



MINISTÉRIO DA CIÊNCIA, TECNOLOGIA E INOVAÇÕES  
**INSTITUTO NACIONAL DE PESQUISAS ESPACIAIS**

sid.inpe.br/mtc-m21d/2022/03.20.18.25-TDI

## DYNAMICS OF DISTURBANCE IN MATOPIBA USING TIME SERIES OF SPECTRAL INDICES

Alana Almeida de Souza

Doctorate Thesis of the Graduate  
Course in Remote Sensing, guided  
by Drs. Lênio Soares Galvão, and  
Thales Sehn Körting, approved in  
April 19, 2022.

URL of the original document:

<<http://urlib.net/8JMKD3MGP3W34T/46HL64H>>

INPE  
São José dos Campos  
2022

**PUBLISHED BY:**

Instituto Nacional de Pesquisas Espaciais - INPE  
Coordenação de Ensino, Pesquisa e Extensão (COEPE)  
Divisão de Biblioteca (DIBIB)  
CEP 12.227-010  
São José dos Campos - SP - Brasil  
Tel.:(012) 3208-6923/7348  
E-mail: pubtc@inpe.br

**BOARD OF PUBLISHING AND PRESERVATION OF INPE  
INTELLECTUAL PRODUCTION - CEPPII (PORTARIA N°  
176/2018/SEI-INPE):****Chairperson:**

Dra. Marley Cavalcante de Lima Moscati - Coordenação-Geral de Ciências da Terra  
(CGCT)

**Members:**

Dra. Ieda Del Arco Sanches - Conselho de Pós-Graduação (CPG)  
Dr. Evandro Marconi Rocco - Coordenação-Geral de Engenharia, Tecnologia e  
Ciência Espaciais (CGCE)  
Dr. Rafael Duarte Coelho dos Santos - Coordenação-Geral de Infraestrutura e  
Pesquisas Aplicadas (CGIP)  
Simone Angélica Del Ducca Barbedo - Divisão de Biblioteca (DIBIB)

**DIGITAL LIBRARY:**

Dr. Gerald Jean Francis Banon  
Clayton Martins Pereira - Divisão de Biblioteca (DIBIB)

**DOCUMENT REVIEW:**

Simone Angélica Del Ducca Barbedo - Divisão de Biblioteca (DIBIB)  
André Luis Dias Fernandes - Divisão de Biblioteca (DIBIB)

**ELECTRONIC EDITING:**

Ivone Martins - Divisão de Biblioteca (DIBIB)  
André Luis Dias Fernandes - Divisão de Biblioteca (DIBIB)



MINISTÉRIO DA CIÊNCIA, TECNOLOGIA E INOVAÇÕES  
**INSTITUTO NACIONAL DE PESQUISAS ESPACIAIS**

sid.inpe.br/mtc-m21d/2022/03.20.18.25-TDI

## **DYNAMICS OF DISTURBANCE IN MATOPIBA USING TIME SERIES OF SPECTRAL INDICES**

Alana Almeida de Souza

Doctorate Thesis of the Graduate  
Course in Remote Sensing, guided  
by Drs. Lênio Soares Galvão, and  
Thales Sehn Körting, approved in  
April 19, 2022.

URL of the original document:

<<http://urlib.net/8JMKD3MGP3W34T/46HL64H>>

INPE  
São José dos Campos  
2022

Cataloging in Publication Data

---

Souza, Alana Almeida de.

So89d Dynamics of disturbance in MATOPIBA using time series of spectral Indices / Alana Almeida de Souza. – São José dos Campos : INPE, 2022.

xxii + 94 p. ; ( sid.inpe.br/mtc-m21d/2022/03.20.18.25-TDI)

Thesis (Doctorate in Remote Sensing) – Instituto Nacional de Pesquisas Espaciais, São José dos Campos, 2022.

Guiding : Drs. Lênio Soares Galvão, and Thales Sehn Körting.

1. Disturbance detection. 2. Time series. 3. Cerrado.  
4. Vegetation indices. I.Title.

CDU 528.8(213.54)

---



Esta obra foi licenciada sob uma Licença [Creative Commons Atribuição-NãoComercial 3.0 Não Adaptada](https://creativecommons.org/licenses/by-nc/3.0/).

This work is licensed under a [Creative Commons Attribution-NonCommercial 3.0 Unported License](https://creativecommons.org/licenses/by-nc/3.0/).



MINISTÉRIO DA  
CIÊNCIA, TECNOLOGIA  
E INOVAÇÕES



**INSTITUTO NACIONAL DE PESQUISAS ESPACIAIS**  
Serviço de Pós-Graduação - SEPGR

**DEFESA FINAL DE DISSERTAÇÃO DE ALANA ALMEIDA DE SOUZA**  
**REG 102318/18, BANCA Nº 082/2022**

No dia 19 de abril de 2022, por teleconferência, o(a) aluno(a) mencionado(a) acima defendeu seu trabalho final (apresentação oral seguida de arguição) perante uma Banca Examinadora, cujos membros estão listados abaixo. O(A) aluno(a) foi APROVADO(A) pela Banca Examinadora, por unanimidade, em cumprimento ao requisito exigido para obtenção do Título de Doutora em Sensoriamento Remoto. O trabalho precisa da incorporação das correções sugeridas pela Banca Examinadora e revisão final pelo(s) orientador(es).

**Novo Título: "Dynamics of disturbance in MATOPIBA using time series of spectral Indices"**

**Membros da banca:**

Dra. Maria Isabel Sobral Escada – Presidente – INPE

Dr. Lênio Soares Galvão – Orientador – INPE

Dr. Thales Sehn Körting– Orientador – INPE

Dr. Cláudio Aparecido Almeida – Membro Interno – INPE

Dr. Edson Eyji Sano – Membro Externo – Embrapa Cerrados

Dra. Yhasmin Mendes de Moura - Membro Externo - Karlsruhe Institute of Technology (KIT)



Documento assinado eletronicamente por **Thales Sehn Korting, Pesquisador**, em 26/04/2022, às 14:01 (horário oficial de Brasília), com fundamento no § 3º do art. 4º do [Decreto nº 10.543, de 13 de novembro de 2020](#).



Documento assinado eletronicamente por **Maria Isabel Sobral Escada, Tecnologista**, em 26/04/2022, às 17:34 (horário oficial de Brasília), com fundamento no § 3º do art. 4º do [Decreto nº 10.543, de 13 de novembro de 2020](#).



Documento assinado eletronicamente por **Lênio Soares Galvão, Pesquisador**, em 27/04/2022, às 09:27 (horário oficial de Brasília), com fundamento no § 3º do art. 4º do [Decreto nº 10.543, de 13 de novembro de 2020](#).



Documento assinado eletronicamente por **EDSON EYJI SANO (E), Usuário Externo**, em 27/04/2022, às 11:21 (horário oficial de Brasília), com fundamento no § 3º do art. 4º do [Decreto nº 10.543, de 13 de novembro de 2020](#).



Documento assinado eletronicamente por **Yhasmin mendes de moura (E), Usuário Externo**, em 05/05/2022, às 07:42 (horário oficial de Brasília), com fundamento no § 3º do art. 4º do [Decreto nº 10.543, de 13 de novembro de 2020](#).



Documento assinado eletronicamente por **Claudio Aparecido de Almeida, Tecnologista**, em 05/05/2022, às 14:05 (horário oficial de Brasília), com fundamento no § 3º do art. 4º do [Decreto nº 10.543, de 13 de novembro de 2020](#).

---



A autenticidade deste documento pode ser conferida no site <http://sei.mctic.gov.br/verifica.html>, informando o código verificador **9620239** e o código CRC **53A85AB3**.

---

Referência: Processo nº 01340.002273/2022-14

SEI nº 9620239

*“Our lives begin to end the day we become silent about things that matter.”*

*Martin Luther King Jr.*



To my mother and grandmother

*in memoriam*



## ACKNOWLEDGEMENTS

(In Portuguese)

O período em que esta tese foi concebida foi de muitos desafios e superações. Perdi minha mãe e avó materna no primeiro ano da tese. Um psicólogo me fez perceber que minha fuga foi me sobrecarregar de trabalho e estudos. Outro desafio foi a dedicação à ciência e ao meio ambiente num período em que o negacionismo, corte de verbas às instituições e retrocessos ambientais ganharam tanta força no Brasil. Vivenciamos uma pandemia de covid-19. O mundo mudou... e permaneceu o mesmo... Muitos dizem que se dedicar à ciência no Brasil é um ato de resistência. Não deixa de ser. Mas também teve um quê de privilégio ter condições de viver com uma bolsa de estudos que está sem reajuste há quase 10 anos. O que me motivou e motiva é a certeza de que conhecimento é um bem precioso (se usado para o bem), capaz de mudar vidas e o mundo para melhor. A certeza de estar entre os melhores profissionais e cientistas do Brasil e do mundo, ao estar no INPE, me enche de orgulho e só tenho a agradecer a cada um dos que cruzaram meu caminho nesses tempos. Em especial, agradeço:

A Deus, que me dá mais do que mereço;

Aos meus orientadores, Dr. Lênio Galvão e Dr. Thales Körting, por fornecerem todo o suporte ao desenvolvimento da pesquisa;

Ao Dr. Cláudio Almeida, pelas contribuições no desenvolvimento da proposta de estudo e artigo. Pela confiança em meu trabalho e parceria profissional que se inicia;

À Dra. Isabel Escada, pelas contribuições no desenvolvimento da proposta de estudo;

À Dra. Ieda Sanches, que tão incansavelmente se dedicou à coordenação da pós-graduação e aos seus alunos durante quase todo o período dessa tese. Por também apostar em mim;

A todo o corpo docente e discente do INPE, com quem pude aprender tanto;

Ao amor da minha vida, Alexandre Ciuffa;

Aos meus familiares, meu porto-seguro;

À Dona Débora, que me recebeu em sua casa com tanto carinho no meu ir e vir a São José dos Campos.

O presente trabalho foi realizado com apoio da Coordenação de Aperfeiçoamento de Pessoal de Nível Superior - Brasil (CAPES) - Código de Financiamento 001.



## ABSTRACT

The Cerrado is the second largest biome in Brazil, occupying around 2 million km<sup>2</sup>. It is considered a global hotspot of biodiversity that is threatened by agribusiness expansion and land degradation. The efforts to monitor the Cerrado by remote sensing are challenging, especially due to the confounding effects of the vegetation phenology with anthropogenic changes. In this study, data-driven approaches based on image time series of vegetation indices (VIs) processed on the Google Earth Engine platform were evaluated for the analysis of vegetation clearing and land degradation in the MATOPIBA region, the newest agricultural frontier in the Cerrado. For the detection of vegetation clearing in the 1985–2018 period, the LandTrendr algorithm was applied to the Normalized Difference Vegetation Index (NDVI) obtained from Landsat satellite instruments. In the evaluation of land degradation (2001–2015), the Trends.Earth algorithm considered NDVI data calculated from the Moderate Resolution Imaging Spectroradiometer (MODIS). By combining different datasets into the analysis, the relationships among savanna clearings, land degradation, topographic attributes, and fire frequency were evaluated. For recent disturbances events, seven VIs were calculated from the Landsat time series (2017–2019) and used as input data to the Continuous Change Detection and Classification (CCDC) algorithm. The effects of disturbance on these VIs and the accuracy of CCDC, considering individual VIs, ensemble VIs, and the type of disturbance (savanna clearing or fire), were assessed. Finally, the possible existence of seasonal patterns of disturbance in the study area was discussed. The results showed that 31.6% of native vegetation has been cleared in the MATOPIBA until 2018. The number of fire events increased with vegetation clearing. The number of land-degraded areas increased with fire frequency over agricultural fields, but remained relatively stable over native vegetated areas. The overall accuracy of CCDC detection of disturbance ranged from 51.2% to 65.9% for single VIs. It increased to 71.2% for ensemble VIs, whose multivariate approach reduced the omission errors. For detecting disturbance events, the most important VIs used near-infrared and shortwave infrared reflectance bands on their formulations (Normalized Burn Ratio - NBR, NBR2, and Moisture Stress Index - MSI). The CCDC accuracy was generally higher for detecting clearing than for mapping burned areas. In contrast, the recorded date of disturbance occurrence was less precise for detecting clearing than for recording events of fire, especially due to the existence of some gradual processes of vegetation degradation until complete clearing. The findings showed the existence of a seasonal pattern of disturbance occurrence. Savanna clearing predominated in the transition from the rainy to the dry season (April to July). It preceded most events of fire between August and October that occurred near the consolidated areas of agriculture and extended into the native vegetation areas.

Keywords: Disturbance detection. Time series. Cerrado. Vegetation indices.



# DINÂMICAS DE DISTÚRBIOS NO MATOPIBA USANDO SÉRIES TEMPORAIS DE ÍNDICES ESPECTRAIS

## RESUMO

O Cerrado é o segundo maior bioma do Brasil, ocupando cerca de 2 milhões de km<sup>2</sup>. É considerado um hotspot global de biodiversidade que está ameaçado pela expansão do agronegócio e pela degradação das terras. Os esforços de monitoramento do Cerrado por sensoriamento remoto são desafiadores, especialmente devido à dificuldade em discriminar variações fenológicas da vegetação daquelas resultantes de mudanças antrópicas. Neste estudo, abordagens baseadas em dados de séries temporais de índices de vegetação (IVs) processadas na plataforma *Google Earth Engine* foram avaliadas para a análise de desmatamento e degradação das terras na região do MATOPIBA, a nova fronteira agrícola do Cerrado. Para a detecção de desmatamento no período 1985-2018, aplicou-se o algoritmo LandTrendr ao Índice de Vegetação por Diferença Normalizada (NDVI) obtido a partir de instrumentos do satélite Landsat. Na avaliação da degradação da produtividade da vegetação (2001–2015), utilizou-se o algoritmo Trends.Earth para analisar dados de NDVI calculados a partir do *Moderate Resolution Imaging Spectroradiometer* (MODIS). Ao combinar diferentes conjuntos de dados na análise, discutiu-se as relações entre supressão de savanas, degradação da terra, atributos topográficos e frequência de fogo. Para eventos de distúrbios recentes, investigou-se sete IVs calculados a partir da série temporal Landsat (2017–2019) e do algoritmo de Detecção e Classificação Contínua de Mudanças (CCDC). Os efeitos dos distúrbios sobre os IVs e a precisão da detecção do CCDC considerando IVs individuais, IVs em conjunto e o tipo de distúrbio (supressão do Cerrado e fogo), também foram avaliados. Por fim, analisou-se a possível existência de padrões sazonais de distúrbios na área de estudo. Os resultados mostraram que 31,6% da vegetação nativa foi removida no MATOPIBA até 2018. O número de eventos de fogo aumentou com o desmatamento da vegetação. A quantidade de áreas degradadas aumentou com a frequência de fogo em áreas agrícolas, mas permaneceu relativamente estável em áreas com vegetação nativa. A precisão geral da detecção de distúrbios pelo CCDC variou de 51,2% a 65,9% para IVs isoladamente. Ela aumentou para 71,2% para IVs usados em conjunto, cuja abordagem multivariada reduziu os erros de omissão. Para detectar eventos de distúrbios, os IVs mais importantes utilizaram bandas de reflectância do infravermelho próximo e infravermelho de ondas curtas em suas formulações (*Normalized Burn Ratio* - NBR, NBR2, e *Moisture Stress Index* - MSI). A precisão do CCDC foi geralmente maior para detecção de desmatamento do que para mapeamento de áreas queimadas. Em contrapartida, a data registrada da ocorrência do distúrbio foi menos precisa para detectar o desmatamento do que para registrar os eventos de fogo, especialmente devido à existência de alguns processos graduais de degradação da vegetação até o desmatamento completo.

Nossos resultados mostraram a existência de um padrão sazonal de ocorrência de distúrbios. A supressão do cerrado predominou na transição da estação chuvosa para a seca (abril a julho). A maioria dos eventos de fogo ocorreu entre agosto e outubro, próximo às áreas consolidadas de agricultura, e se estendeu até as áreas de vegetação nativa.

Palavras-chave: Detecção de distúrbios. Séries temporais. Cerrado. Índice de vegetação.

## LIST OF FIGURES

	<u>Pág.</u>
Figure 4.1 - Study area.....	20
Figure 4.2 - Dynamics of savanna clearings over the nine mesoregions of MATOPIBA at different periods of analysis.....	27
Figure 4.3 - Examples of clearing detection over three types of savannas from the MATOPIBA region.....	28
Figure 4.4 - Temporal variations in savanna-cleared areas over the MATOPIBA region.....	30
Figure 4.5 - Dynamics of savanna clearings detected by the LandTrendr algorithm per mesoregion of MATOPIBA.....	31
Figure 4.6 - Changes over time in the savanna-cleared area over the Sudoeste Piauiense.....	32
Figure 4.7 - Period of savanna clearings detected by the LandTrendr algorithm over a site located at the <i>Sudoeste Piauiense</i> .....	33
Figure 4.8 - Land degradation in MATOPIBA region.....	34
Figure 4.9 - (a) Average annual precipitation (2001-2015) over the MATOPIBA region calculated from the Tropical Rainfall Measuring Mission (TRMM) data. (b) Fire frequency determined from MODIS data in the 2001-2015 period. (c) Spatial distribution of the major soil types.....	35
Figure 4.10 - Digital Elevation Model of the MATOPIBA region.....	36
Figure 4.11 - Relationship between the cumulative savanna-clearing area detected per year by LandTrendr and the cumulative burned-area calculated per year from the MODIS MCD64A1 product.....	38
Figure 4.12 - Variations in Trends.Earth metrics and fire frequency for a site located at the <i>Sudoeste Piauiense</i> .....	39
Figure 4.13 - Relationship between the proportion of land-degraded areas and fire frequency for a site located at the <i>Sudoeste Piauiense</i> .....	40
Figure 5.1 Main methodological steps used for detecting disturbance over the savannas.....	49
Figure 5.2 - Location of the study area in the <i>Cerrado</i> biome in Brazil.....	51

Figure 5.3 - Variations in monthly accumulated precipitation over the study area during the rainy and dry seasons of 2019.....	52
Figure 5.4 - (a) OLI/Landsat-8 surface reflectance spectra of woodland savanna before and after a clearing event in 2019. (b) Spectra from a shrub savanna area affected by fire in the same year.....	58
Figure 5.5 - Landsat time-series examples of disturbance in 2019 in seasonal profiles.....	60
Figure 5.6 - Variations in commission and omission errors for the CCDC detection of disturbance (clearing plus fire), using different vegetation indices (VIs) and ensemble VIs.....	63
Figure 5.7 - CCDC performance of each vegetation index (VI) and ensemble VIs to correctly detect disturbance over areas affected by fire ( $n = 147$ samples) and savanna clearing ( $n = 147$ samples).....	64
Figure 5.8 - Time accuracy of CCDC-detection over (a) cleared- and (b) burned-savanna areas.....	65
Figure 5.9 - Monthly average of Landsat cloud-free pixels in the study area during the rainy and dry seasons of 2019.....	66
Figure 5.10 - Temporal local patterns of disturbance over areas affected by clearing and fire in 2019 for the reference samples. Savanna clearing events predominate between April and July, while fire disturbance mainly occurs between August and October.....	67
Figure 5.11 - CCDC-detected disturbance over two periods of predominant occurrence of (a) savanna clearing (April–July) and (b) fire (August–October)..	68
Figure 5.12 - Savanna-cleared area in 2019 mapped in the study area by the <i>Sistema de Detecção de Desmatamento em Tempo Real</i> (DETER Cerrado) from the Brazilian National Institute of Space Research (INPE).....	69
Figure 5.13 - Burned area in two distinct periods of 2019, registered by the 250-m MODIS FireCCI v.5.1 product (European Space Agency—ESA): (a) April to June and (b) August to October.....	70

## LIST OF TABLES

	<b><u>Pág.</u></b>
Table 4.1 - LandTrendr parameters selected to evaluate the dynamics of savanna clearings in the MATOPIBA region, using composite NDVI time series (1985-2018) obtained from the TM, ETM+ and OLI Landsat instruments.....	23
Table 4.2 - Full area-weighted error matrix for cleared and non-cleared savanna areas in the MATOPIBA region. $W_i$ is the proportion of the area of a given class concerning the total area.....	29
Table 5.1 - Vegetation indices (VIs) used in the CCDC algorithm for detecting disturbance over the savannas.....	54
Table 5.2 - Overall accuracy (OA) with confidence intervals (CI) for the CCDC detection of disturbance over savannas using different vegetation indices (VIs) and ensemble VIs. Producer's (PA) and User's (UA) accuracies are also indicate for the disturbance and non-disturbance classes.....	62



## LIST OF ABBREVIATIONS

BFAST	Break Detection For Additive Season and Trend
CCI	Climate Change Initiative
CCDC	Continuous Change Detection and Classification
DETER	<i>Sistema de Detecção de Desmatamento em Tempo Real</i>
DEM	Digital Elevation Model
ETM+	Enhanced Thematic Mapper Plus
EVI	Enhanced Vegetation Index
EWMACD	Exponentially Weighted Moving Average Change Detection
GEE	Google Earth Engine
GRND	Green-Red Normalized Difference
INPE	<i>Instituto Nacional de Pesquisas Espaciais</i>
LandTrendr	Landsat-based Detection of Trends in Disturbance and Recovery
LST	Land Surface Temperature
LOESS	Locally weighted scatterplot smoothing
MODIS	Moderate Resolution Imaging Spectrometer
MSI	Moisture Stress Index
NIR	Near Infrared
NBR	Normalized Burn Ratio
NDVI	Normalized Difference Vegetation Index
OLI	Operational Land Imager
PRODES	<i>Programa de Monitoramento da Floresta Amazônica Brasileira por Satélite</i>
RUE	Rain Use Efficiency

SAVI	Soil-Adjusted Vegetation Index
SLC	Scan Line Corrector
SRTM	Shuttle Radar Topography Mission
SWIR	Shortwave Infrared
TM	Thematic Mapper
UNCCD	United Nations Convention to Combat Desertification
VCT	Vegetation Change Tracker
VI	Vegetation Indices
VeRDET	Vegetation Regeneration and Disturbance Estimates through Time

# CONTENTS

	<u>Pág.</u>
<b>1 INTRODUCTION.....</b>	<b>1</b>
1.1 General objective .....	4
1.2 Specific objectives .....	4
<b>2 LITERATURE REVIEW.....</b>	<b>6</b>
2.1 Trends in change detection methods.....	6
2.2 Disturbance detection in the Cerrado with time series of satellite images ...	8
<b>3 THE MATOPIBA REGION .....</b>	<b>12</b>
<b>4 DYNAMICS OF SAVANNA CLEARING AND LAND DEGRADATION IN THE NEWEST AGRICULTURAL FRONTIER IN BRAZIL.....</b>	<b>15</b>
4.1 Introduction .....	15
4.2 Methodology .....	19
4.2.1 Study area .....	19
4.2.2 Analysis of the savanna clearings over time.....	21
4.2.2.1 Accuracy assessment and area estimates .....	23
4.2.3 Land degradation analysis.....	24
4.2.4 Influence of topographic attributes and fire on clearing and degradation	25
4.3 Results .....	26
4.3.1 Dynamics of savanna clearings from Landsat NDVI data.....	26
4.3.2 Analysis of land degradation from MODIS NDVI data .....	33
4.3.3 Relationships of clearing and degradation with topography and fire .....	35
4.4 Discussion .....	40
4.5 Conclusions.....	45
<b>5 ON A DATA-DRIVEN APPROACH FOR DETECTING DISTURBANCE IN THE BRAZILIAN SAVANNAS USING TIME SERIES OF VEGETATION INDICES.....</b>	<b>46</b>
5.1 Introduction .....	46
5.2 Data and methodology .....	49

5.2.1 Selection of the study area .....	50
5.2.2 Pre-processing of Landsat time series and selection of VIs for CCDC... 52	52
5.2.3 Continuous Change Detection and Classification (CCDC).....	54
5.2.4 Data analysis from sampling and response designs .....	55
5.2.4.1 Accuracy assessment per VI, ensemble VIs, and type of disturbance 55	55
5.2.4.2 Accuracy of the detected time of disturbance.....	57
5.2.4.3 Seasonal patterns of Savanna clearing and fire events.....	57
5.3 Results .....	58
5.3.1 Time series of vegetation indices and the detection of disturbance .....	58
5.3.2 Variations in accuracy metrics per VI, ensemble VIs, and type of disturbance .....	61
5.3.3 Assessment of the correct time of disturbance.....	64
5.3.4 Seasonal patterns of occurrence between savanna clearing and fire ....	67
5.4 Discussion .....	70
5.5 Conclusions.....	74
<b>6 GENERAL DISCUSSION.....</b>	<b>76</b>
<b>7 CONCLUSIONS.....</b>	<b>79</b>
7.1 Future Works .....	79
<b>REFERENCES.....</b>	<b>81</b>

## 1 INTRODUCTION

The Cerrado is the second largest biome in Brazil, occupying around 2 million km<sup>2</sup> or 24% of the national territory (IBGE, 2012). The Cerrado shares ecological transition zones with four of the six Brazilian biomes: Amazon (rainforest), Caatinga (semi-arid region), Pantanal (wetland), and Atlantic Forest (coastal forest). The vegetation structure is heterogeneous with grasses, shrubs, and trees in variable proportions. Besides being considered a global hotspot of biodiversity (MYERS et al., 2000), the Cerrado hosts the headwaters of many Brazilian hydrographic basins, including the Xingu, Paraná, São Francisco, and Araguaia-Tocantins watersheds (LIMA; SILVA, 2005). The biome has also many traditional communities and indigenous people, who depend directly on this ecosystem. Despite the importance of the Cerrado, only 5.4% of the biome are conservation units for sustainable use, and 2.5% are strictly protected areas. Indigenous territories occupy 4.5% of the area and many traditional communities still wait for the official recognition of their territories.

The Cerrado is also a Brazilian agribusiness power, having half of the agricultural lands in Brazil (SPERA, 2017). The legal protection of private rural lands, regulated by the Brazilian Forest Code, is weak compared with the Amazon (SPAROVEK et al., 2012). It is estimated that around 440,000 km<sup>2</sup> of native vegetation can be legally cleared in the Cerrado (GUIDOTTI et al., 2017). Most native vegetated areas are located in the MATOPIBA region. The MATOPIBA, an acronym for the names of the four Brazilian states that compose this region (Maranhão, Tocantins, Piauí, and Bahia), is the newest and probably the last agricultural frontier in the Cerrado (GRAESSER et al., 2015; RAUSCH et al., 2019). The native savannas in MATOPIBA, originally about 630,000 km<sup>2</sup>, have been converted for single cropping (e.g. soybean, maize, and cotton plantations) and double cropping (e.g. soy-corn or soy-cotton rotations) activities (SPERA et al., 2016). Therefore, this region is an example of the conflict between environmental and agricultural policies that will determine the distribution between the original cover and converted areas in the coming years (SANO et al., 2019a).

More than 50% of the original Cerrado cover has been replaced mainly by planted pastures and agricultural areas (MMA, 2015; SANO et al., 2019b; SOUZA et al., 2020a; INPE, 2021). This conversion process is still going on at a fast pace. In the conversion process and land management, fire is usually used. Although the Cerrado contains vegetation adapted to fire, its indiscriminate use affects biodiversity, increases carbon emissions, compromises ecosystem services, and promotes land degradation (MIRANDA et al., 2009; PIVELLO et al., 2010).

Understanding the dynamics of clearing and fire in the Cerrado, mainly in the MATOPIBA region, which is poorly known compared to other parts of the biome, is a key component for planning public policies, defining inspection and management actions, and supporting greenhouse gas emissions estimates. The use of satellite images is the only means for large-scale monitoring in this region (SANO et al., 2007). However, systematic and accurate clearing and degradation monitoring in the Cerrado is still challenging using change detection methods.

The biome presents many different floristic and structural compositions that respond differently to climatic seasonality, strongly marked by well-defined dry and rainy seasons. In addition to the phenological response characteristic of each vegetation type, the vegetation's resilience to different types of disturbance is also distinct. These characteristics limit the use of traditional change detection techniques based on the definition of fixed thresholds between the difference of pairs of satellite images for the detection of vegetation suppression and fire, hereinafter generically referred to as disturbance. Thus, it is important to develop data-driven approaches to capture disturbance processes, especially with an adequate temporal and spatial resolution of satellite observations.

The current governmental initiatives for the systematic clearing monitoring of the Cerrado biome are based on the visual interpretation of Landsat-like satellite images. Brazil's National Institute for Space Research (INPE) has two operational projects for monitoring vegetation suppression in the Cerrado: PRODES Cerrado, and DETER Cerrado (BRITO et al., 2018; INPE, 2019). The PRODES Cerrado mapped the entire anthropized area of the Cerrado biome in 2000. From that reference year, the project systematically identified all subsequent anthropic

increments (i.e. newly cleared areas) at a biannual (between 2000 and 2012) and annual frequency (after 2013) (PARENTE et al., 2021). DETER Cerrado focuses on issuing daily clearing alerts to support inspection and control actions. Both initiatives have high accuracies (MEIRA et al., 2019; PARENTE et al., 2021). However, the quality of the monitoring with fast and automated/semi-automated operational change detection methods is one of the challenges that government and non-profit institutions are facing today.

In this context, this study aims to contribute to the detection and analysis of the dynamics of vegetation clearing and land degradation in the Cerrado. For this purpose, change detection algorithms that use time series of vegetation indices with different temporal frequencies were considered. Annual-based composite images from the dry season (strategy to reduce the effects of vegetation phenology) and methods using all available images in a given period of analysis (strategy to explore vegetation phenology) were evaluated. Data-driven approaches with these two temporal frequencies of imagery were processed on the Google Earth Engine's (GEE) cloud-based platform (GORELICK et al., 2017). The use of new algorithms and time series has been showing good results in the detection and qualification of disturbance in forest environments. However, they still need to be evaluated in savanna environments subject to strong climatic seasonality such as in the case of the Cerrado. In addition, image processing on the GEE makes it possible to scale and speed up image processing. Then, our study served as a proof of concept for the evaluation of new approaches for change detection in the Cerrado using cloud processing and time series of vegetation indices.

In addition to evaluating the performance of new disturbance detection algorithms in the Cerrado, this study analyzes the effect of fire on land degradation. The study starts from the following hypotheses:

- The magnitude of the disturbances depends on their type, intensity, and vegetation formation under disturbance. However, the largest spectral magnitude of change (pos-disturbance minus pre-disturbance value) in a pixel-based annual time series is related to native vegetation clearing in the Cerrado;

- The indiscriminate use of fire in the Cerrado causes land degradation, which is detectable using a time series of vegetation indices (VIs);
- The detection of clearing and fire in the Cerrado has distinct sensitivities to the spectral indices used as input data to methods for detecting changes with time series. Therefore, more accurate disturbance maps are expected when using different VIs and their combination in the analyses.

### **1.1 General objective**

The main goal of this study is to evaluate new data-driven approaches for the analysis of vegetation clearing and land degradation in MATOPIBA using time series of VIs focused on two-time intervals: 1) a long-term period (interannual, between 1985 and 2018, with composite dry-season satellite observations per year to reduce the effects of vegetation phenology on the analysis); and 2) a short-term period (intra-annual, between 2017 and 2019, with seasonal satellite observations along each year to consider vegetation phenology in the short time detection of disturbance).

### **1.2 Specific objectives**

The specific objectives are to evaluate:

- a) the accuracy assessment of the disturbance detection from a data-driven analysis of interannual and intra-annual time series of VIs over native vegetation in the Cerrado;
- b) the dynamics of vegetation clearing (1985-2018) and land degradation (2001-2015) in the MATOPIBA region;
- c) the accuracy of the disturbance detection over native vegetation, considering single VIs (univariate input data), ensemble VIs (multivariate input data), and the type of disturbance (clearing and fire) in the Cerrado;
- d) the possible existence of seasonal patterns of occurrence of fire and clearing for a better understanding of the dynamics of disturbance in the Cerrado.

The present thesis is structured in chapters. The first chapter contains a general introduction to the study. Chapter 2 presents trends in change detection methods and an overview of studies in the Cerrado biome focused on disturbance detection with time series. Chapter 3 describes the MATOPIBA region. Chapter 4 presents the article published in *GIScience and Remote Sensing* journal, entitled “Dynamics of savanna clearing and land degradation in the newest agricultural frontier in Brazil” (SOUZA et al., 2020c). Chapter 5 contains the article published in the *Remote Sensing* journal: “On a data-driven approach for detecting disturbances in the Brazilian savannas using time series of vegetation indices”(SOUZA et al., 2021). Chapter 6 discusses the overall results. The overall conclusions of the thesis are presented in Chapter 7.

## **2 LITERATURE REVIEW**

### **2.1 Trends in change detection methods**

Disturbance detection through remote sensing is a constantly evolving area of research. Overlooking the state-of-the-art on the subject has become an arduous task, given the growing number of algorithms in use and development. The different approaches have been consolidated in several review articles (COPPIN et al., 2004; LU et al., 2004; RADKE et al., 2005; HUSSAIN et al., 2013; ZHU, 2017). However, most authors agree that there is no universal detection technique (COHEN et al., 2017; ZHU, 2017). It is up to the analyst to identify the most suitable method for its application in a given study area.

There are some review articles on change detection methods based on time series, but these papers have focused on the assessment of forest environments (BANSKOTA et al., 2014; THONFELD; HECHELTJEN; MENZ, 2015). There is no evaluation of existing methods applied to non-forest environments subject to strong seasonality such as the Cerrado biome.

At the beginning of the studies several decades ago, change detection techniques were based on the comparison between pairs of images. Nowadays, the investigations are using more and more images with one of the two approaches: selecting the best high-quality cloud-free pixel to be inserted into temporal composite images; or capturing intra-annual variations capable of describing the complex dynamics of the Earth's surface (GÓMEZ; WHITE; WULDER, 2016; ZHU, 2017).

The best available pixel approach is mainly used in studies aimed at detecting interannual changes (COHEN; YANG; KENNEDY, 2010; KENNEDY; YANG; COHEN, 2010; HUGHES; KAYLOR; HAYES, 2017; GRIFFITHS; JAKIMOW; HOSTERT, 2018). In these cases, multiple images are used to compose one cloud-free image per year, especially in the period more favorable to obtain images (e.g., dry season with reduced frequency of cloud cover). This strategy aims to reduce the lack of cloud-free images and the seasonal differences caused by solar illumination and vegetation phenology. The best available pixel is the strategy of the MapBiomas initiative, which aims to generate annual land use and

land cover classification of Brazil using machine learning algorithms available in the GEE platform (ALENCAR et al., 2020; SOUZA et al., 2020b). This approach is also used as input data for algorithms of change detection using time series, such as the Landsat-based Detection of Trends in Disturbance and Recovery (LandTrendr) (KENNEDY; YANG; COHEN, 2010), Vegetation Change Tracker (VCT) (HUANG et al., 2010), and Vegetation Regeneration and Disturbance Estimates through Time (VerDET) - (HUGHES et al., 2017). The last two algorithms are restricted to forest environments. These methods are offline, i.e. assume the time series data already exist and the main goal is to detect when the characteristics of the time series changed (ZHU, 2017).

Intra-annual detection is possible for methods that allow as input data a sequence of several images over each studied year obtained by a given sensor, satellite constellations, or data fusion from different satellite instruments. Using time series, the main goal is to detect changes in near real-time (or continuously), with minimum delay, i.e. it is an online approach (ZHU, 2017). The Continuous Change Detection and Classification (CCDC) (ZHU; WOODCOCK, 2014), Break Detection For Additive Season and Trend Monitor (BFAST Monitor) (VERBESSELT; ZEILEIS; HEROLD, 2012a), Exponentially Weighted Moving Average Change Detection (EWMACD) (BROOKS et al., 2014), and EDYN (BROOKS et al., 2017) are examples of methods that employ this type of data. Among them, only BFAST has been evaluated in the Cerrado (SOUZA; GALVÃO, 2019; BUENO et al., 2020).

In addition to detecting abrupt changes (e.g., clearing and fire), the use of time series allows the assessment of gradual trends in spectral values of the pixels, which is indicative of degradation or vegetation recovering processes. Unlike abrupt changes, gradual changes occur over several years. The gradual change relates to landscapes undergoing a systematic shift through time in spectral response, such as the increasing biomass associated with plant succession and vegetation regrowth; the decreasing biomass associated with some particular agent of stress; or the gradual shifts in species composition related to several potential factors (VOGELMANN et al., 2016). The main gradual change evaluated with remote sensing products is land degradation (changes in

vegetation productivity), which has been studied with NDVI data from sensors that can provide daily information such as the Advanced Very High Resolution Radiometer (AVHRR) and the Moderate Resolution Imaging Spectroradiometer (MODIS) (GAO et al., 2006; JACQUIN; SHEEREN; LACOMBE, 2010; SCHUCKNECHT et al., 2013; SIMS et al., 2019). Linear trends of NDVI are usually considered indicators of vegetation dynamics and are widely used as proxies for land degradation (BAI et al., 2008; TUCKER, , PINZON, 2016; EASDALE et al., 2019).

Validating gradual changes might include measures of spatial density of plants, species composition, plant vigor/health, and soil moisture availability, among others. These measurements are sometimes hard to be obtained in the field. Then, the history of land use, type of soil and land management, and the climate classification are important factors to explain the gradual changes observed in the time series of VIs (VOGELMANN et al., 2016). Despite the challenges in validating gradual changes, Vogelmann et al. (2016) have moved remote sensing analysis closer to an ecological view of landscape dynamics (KENNEDY et al., 2014).

## **2.2 Disturbance detection in the Cerrado with time series of satellite images**

The analysis of changes in the Cerrado using remote sensing images has been usually based on vegetation indices. The relationship between spectral indices and biophysical parameters in the Cerrado has been evaluated in several studies (RATANA; HUETE; FERREIRA, 2005; LIESENBERG; GALVÃO; PONZONI, 2007; SOUZA; GALVÃO; SANTOS, 2010; JACON, 2016; SCHWIEDER et al., 2018). VIs were also explored for land use and land cover classification in the Cerrado (COSTA, 2014; SCHWIEDER et al., 2016; BENDINI, 2018; GIROLAMO NETO, 2018; PICOLI et al., 2018; ALENCAR et al., 2020; SOUZA et al., 2020b).

Despite being the tendency, the use of annual temporal composites of bands or VIs, or all available images in automatic change detection methods (ZHU, 2017), is still scarce in the Cerrado. The studies that used several images in one year

have limitations regarding the identification of the date when the changes have occurred (SILVEIRA et al., 2018, 2019; BUENO et al., 2019).

None of the interannual studies published to date, focusing on detecting changes, used the best available pixel approach to obtain composite images. The MapBiomas project (<https://mapbiomas.org>) uses annual composites of spectral bands, vegetation indices, and fractional images for the annual land use and land cover classification in the Cerrado. Each annual image is classified independently and, later, temporal filters reduce eventual classification errors. Therefore, MapBiomas approach fits into what Câmara et al. (2016) entitled the “space-first, time-later” approach.

The use of fixed thresholds of change between VI images has been tested to detect vegetation clearing and fire in the Cerrado (BAYMA; SANO, 2015; PESSOA et al., 2015; BARROSO et al., 2017). These studies recognize the limitation of this approach due to the effects of climatic seasonality on vegetation phenology as well as the diversity of plant formations. Furthermore, the change threshold applicable in one year will not necessarily work in other years (SILVA; COSTA; MATRICARDI, 2017). Regarding the detection of burn scars in the Cerrado, the imagery frequency is a critical point, as the time when the spectral signal of burn scars varies between the plant formations (PEREIRA et al., 2016; ARRUDA et al., 2021).

The spatial image segmentation and extraction of spectral and geostatistical metrics, followed by the classification of changing and unchanging segments, have some limitations such as the impossibility of using long time series and the high computational cost (LEITE; DE CARVALHO; DA SILVA, 2017; SILVEIRA et al., 2018; BUENO et al., 2019). Furthermore, as in MapBiomas, the strategy is centered on image classification, that is, it is centered on spatial-spectral domains, with the temporal component being a secondary aspect.

Souza and Galvão (2019) evaluated the impact of land-use conversions in the Cerrado on the surface temperature of MODIS (Land Surface Temperature – LST – product MOD11A2). A time series with monthly averages of the MODIS LST from January 2000 to December 2016 was decomposed into seasonal and trend

components using LOESS (“Locally weighted scatterplot smoothing”). Samples from the original time series of the LST, as well as the trend and seasonality components, were analyzed using the "Changepoint" package in R. The method detected a significant change in the original series and in the trend component of the LST in the year when the vegetation clearing occurred. Furthermore, the change in LST values (pre- and post-change) corroborated the estimates calculated by linear regression. The regression analysis was based on the fraction between the different land use types contained in a MODIS pixel and the average of the LST.

Concerning the degradation analysis, the studies generally use the NDVI-MODIS trend analysis as a proxy of the net primary productivity and land degradation. Pereira et al. (2018) estimated the area of degraded pastures in the Cerrado by analyzing the trends of cumulative NDVI anomalies over time used as a proxy for pasture degradation. According to this study, around 39% of the Cerrado pastures are currently degraded, encompassing 18.2 million hectares.

Santana (2019) used trend analysis in NDVI–MODIS time series (2001-2016) to evaluate the influence of different fire occurrences on vegetation phenology of the Brazilian savannas in a group of protected areas in the Jalapão region. Full protection units presented more than 60% of areas with a positive trend. Jalapão Environmental Protection Area, despite being a conservation unit for sustainable use, has low agricultural use, resulting in more than 90% of areas with positive changes. Conservation units with high agricultural use presented more than 70% of pixels with negative trends. The vegetation converted into crops was the one with the greatest changes, showing decreases up to 0.01 NDVI annually not related to the occurrence of fire. Deforestation causes a change in the VI response, resulting in negative trends when the NDVI of the crop is lower than that of the natural vegetation, or positive trends when the NDVI is higher.

Bueno et al. (2020) identified how much vegetation disturbance maps derived from Landsat spectral indices agree spatially. Vegetation disturbance maps, provided by one change detection algorithm (BFAST Monitor) and seven different spectral indices (EVI, MSAVI, NBR, NBR2, NDMI, NDVI, and SAVI), indicated a

low rate of spatial agreement when compared among themselves. The NDVI presented the highest overall accuracy over savanna (59.6%), with an omission error of 67.4% and commission error of 13.4%. Wetness indices produced greater detection accuracies in comparison to greenness-related indices free of saturation. Bueno et al. (2020) found that distinct input data can produce non-spatially correlated disturbance maps. However, they did not explore if an ensemble metric approach could result in better accuracies of disturbance detection.

### 3 THE MATOPIBA REGION

The MATOPIBA is composed of parts of the Maranhão, Piauí, and Bahia states and the whole Tocantins state, totaling 337 municipalities. In MATOPIBA, 91% of the total area includes the Cerrado biome. The Amazon and Caatinga biomes comprise 7% and 2% of the region, respectively. The states of Tocantins and parts of Maranhão also reside within Brazil's Legal Amazon (IBGE, 2017). The vegetation is predominantly formed by shrub savanna, mainly by Cerrado *stricto sensu*. In the savanna grasslands, *Campo Sujo* predominates, while the woodland savanna is composed, predominantly, of the riparian forests, beyond wooded vegetation at North and East Maranhense (INPE, 2021).

The region has two well-defined seasons: a dry season (May to September) and a rainy season (October to April). The average annual rainfall is 800 mm on the east and 2,000 mm on the west (SANO, 2019). During the rainy season, there is a high production of biomass. As the dry season progresses, the biomass produced dries up, favoring the occurrence of fire. For thousands of years, natural fire and anthropogenic fire coexist in the Cerrado region. This suggests that fire, together with the seasonality of precipitation and the soil poor in nutrients, is one of the determinants of the Cerrado vegetation forms (MIRANDA et al., 2009; OLIVERAS et al., 2013).

From a geomorphological point of view, the MATOPIBA can be roughly divided into plateaus and depressions (SANO, 2019). The agriculture in MATOPIBA is highly mechanized and is predominant at the plateaus. The depressions are predominantly occupied by family farming of those who already inhabited the region before the arrival of agribusiness (FAVARETO et al., 2018; FAVARETO, 2019). Soybean, maize, and cotton are the main crops over the plateaus. There is a great variety of soils with a predominance of Latosols (31.1%), Argisols (12.8%), Petric Plintosols (8.7%), Orthic Quartzarenic Neosols (8.7%), and Litholic Neosols (7.2%) in the higher relief. Argiluvic and Haplic Plintosols (3.9%), Gleissolos (1.0%), and Planosols (0.9%) predominate in the lower relief (BOLFE et al., 2016).

Unlike most of the Cerrado, MATOPIBA does not have a history of large-scale cattle ranching. As a result, cropland expansion in MATOPIBA is advancing primarily through clearing native vegetation rather than by using previously cleared pasturelands (SPERA et al., 2016). Fire and agricultural expansion have a direct relationship in the region (MENEZES, 2016). The beginnings of agricultural expansion were in the 1960s, but it intensified in the 1970s with the National Integration Program, which invested in road infrastructure in the region. In the 1980s, there was a strong incentive to establish soybean cultivation for export in the western region of Bahia. This was possible through the second stage of the Japanese-Brazilian Program for the Development of the Cerrados (known as PRODECER), which took place from 1985 to 1990. The Brazilian Agricultural Research Corporation (EMBRAPA) had a paramount role in the adaptation of soybean to low latitudes and more acidic soils. Another stage of PRODECER took place from 1995 to 2001, with actions carried out in the states of Tocantins and Maranhão.

Although better known than other projects, PRODECER was not the only public program implemented in the region. There were programs to redeploy land, finance irrigation equipment, and provide rural technical assistance, for example, in the 1970s and 1980s. These programs benefited medium and large farmers. The availability of cheap land and water was also a major incentive for rural producers to migrate from southern Brazil to MATOPIBA. In just a few decades, a region of low economic dynamism has turned into a coveted frontier that is now home to 10 of the 100 largest soy producers in the country and some of the fastest-growing cities in population size. However, it is worth noting that recent works report that the current Brazilian rural elite in MATOPIBA has been replaced by the growing interest of transnational companies that have been investing in land as a financial asset (FAVARETO et al., 2018).

The process of formation of MATOPIBA was complex and resulted in a region with many contrasts from social, economic, and environmental point-of-views. There were lots of socioeconomic inequality, land grabbing, and water use conflicts along with high rates of deforestation (FAVARETO, 2019). The region

contains 42 conservation units, 28 indigenous lands, 865 agrarian reform settlements, and 34 quilombola areas (EMBRAPA TERRITORIAL, 2022).

## 4 DYNAMICS OF SAVANNA CLEARING AND LAND DEGRADATION IN THE NEWEST AGRICULTURAL FRONTIER IN BRAZIL<sup>1</sup>

### 4.1 Introduction

Tropical savannas in Brazil, locally known as Cerrado, comprise the second largest biome of the country (24% in area) after the tropical forests of the Amazon (49%) (FERREIRA et al., 2011; INSTITUTO BRASILEIRO DE GEOGRAFIA E ESTATÍSTICA (IBGE), 2012). They cover approximately 204 million hectares (SANO et al., 2019a). The savannas show gradients ranging from grasslands to woodlands, which are controlled by several factors such as soil moisture, soil composition, and precipitation (SILVA; BATES, 2002; SOUZA; GALVÃO; SANTOS, 2010; JACON et al., 2017). Because of the high diversity of vegetation species well adapted to natural and human-induced fires and the strong rainfall seasonality, the Cerrado is one of the world's hotspots of biodiversity (RATTER; BRIDGEWATER, and RIBEIRO, 2006).

In addition to its ecological importance, the Cerrado is also an essential region from an agricultural point of view having half of the agricultural lands from Brazil (SPERA, 2017). Approximately half of the biome has been converted into pasture and croplands, which transformed the region into a leading producer of major export crops such as soybean, maize, and cotton (SANO et al., 2010; BEUCHLE et al., 2015; NOOJIPADY et al., 2017). As was also observed in tropical forests of the Amazon, soybean production has been an important driver of vegetation clearing in the Cerrado (GIBBS et al., 2015). In tropical forests, the Amazon Soy Moratorium was proposed to reduce the influence of this driver on deforestation rates. Using this agreement, the major exporting companies of this commodity are committed to not buying and financing soybean production from deforested areas in the Amazon after July 2006 (LIMA et al., 2019). While this moratorium has effectively reduced tropical forest conversion for soybeans in the Amazon,

---

<sup>1</sup> This chapter is an adapted version of the paper: SOUZA, A. A.; GALVÃO, L. S.; KORTING, T. S.; SOUZA, A. A. DE. Dynamics of savanna clearing and land degradation in the newest agricultural frontier in Brazil. **GIScience & Remote Sensing**, p. 1–20, 2020.

one of the spillover effects on the Cerrado was just the opening of new agricultural frontiers for soybean production (DOU et al., 2018; NEPSTAD et al., 2019). Because a similar type of agreement does not cover the Cerrado, the global demands for agricultural commodities have produced savanna-clearing rates that recently exceeded the rates of tropical forest conversion in the Amazon (ZALLES et al., 2019; INPE, 2019; RATTER; BRIDGEWATER, and RIBEIRO, 2006).

The MATOPIBA, an acronym for the names of the four Brazilian states that compose this region (Maranhão, Tocantins, Piauí, and Bahia), is the newest and probably the last agricultural frontier in the Cerrado (GRAESSER et al., 2015; RAUSCH et al., 2019). The native savannas have started to face intensive clearing for single cropping (e.g., soybean, maize, and cotton plantations) or double cropping (e.g., soy-corn or soy-cotton rotations) activities (SPERA et al., 2016). Compared to other areas of the biome, the dynamic of vegetation clearing over the MATOPIBA is poorly known. This knowledge is important to simulate trajectories of soybean expansion in the MATOPIBA region. It contributes to defining environmental policies addressing the tradeoffs between the increasing food production, the preservation strategies of biodiversity, and the ecosystem services (ARAÚJO et al., 2019; NEPSTAD et al., 2019).

For savanna clearing and crop management, fire is an important player in MATOPIBA. Fire can alter the structure and composition of the native vegetation and affect the carbon and water fluxes in the ecosystem (MIRANDA et al., 2009; PIVELLO et al., 2010; BUSTAMANTE et al., 2012; GARCIA; BALLESTER, 2016; TRABAQUINI et al., 2017). The resultant land degradation can become an important environmental problem. It produces a long-term decline in productivity due to human-induced disturbances (EASDALE et al., 2019). Although important for the conservation and sustainable use of the Cerrado biome, the relationship between savanna clearing, land degradation, and fire has not been studied yet over the MATOPIBA region.

In this context, remote sensing is an alternative to monitor the dynamics of vegetation clearing and land degradation on a broad scale over the Cerrado. Satellite data allows the detection of clearing and the identification of degraded

lands. The modifications in soil surface properties and land cover changes affect land productivity (XIE et al., 2019). We can use burned-area products obtained from satellite data for the analysis of vegetation clearing dynamics and land degradation. Furthermore, topographic attributes calculated from the Shuttle Radar Topography Mission (SRTM) Digital Elevation Model (DEM) can be compared with patterns of land occupation. The geospatial analysis of such big data may benefit from the use of the Google Earth Engine (GEE) cloud-computing platform (GORELICK et al., 2017). Recent examples of the use of the GEE platform over crops and savannas have been published by Alencar et al. (2020), Fuentes, Millard, and Laurin (2020), Gumma et al. (2020); Liu et al. (2020). A comprehensive review of the status of this platform for different applications has been presented by Tamiminia et al. (2020).

For the analysis of savanna clearings, algorithms that capture abrupt human-induced disturbance events can quantitatively inspect time series of historical Landsat data (KENNEDY et al., 2018). This is the case of the LandTrendr (Landsat-based detection of Trends in Disturbance and Recovery) algorithm on the GEE platform. LandTrendr is a temporal segmentation and fitting algorithm that models change trajectories as a series of sequential line segments (KENNEDY; YANG; COHEN, 2010). To reduce the influence of vegetation phenology on clearing detection, yearly satellite data acquired during the dry season over the savannas should be considered as input data for the LandTrendr. Looking for abrupt changes over time in the magnitude of the Landsat-derived Normalized Difference Vegetation Index (NDVI), the LandTrendr may detect clearing events that occur over the savannas as well as the year of their occurrence.

For the analysis of land degradation, different approaches have been proposed using temporal trends in NDVI (EASDALE et al., 2019). These approaches have been recommended by the United Nations Convention to Combat Desertification (UNCCD) to relate changes in productivity with land degradation (SIMS et al., 2017). They are mostly based on the inspection of long-term changes in NDVI as a proxy for land degradation (JACQUIN; SHEEREN; LACOMBE, 2010; PEREIRA et al., 2018; GONZALEZ-ROGLICH et al., 2019). An example is the Trends.Earth

algorithm, specially designed to monitor land degradation with Earth observations (CONSERVATION INTERNATIONAL, 2019). Using this algorithm on the GEE platform, we can assess the land productivity from metrics of change (e.g., productivity trajectory and state) derived from the Moderate Resolution Imaging Spectroradiometer (MODIS) NDVI time series. When compared to Landsat instruments, MODIS acquires daily data that are used to produce regularly spaced time series at 16-day composite intervals. This temporal specification is adequate for seasonal and inter-annual analyses of this vegetation index for land degradation studies. In the Trends.Earth algorithm, the trajectory metric (rate of change in land productivity over a long time) is calculated using linear regressions at the pixel level that are run on annual integrals of NDVI. By using the non-parametric Mann-Kendall test, the algorithm detects statistically significant positive or negative trends, which are potential indicators of long-term vegetation recovery or land degradation, respectively (GONZALEZ-ROGLICH et al., 2019). To detect recent changes in land productivity, the Trends.Earth uses the state metric. To calculate this metric, the mean NDVI values at the pixel level for a baseline (e.g., 12-year period) and a recent period (e.g., three years) are compared to the frequency distribution of historical values in that pixel (CONSERVATION INTERNATIONAL, 2019). Recent improvements or declines in land productivity are detected from the sign of change between both periods.

In this study, we evaluated the dynamics of savanna clearings and land degradation in the MATOPIBA region using these two algorithms implemented on the GEE platform (LandTrendr and Trends.Earth) and different satellite products. Savanna clearings between 1985 and 2018 were detected from the Landsat NDVI data and LandTrendr algorithm. For studying land degradation, we used MODIS NDVI time series as input data for the Trends.Earth algorithm. The time interval selected for land degradation analysis (2001-2015) followed the recommendations by the Good Practice Guidance (SIMS et al., 2017), a document adopted by the UNCCD. Finally, we discussed the relationships among savanna clearings, land degradation, topographic attributes, and fire frequency.

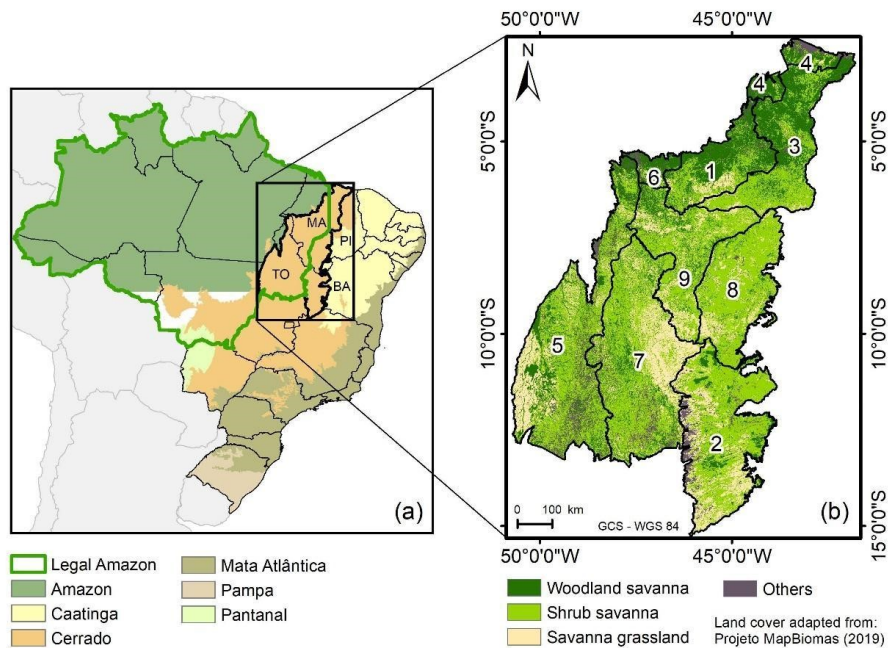
## 4.2 Methodology

### 4.2.1 Study area

Located in the northeast of Brazil, the MATOPIBA region includes parts of the states of Maranhão, Tocantins, Piauí, and Bahia (337 municipalities). From the total area of MATOPIBA, 95% occur over the savannas, including nine of the 10 mesoregions (Figure 4.1). The last mesoregion (*Vale São Franciscano da Bahia*) occurs predominantly over the Caatinga biome. Mesoregions are subdivisions of Brazilian states, encompassing municipalities with high levels of economic and social similarity (ARAÚJO et al., 2019).

The MATOPIBA is the newest and probably the last agricultural frontier over the savannas in Brazil since the early 2000s. In 2015, a Brazilian Decree officially created the MATOPIBA region and established government support to develop the region (SPERA et al., 2016). By an ordinance of the Brazilian *Ministério do Meio Ambiente* (MMA), the MATOPIBA has been a priority region for actions of illegal-clearing control and land-degradation recovery aiming at sustainable development.

Figure 4.1 - Study area.



(a) Location of MATOPIBA in the northeast of the *Cerrado* biome in Brazil, including parts of the states of Maranhão (MA), Tocantins (TO), Piauí (PI) and Bahia (BA). The limits with other biomes are indicated. The nine mesoregions of MATOPIBA are: 1 – *Centro Maranhense*; 2 – *Extremo Oeste Baiano*; 3 – *Leste Maranhense*; 4 – *Norte Maranhense*; 5 – *Ocidental do Tocantins*; 6 – *Oeste Maranhense*; 7 – *Oriental do Tocantins*; 8 – *Sudoeste Piauiense*; and 9 – *Sul Maranhense*. (b) Representation of the native vegetation cover in 1985, which was mostly composed of savanna grassland (*Formações Campestres*), shrub savanna (*Formações Savânicas*) and woodland savanna (*Formações Florestais*). “Others” indicated non-savanna classes.

Source: Author’s production.

The MATOPIBA has well-defined rainy (October to May) and dry (June to September) seasons, presenting average annual precipitation of 1100 mm (SANO et al., 2019a). The two crops planted predominantly over well-developed deep and permeable Oxisols are soybean and maize. The low fertility of soils is generally compensated by soil and crop management practices. From a geomorphological point-of-view, the Cerrado is roughly divided into plateaus (known as *chapadas*) and depressions (SANO et al., 2019a). In MATOPIBA, mechanized agriculture occurs over the plateaus because of the more favorable

slope conditions for the displacement of tractors. As shown in Figure 4.1b, the native vegetation cover in 1985 was mostly composed of savanna grasslands (*Formações Campestres*), shrub savannas (*Formações Savânicas*) and woodland savannas (*Formações Florestais*) (SOUZA et al., 2020b).

#### **4.2.2 Analysis of the savanna clearings over time**

To obtain yearly maps of savanna clearings between 1985 and 2018 over the MATOPIBA region, we used the LandTrendr algorithm on the GEE platform and a dry-season composite approach. We selected all the available satellite images acquired during the dry season (July-August-September) of each year by the Thematic Mapper (TM)/Landsat-5, Enhanced Thematic Mapper Plus (ETM+)/Landsat-7, and Operational Land Imager (OLI)/Landsat-8. By constraining the image selection to the dry season, we reduced the vegetation phenology and view-illumination effects on clearing detection (SILVEIRA et al., 2019). Moreover, the dry season is also a more favorable period to obtain cloud-free images than the rainy season. The C-Function of Mask (CFMask) algorithm was used to exclude clouds and cloud shadows from the analysis (FOGA et al., 2017). For a given year, the masks were applied to each image of the dry season period before creating the composite image with high-quality atmospheric pixels. This composite approach tends to result in one cloud-free image per year. However, if a given cloud-free pixel does not exist for the composite image of a given year, this pixel is masked for the LandTrendr. If a savanna-clearing change occurs over this masked pixel, the detection of this event is generally delayed until the next cloud-free observation in the subsequent years.

Using atmospherically corrected surface reflectance images (30-m spatial resolution) geometrically rectified and screened for clouds and shadows, we generated 34 composite images. Therefore, one composite dry season image was obtained per year between 1985 and 2018. For this purpose, the medoid approach was used (FLOOD, 2013). For a given pixel and band of the Landsat images, we retrieved the reflectance that was numerically closer to the median of all corresponding pixels coming from the dry season images selected in a given year. Before this procedure, the reflectance of the OLI bands was radiometrically

adjusted to that of the ETM+ bands, using slopes and intercepts from the reduced major axis regressions reported by Roy et al. (2016). After applying the medoid approach, we obtained the NDVI images, which were used as input data for the LandTrendr algorithm.

The parameters used to run LandTrendr are listed in Table 1 and are described in detail by Kennedy, Yang, and Cohen (2010). In our work, we assume that the savanna clearings produce abrupt changes in the NDVI time series at short intervals of time. To avoid the detection of events associated with fire, we did not consider transitory modifications in NDVI that rapidly recovered the pre-disturbance values in the subsequent year of detection. The LandTrendr shows the site location of the vegetation changes and the year of the occurrence of the events. Only the greatest change over time was marked as associated with savanna clearings, which generally corresponded to the native vegetation removal (KENNEDY; YANG; COHEN, 2010; KENNEDY et al., 2018).

Table 4.1 - LandTrendr parameters selected to evaluate the dynamics of savanna clearings in the MATOPIBA region, using composite NDVI time series (1985-2018) obtained from the TM, ETM+ and OLI Landsat instruments.

<b>Parameter</b>	<b>Value</b>	<b>Description</b>
maxSegments	6.0	Maximum number of segments to be fitted on the time series
spikeThreshold	0.5	Threshold for dampening the spikes (1.0 means no dampening)
vertexCountOvershoot	3.0	The initial model can overshoot the maxSegments + 1 vertices by this amount. Later, it will be pruned down to maxSegments + 1
preventOneYearRecovery	true	Prevent segments that represent one-year recoveries
recoveryThreshold	0.25	If a segment has a recovery rate faster than $1/\text{recoveryThreshold}$ (in years), then the segment is disallowed
pvalThreshold	0.05	If the p-value of the fitted model exceeds this threshold, then the current model is discarded and another one is fitted using the Levenberg-Marquardt optimizer
bestModelProportion	0.75	Takes the model with most vertices that has a p-value that is at most this proportion away from the model with lowest p-value
minObservationsNeeded	6.0	Minimum observations needed to perform output fitting
Magnitude	200	NDVI value from starting year minus NDVI value from ending year for segment of change (x1000)

Source: Oregon State University (2021).

#### 4.2.2.1 Accuracy assessment and area estimates

The sample size definition and the location of samples for accuracy assessment and area estimates of the clearing-detection results were supported by the AREA2 algorithm on the GEE platform. It allows users to design a sample

according to the recommended practices and international guidance. To define the strata, we used stratified random sampling (OLOFSSON et al., 2014) based on a simplified class version (cleared and non-cleared savanna classes) of the land-use and land-cover (LULC) map of the Projeto MapBiomás (2019). Considering only two classes (cleared and non-cleared savannas), we selected 462 pixels over distinct sites in the region. This number of pixels was determined using the formula proposed by Cochran (1977). The formula uses the standard error of the estimated overall accuracy (0.01) and the anticipated user's accuracies of the two classes (0.70). From the 462 selected samples, we verified 142 disturbed sites and 320 non-disturbed sites. The reference dataset was a combination of high-resolution imagery and time-series graphical inspections.

The error matrix was created by cross-tabulation of the two-class labels allocated by the LandTrendr classification (cleared versus non-cleared savanna classes) against the reference data for the sample sites. We also checked the correct year of the cleared-savanna event detected by the LandTrendr algorithm. The error matrix was summarized in terms of proportion of area and estimates of overall accuracy, user's accuracy (and its related measure of commission error), and producer's accuracy (and its related measure of omission error). This matrix provided the basis to produce error-adjusted area estimates of cleared and non-cleared classes, avoiding bias associated with the mapped area obtained from pixel counting.

#### **4.2.3 Land degradation analysis**

For a detailed evaluation of land degradation, we inspected long-term trends (2001-2015) of the MODIS NDVI. This vegetation index has been largely used as a proxy for land degradation (EASDALE et al., 2019). This period of analysis was defined based on the general principles for how countries can access land cover data to monitor degraded lands, as proposed by the UNCCD group for Sustainable Development Goals (SIMS et al., 2017). NDVI data from the Collection 6 16-day MOD13Q1 vegetation index product, generated at 250-m spatial resolution, served as input data for the Productivity module of the Trends.Earth. This is a free and open-source tool for the assessment of land

conditions using Earth observation data and cloud processing on the GEE platform (CONSERVATION INTERNATIONAL, 2019). The annual integrals of NDVI were used to perform the trajectory analysis. They were corrected for the effects of climate using the Rain Use Efficiency (RUE) method (WESSELS; VAN DEN BERGH; SCHOLE, 2012).

To evaluate land degradation, two Trends.Earth land productivity metrics were calculated from the MODIS NDVI time series: trajectory and state. While the trajectory metric captures changes in productivity over a long time (2001-2015 in our case), the state detects recent modifications in productivity (past 3–5 years). Therefore, to measure state, we followed the recommendation by the UNCCD and defined 2001-2012 as the historical baseline period. We assumed 2013-2015 as the recent period of comparison, from which the mean NDVI values were computed (GONZALEZ-ROGLICH et al., 2019).

The final step of the land degradation analysis was to combine the two metrics (trajectory and state) to generate three dynamic classes of land productivity: (a) improvement areas with statistically significant positive trends in NDVI trajectories; (b) stable areas without significant trends in NDVI trajectories; and (c) degradation areas with statistically significant negative trends in NDVI trajectories. During the combined analysis of these metrics, if there was a decline in one of the two metrics at a particular pixel, we assigned that pixel to the degradation class.

#### **4.2.4 Influence of topographic attributes and fire on clearing and degradation**

The dynamics of savanna clearings and land degradation were also evaluated considering variations in topographic attributes and fire frequency. The slope and elevation metrics were calculated from the SRTM DEM at 30 m spatial resolution. We obtained fire frequency from the Collection 6 monthly MODIS MCD64A1 Burned Area product, generated at 500 m spatial resolution. We aggregated the monthly data into annual binary observations of burned and unburned areas for the 2001-2018 period. Using map algebra, the intersection between burned areas across years was determined on a per-pixel basis. By adopting this procedure, fire frequency in the data analysis of a given pixel could vary from zero for

unburned areas up to 18 times (pixel-area burned every year between 2001 and 2018).

In the last step of the data analysis, we inspected for possible associations between cleared areas, topographic attributes (slope and elevation), and burned areas. The relationships between cleared and burned areas were established. In addition, we compared the fire frequency with the percentage of degraded areas over agricultural lands and native vegetation. For this purpose, we resampled the 250-m land degradation map, derived from Trends.Earth analysis, into the 500-m fire frequency map, generated from the MODIS MCD64A1 product. By overlaying both maps, we calculated the proportion of degraded areas observed over agricultural areas and native vegetation, as a function of fire frequency.

### **4.3 Results**

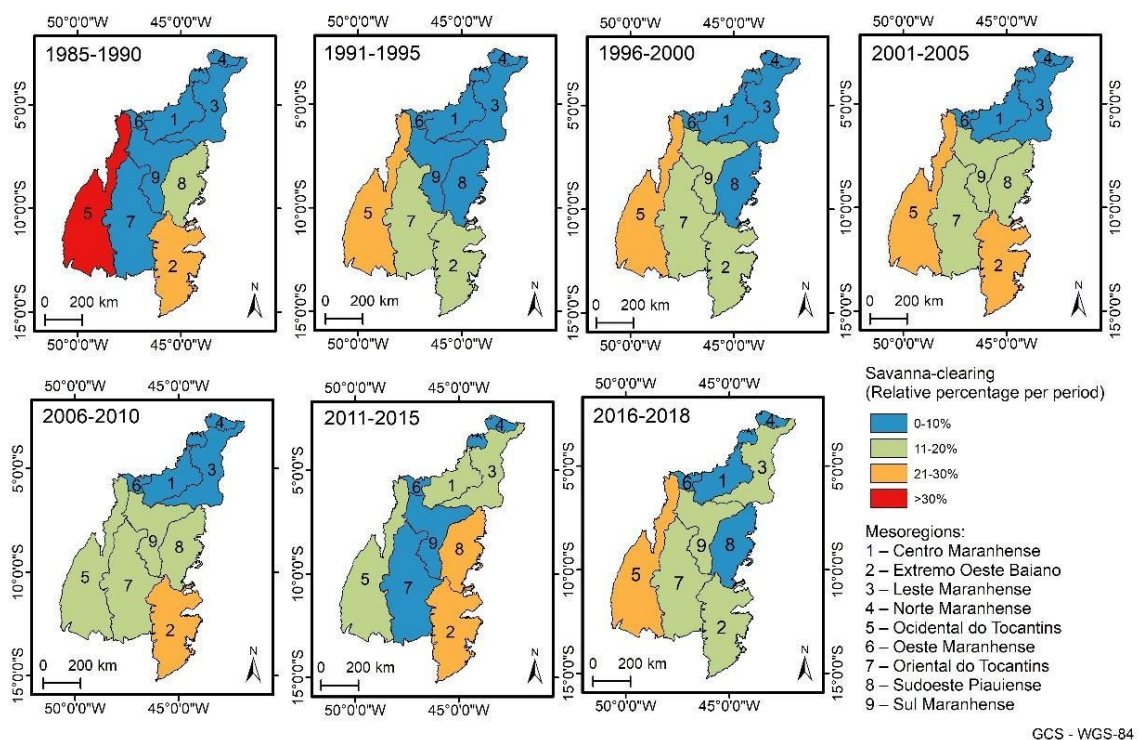
#### **4.3.1 Dynamics of savanna clearings from Landsat NDVI data**

Figure 4.2 shows the dynamics of savanna clearings captured by the LandTrendr algorithm in the 1985-2018 period. The automated detection of clearing during the dry season of each year (July to September) corresponded to the largest change observed in Landsat NDVI trajectories. When compared to savanna grassland areas, this change was generally stronger over woodland savanna and shrub savanna areas (Figure 4.3). Less intense NDVI variations at short time intervals in Figure 4.3 were usually associated with image pre-processing issues (e.g., atmospheric correction and cloud masking) or with land cover changes following clearing. Based on Figure 4.3, we anticipate that the accuracy of detection by LandTrendr will probably increase with vegetation cover from savanna grasslands to woodland savannas. Woodland savannas presented stronger NDVI changes due to clearing than savanna grasslands (Figure 4.3).

In MATOPIBA, large relative proportions of savanna clearing over the mesoregions *Ocidental do Tocantins* (33.4%) and *Extremo Oeste Baiano* (28.1%) marked the first period of detection by the LandTrendr algorithm (1985-1990) (Figure 4.2). From 1991 to 2005, the clearing activities progressed toward the *Oriental do Tocantins*, *Sudoeste Piauiense*, and *Sul Maranhense*, as indicated by the predominance of green color (Figure 4.2). In this period, these

mesoregions showed relative proportions of 12.8%, 11.9%, and 17.0%, respectively. The signature of the Amazon Soy Moratorium in 2006 produced spillover effects on the *Cerrado* areas of MATOPIBA. The moratorium contributed to consolidate the agriculture expansion into *Extremo Oeste Baiano* and *Sudoeste Piauiense* and toward the north (mesoregions *Centro* and *Leste Maranhense*). In the 2011-2015 period, following the soybean expansion in MATOPIBA, these four mesoregions (1, 2, 3, and 8 in Figure 4.2) were responsible for 68.1% of the total cleared areas detected by the LandTrendr. In the most recent period of analysis (2016-2018), *Ocidental do Tocantins* presented the largest proportion of cleared areas (26.3%), as represented by orange color in Figure 4.2.

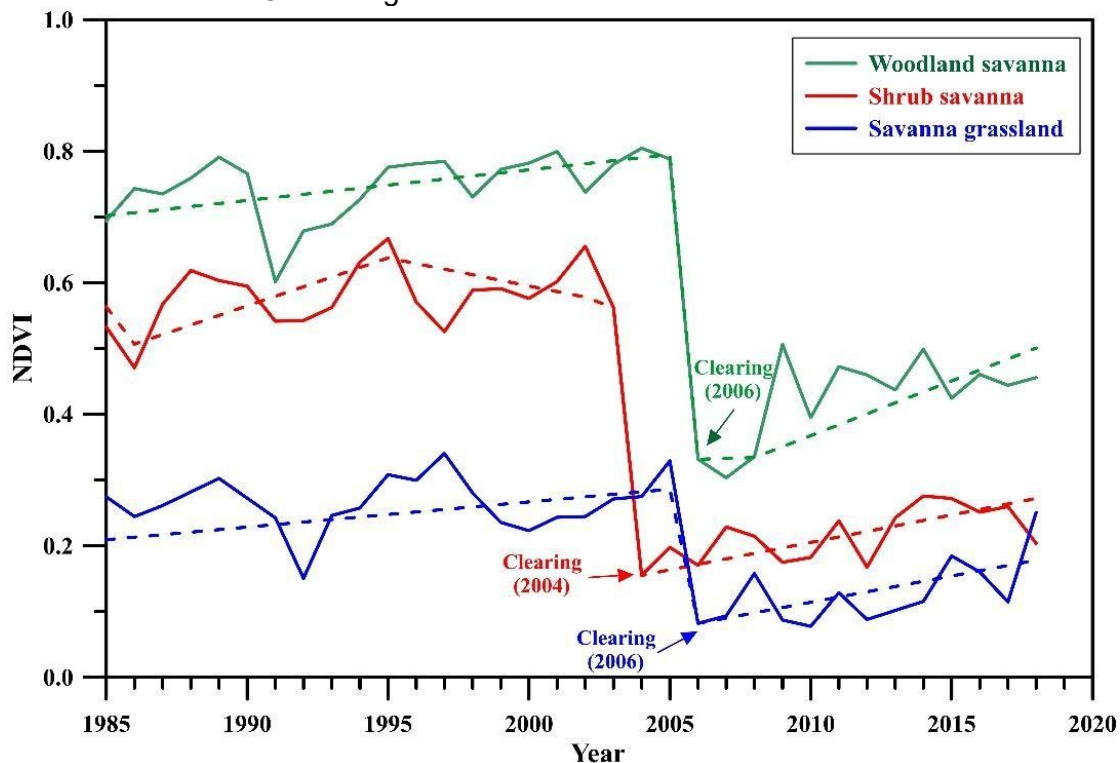
Figure 4.2 - Dynamics of savanna clearings over the nine mesoregions of MATOPIBA at different periods of analysis.



Relative percentages per period are shown. The LandTrendr algorithm was used with Landsat NDVI data for clearing detection.

Source: Author's production.

Figure 4.3 - Examples of clearing detection over three types of savannas from the MATOPIBA region.



The LandTrendr algorithm detected the largest modification in fitted segments (dashed lines) of the long-term composite Landsat NDVI time series as savanna clearing.

Source: Author's production.

Validation of the results of Figure 4.2 produced an overall classification accuracy of 74.3% (Table 4.2). Considering one year of a confidence interval, the year of change was correctly detected by the LandTrendr algorithm in 96% of the cases. In Table 4.2, the savanna-cleared class presented a user's accuracy of 69.4%. Along with the producer's accuracy, the validation indicated a very conservative clearing detection by LandTrendr. The error matrix provided the basis for estimating cleared and non-cleared areas. In the 1985-2018 period of analysis, the total cleared-area of savannas detected by LandTrendr in MATOPIBA was 19,917,400 ha, which represents 31.6% of the total area (Table 4.2).

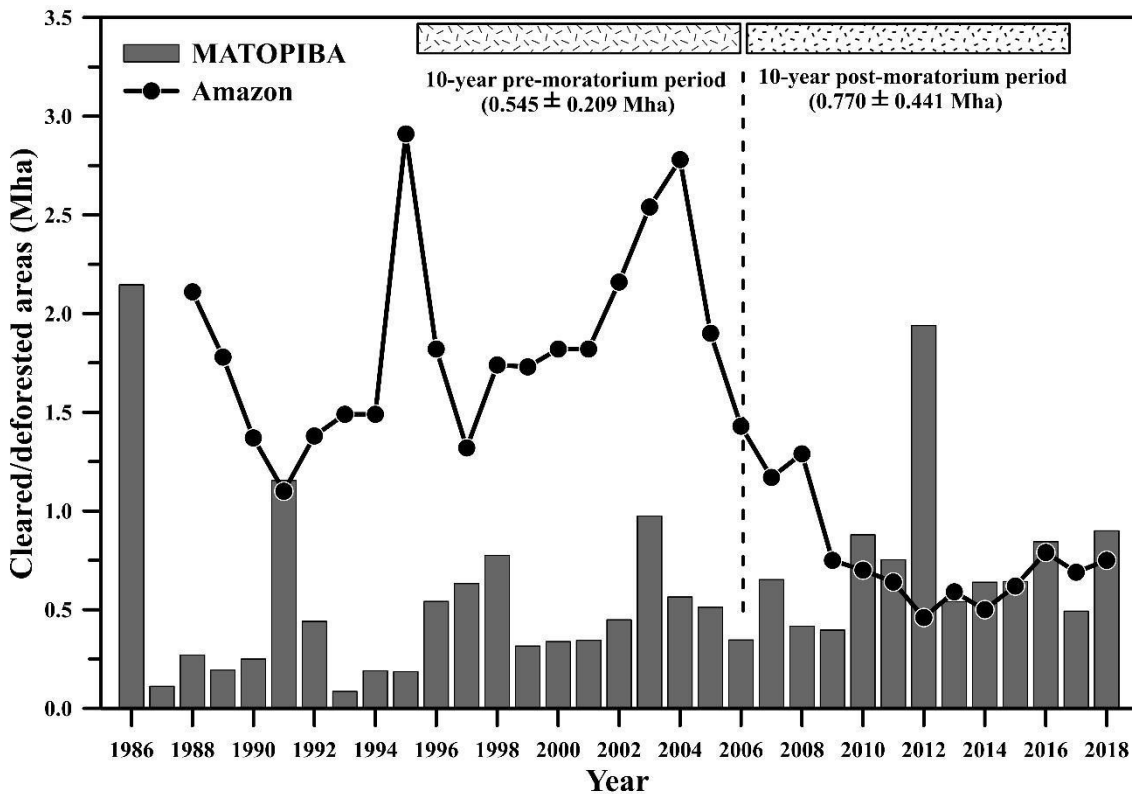
Table 4.2 - Full area-weighted error matrix for cleared and non-cleared savanna areas in the MATOPIBA region.  $W_i$  is the proportion of the area of a given class concerning the total area.

Savanna Class	Cleared	Non-cleared	$W_i$	Pixels	Total Area Mapped (ha)	Area Adjusted (ha)	User's Accuracy (%)	Producer's Accuracy (%)	Overall Accuracy (%)
Cleared	0.107	0.047	0.154	62	9,646,300	19,917,400	69.4	33.8	74.3
Non-cleared	0.209	0.636	0.846	400	53,315,200	43,044,100	75.3	93.1	
					62,961,500	62,961,500			

Source: Author's production.

Savanna-clearing areas varied across years from 0.086 Mha to 2.146 Mha per year, having well-defined peaks in 1986, 1991, and 2012 (Figure 4.4). Results of Figure 4.4 showed average cleared areas of  $0.503 \pm 0.655$  Mha over the first decade of evaluation (1986-1995). When we considered the possible spillover effects of the Amazon Soy Moratorium into the savanna clearings of MATOPIBA, this average value increased to  $0.545 \pm 0.209$  Mha in the 10-year pre-moratorium period before the signature in 2006. It then accelerated to  $0.770 \pm 0.441$  Mha in the 10 years following this agreement. Thus, the average savanna cleared-areas increased 41% when compared to the values observed in the decade preceding the moratorium. In Figure 4.4, the peak of savanna clearing in 2012 was just coincident with the lowest areas of Amazonian deforestation reported by INPE (2019) over the entire time series. In the post-moratorium decade, savanna-cleared and tropical-deforested areas presented a non-linear (logarithmic) relationship with a coefficient of determination ( $R^2$ ) of 0.50 (results not shown).

Figure 4.4 - Temporal variations in savanna-cleared areas over the MATOPIBA region.



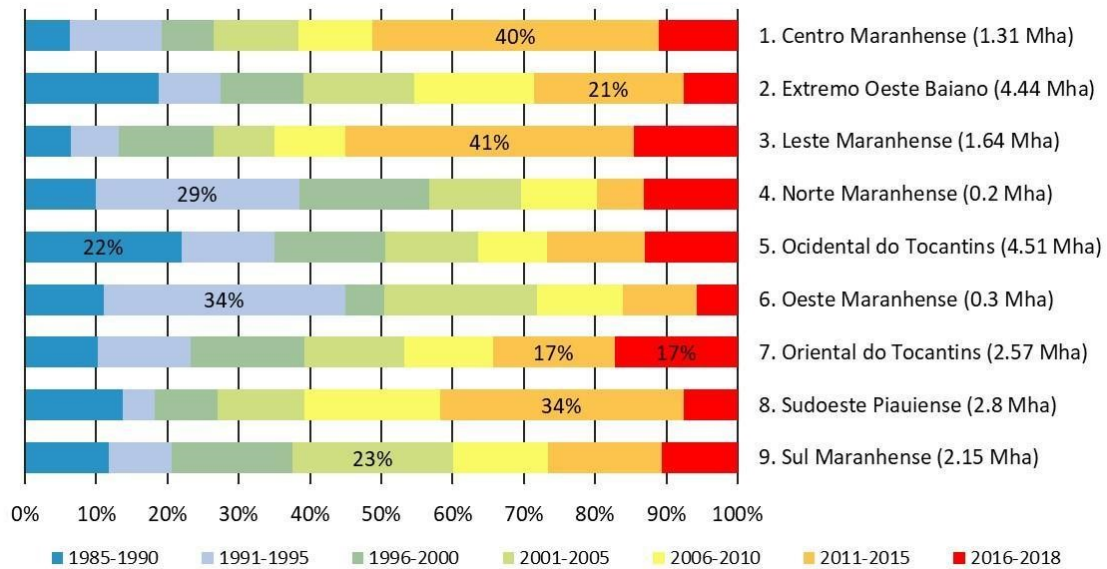
Average and standard deviation values of clearing are indicated for ten-year periods pre- and post-Amazon Soy Moratorium. Results between 1986 and 1995 were  $0.503 \pm 0.655$  Mha. We also plotted the Amazonian deforested areas reported by INPE (2019) for comparison.

Source: Author's production.

The accumulated cleared areas per mesoregion are shown in Figure 4.5 along with the percentages of cleared areas per period of analysis. Therefore, for each color bar, the calculations considered the total cleared area of the mesoregion indicated in this figure. By inspecting Figure 4.5, we can rapidly identify the period of native vegetation conversion for land use in MATOPIBA. The most recent agricultural expansion in the post-moratorium period (2006-2018) was observed over the *Centro Maranhense*, *Extremo Oeste Baiano*, *Leste Maranhense*, and *Sudoeste Piauiense*. These mesoregions had the highest cumulative percentages of savanna-cleared areas between 2006 and 2018 (Figure 4.5). Confirming the trends observed in Figure 4.5, the *Sudoeste Piauiense* showed a

well-defined peak of vegetation clearing in 2012 (Figure 4.6), which was inversely related to the reduction in Amazonian tropical deforestation resulting from the Soy Moratorium. Detailed inspection of sites at the *Sudoeste Piauiense* confirmed the increasing number of clearing events for soybean planting after 2006, as indicated by the predominance of yellow, orange, and red colors in Figure 4.7.

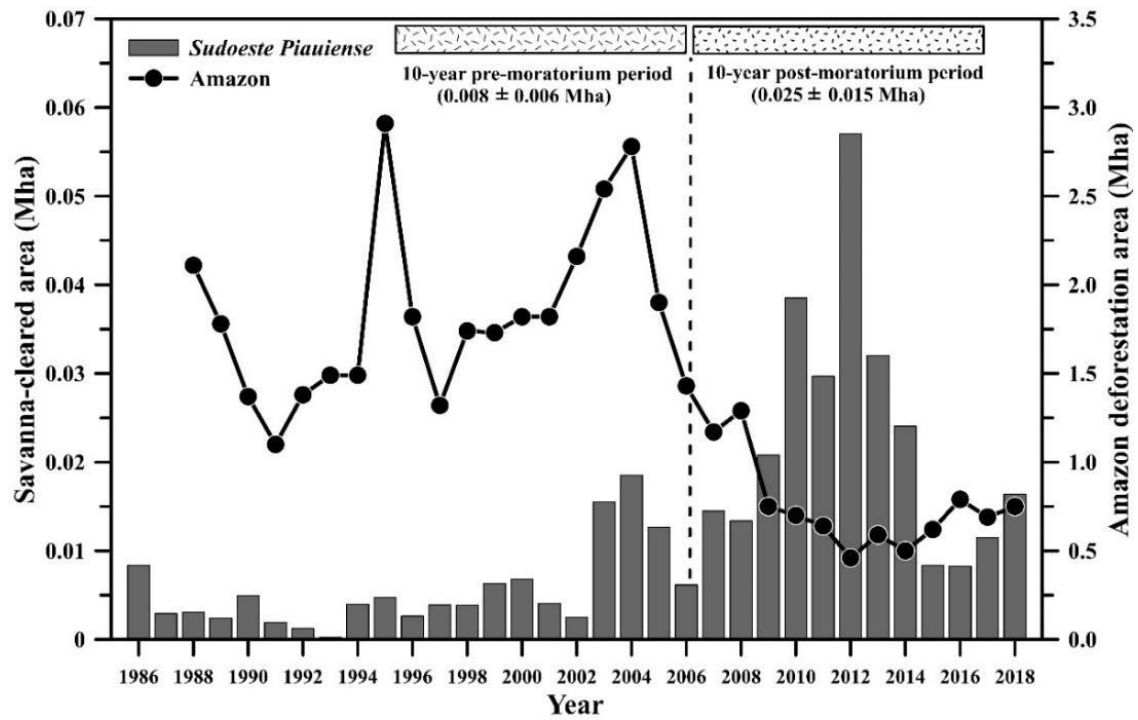
Figure 4.5 - Dynamics of savanna clearings detected by the LandTrendr algorithm per mesoregion of MATOPIBA.



Numbers indicate the periods presenting the highest cumulative percentages of clearing on each mesoregion. The total cleared area per mesoregion (in Mha) is shown between parentheses.

Source: Author's production.

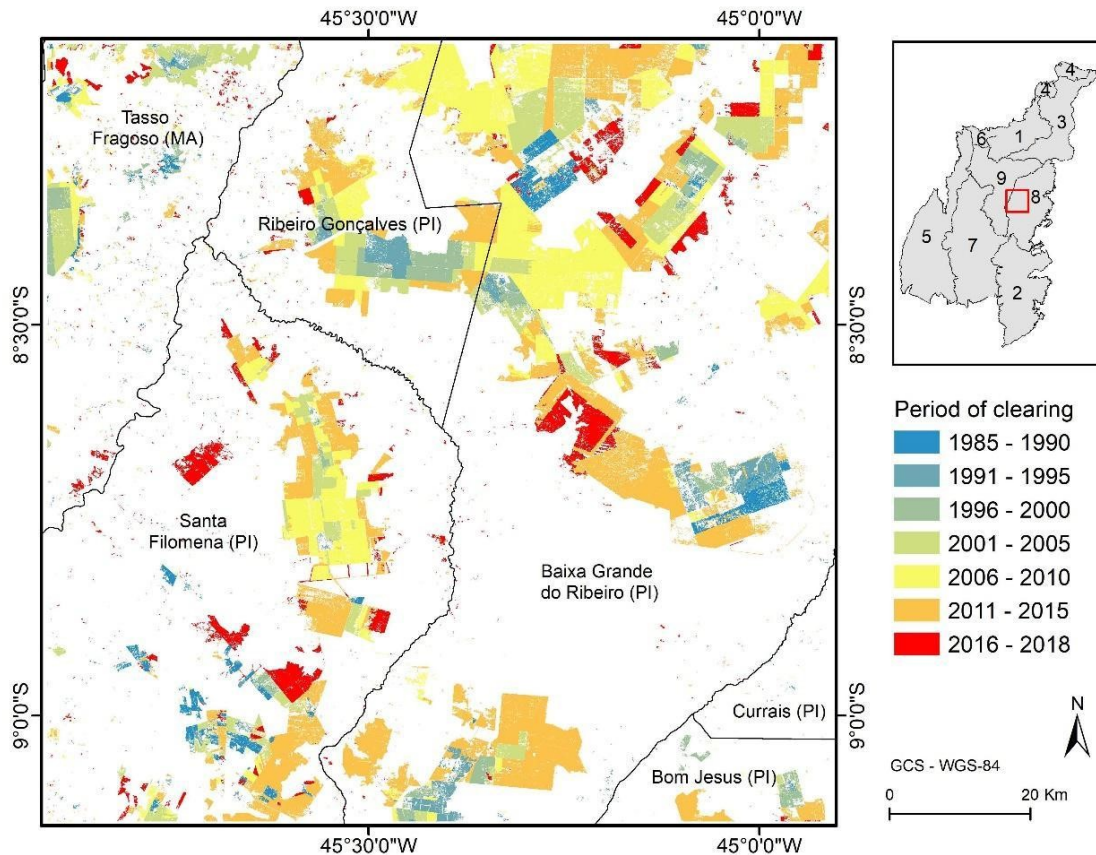
Figure 4.6 - Changes over time in the savanna-cleared area over the Sudoeste Piauiense.



We also plotted the Amazonian deforested areas reported by INPE (2019) for comparison.

Source: Author's production.

Figure 4.7 - Period of savanna clearings detected by the LandTrendr algorithm over a site located at the *Sudoeste Piauiense* (square in red).



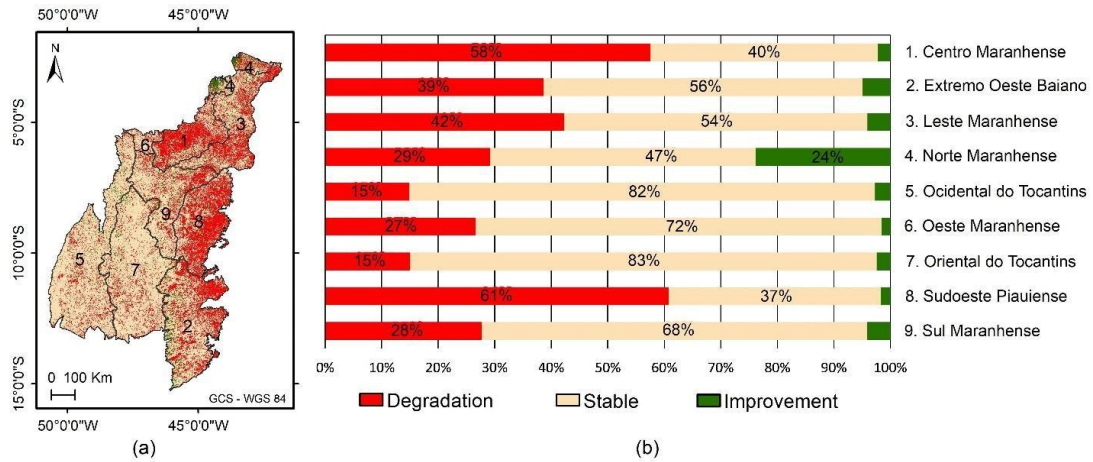
Some municipalities are indicated for reference.

Source: Author's production.

#### 4.3.2 Analysis of land degradation from MODIS NDVI data

When we inspected long-term trends (2001-2015) of MODIS NDVI (Collection 6 16-day MOD13Q1 product) using the Trends.Earth algorithm, we observed distinct patterns of land degradation in the MATOPIBA region (Figure 4.8). To determine the proportions of the three Trends.Earth classes (degradation, stable and improvement), we considered the total area of the mesoregion (cleared and native vegetation areas). Areas of improvement in land productivity were comparatively smaller than the areas of land degradation (Figure 4.8a). The mesoregions that showed the largest proportions of land degradation were the *Sudoeste Piauiense* (61%) and the *Centro Maranhense* (58%) (Figure 4.8b).

Figure 4.8 - Land degradation in MATOPIBA region.

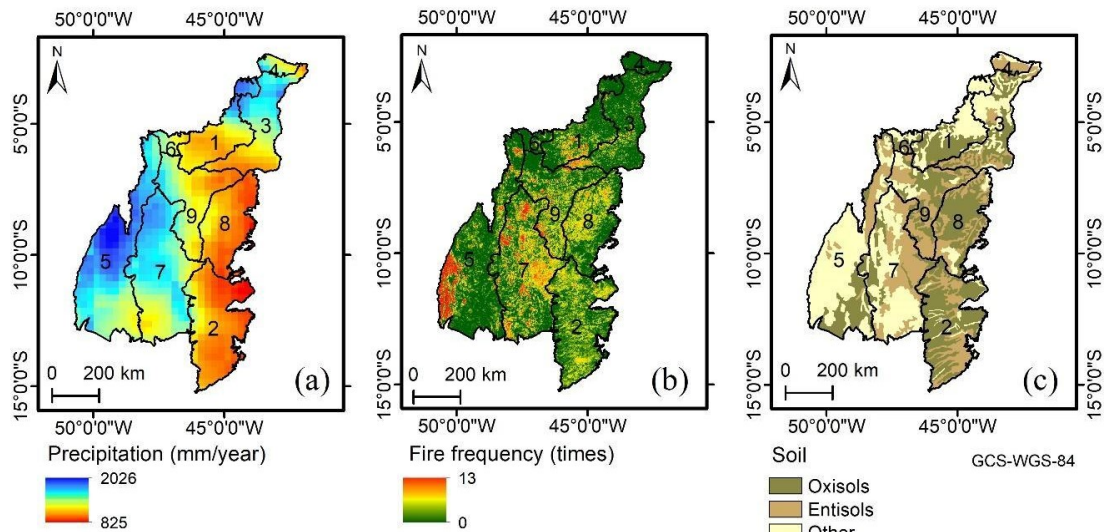


(a) Dynamics of land degradation over the nine mesoregions of MATOPIBA, obtained from trajectory and state Trends.Earth metrics and MODIS NDVI time series (2001-2015). (b) The proportion of land-degraded areas on each mesoregion, indicated by numbers in the red bars.

Source: Author's production.

This spatial pattern of land degradation shown in Figure 4.8a was coincident with areas having the lowest average annual precipitation in the transition zone between the *Cerrado* (savannas) and the semi-arid region of the *Caatinga* biome (Figure 4.9a). Fire events were also observed in this zone with a variable frequency of occurrence, reaching values up to 13 times (Figure 4.9b). At these mesoregions (*Sudoeste Piauiense* and *Centro Maranhense*), greater proportions of low-fertility sandy soils (*Latossolo Amarelo* (Oxisols) and *Neossolo Quartzarênico* (Entisols)) are also usually observed (Figure 4.9c). The combination of these factors (climate, soil composition, and fire frequency) with inadequate crop/soil management practices can cause land degradation. This association can explain the long-term negative trends in NDVI captured by the Trends.Earth in portions of the MATOPIBA region.

Figure 4.9 - (a) Average annual precipitation (2001-2015) over the MATOPIBA region calculated from the Tropical Rainfall Measuring Mission (TRMM) data. (b) Fire frequency determined from MODIS data in the 2001-2015 period. (c) Spatial distribution of the major soil types.



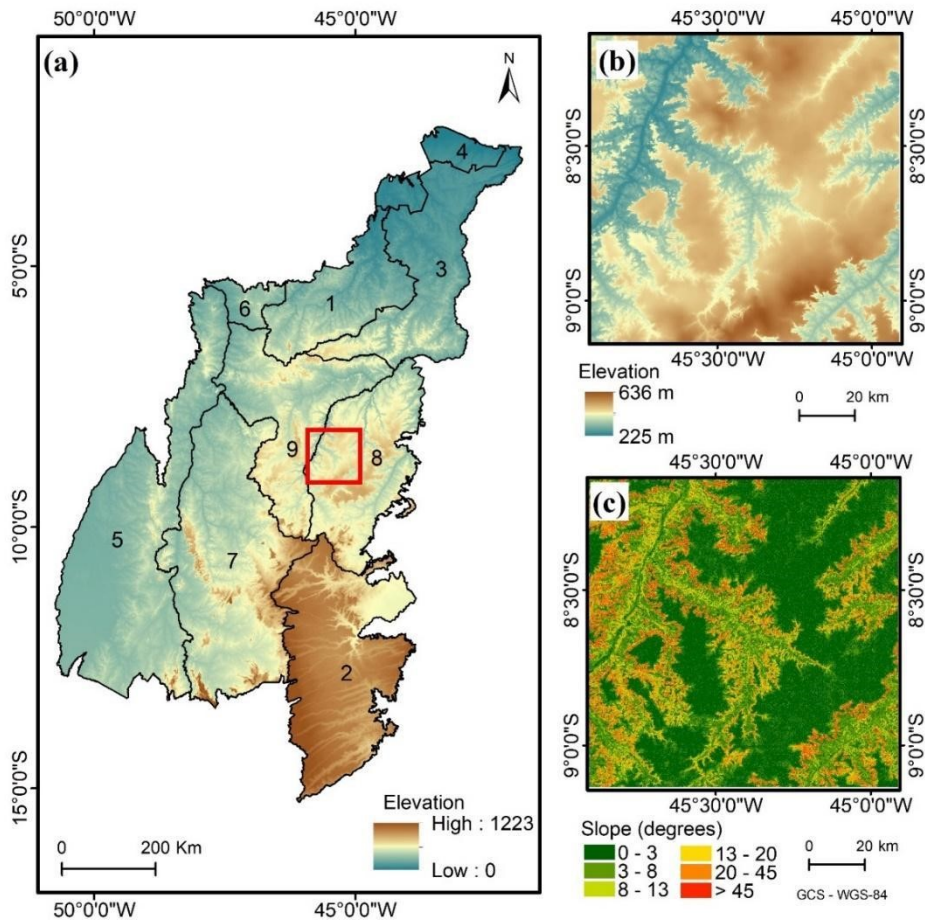
The mesoregions are defined in Figure 4.1.

Source: Adapted from Santos et al. (2011).

### 4.3.3. Relationships of clearing and degradation with topography and fire

The highest elevations (up to 1223 m) of MATOPIBA were observed at the *Extremo Oeste Baiano* (mesoregion 2), while the lowest elevations occurred at the *Leste* and *Norte Maranhense* (mesoregions 3 and 4 in Figure 10a). Most of the MATOPIBA (94%) have slope values lower than 10°. Areas of high elevation (brown color in Figure 4.10b) and low slope (green color in Figure 4.10c) form the plateaus (*chapadas*), which are adequate places for mechanized agriculture. Our results using LandTrendr showed that 83.4% of the savanna-cleared areas occurred at slopes lower than 3°, while 13.4% and 2.1% of them were observed at slope intervals of 4°-8° and 9°-13°, respectively.

Figure 4.10 - Digital Elevation Model of the MATOPIBA region.



(a) SRTM-derived Digital Elevation Model (DEM) of the MATOPIBA region, showing variations in elevation per mesoregion. Detailed changes in elevation and slope for a site located at the *Sudoeste Piauiense* are shown in (b) and (c), respectively. The location of the site (red square) is indicated in (a).

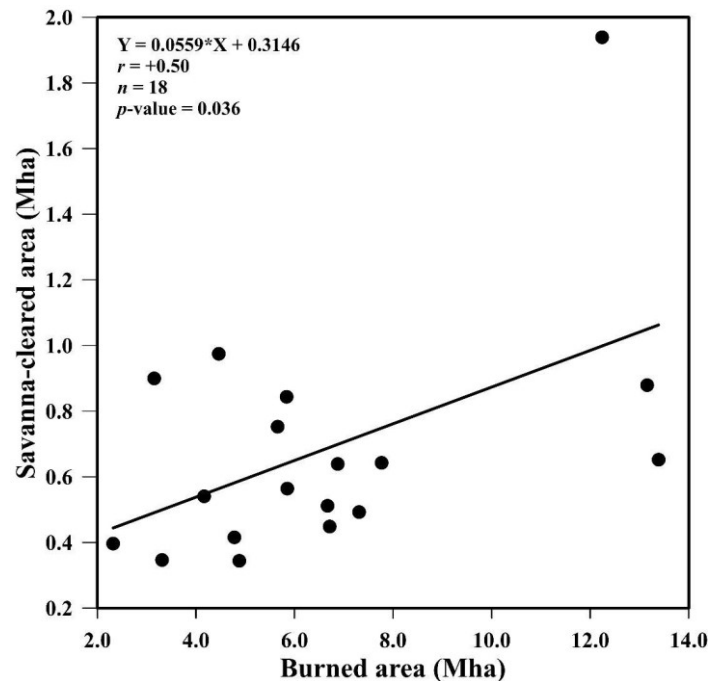
Source: Author's production.

Cleared areas at lower elevations and higher slopes (geomorphological depressions) generally involved smallholder farming that was already present before the recent agribusiness expansion. The average size of the cleared areas detected by LandTrendr was significantly different between the depressions (< 1 ha) and plateaus (larger cleared areas). Because of the large-scale expansion of the agribusiness over the flat terrains, the size of the cleared areas has increased over the plateaus since 1995 when compared to the depressions. It presented

values 416% greater than that observed between 2000 and 2018 over the depressions.

Fire is an important factor associated with clearing in MATOPIBA. The number of fire events generally increased with vegetation clearing. However, when we correlated the amount of cumulative cleared-area per year, estimated by LandTrendr in the 2001-2018 period, with the corresponding amount of MODIS-detected burned area, we observed a Pearson's correlation coefficient ( $r$ ) of +0.50 (Figure 4.11). This value obtained over the entire MATOPIBA region was statistically significant at the 0.05 level. Therefore, the amount of burned areas per year increased with increasing savanna clearing (positive  $r$  value in Figure 4.11). However, as observed in this figure, the cumulative burned area each year was much greater than that observed for savanna clearing. Slightly higher  $r$  values were observed at some mesoregions such as *Sudoeste Piauiense* ( $r = +0.55$ ;  $p$ -value = 0.018). In both cases, this moderate relationship between clearing and fire is explained by the multi-purpose use of fire in clearing activities and crop management practices. Moreover, fire events over converted areas generally extend into the native vegetation. We did not separate these areas in our correlation analysis.

Figure 4.11 - Relationship between the cumulative savanna-clearing area detected per year by LandTrendr and the cumulative burned-area calculated per year from the MODIS MCD64A1 product.



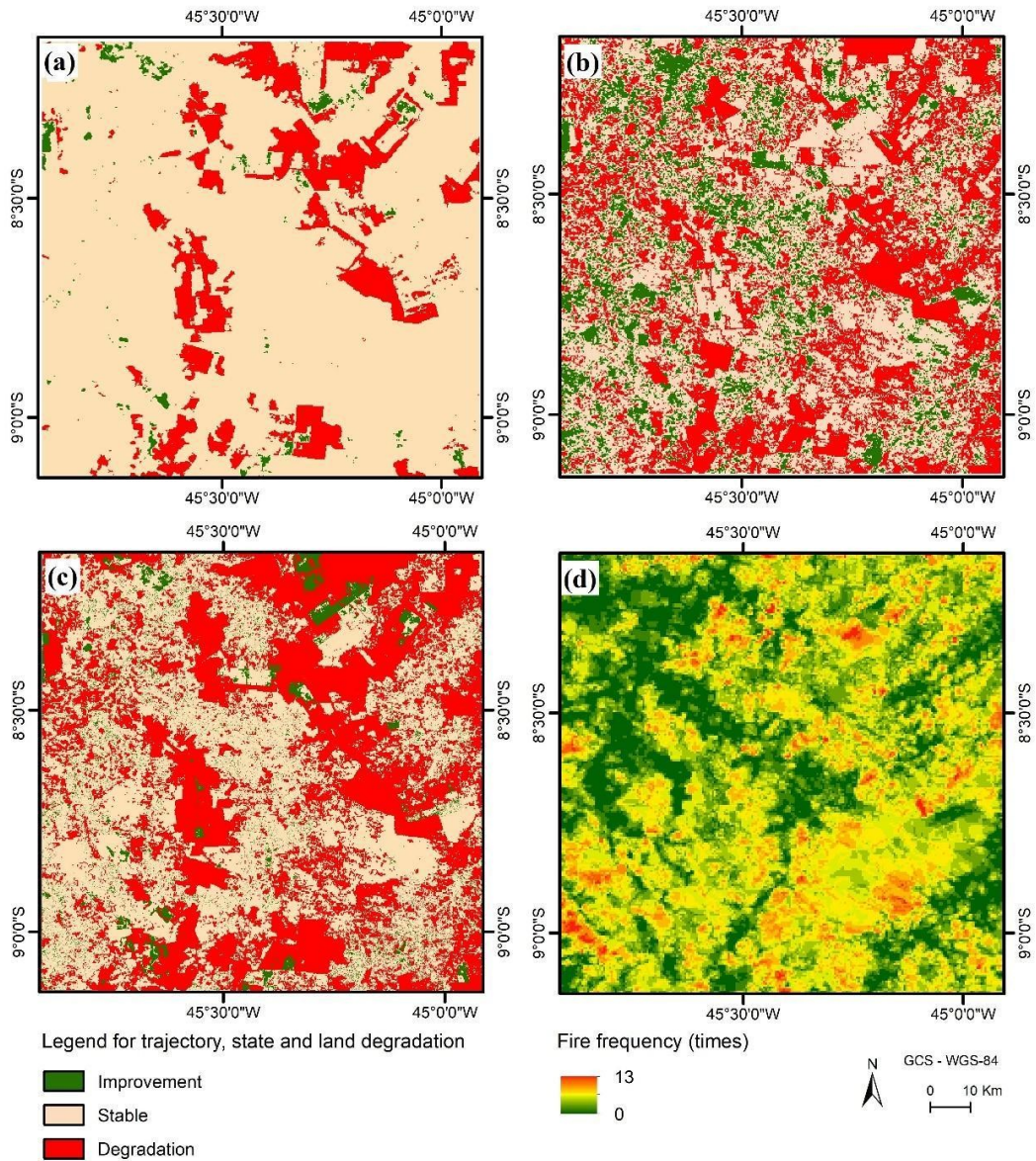
The cumulative areas per year corresponded to the period between 2001 and 2018 ( $n = 18$  years) over the entire MATOPIBA region.

Source: Author's production.

In addition to the relation with clearing, fire affects land productivity. An example is presented in Figure 4.12. This figure shows Trends.Earth results over a selected site at the Sudoeste Piauiense. Areas in red in Figure 4.12(a) indicated long-term negative trajectories in the NDVI (a proxy for land degradation), considering the period of analysis (2001-2015). Recent declines in land productivity over the last three years of analysis (2013-2015) were indicated in red color by the state metric (Figure 4.12b). The occurrence of land degradation areas, assigned from the combination of both metrics in Figure 4.12c, was associated with fire frequency. Fire frequency reached local values up to 13 times in the period of analysis (Figure 4.12d). However, as shown in Figure 4.13, the proportion of land-degraded areas increased with fire frequency over the agricultural areas. By contrast, it remained relatively stable over the savanna

areas of native vegetation. This type of vegetation is well adapted to natural and human-induced fires.

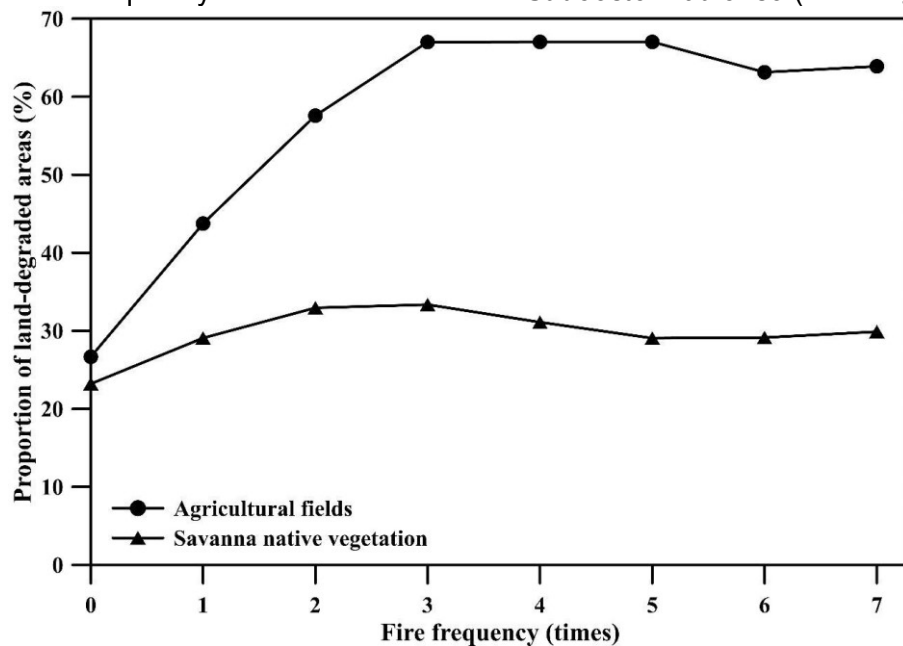
Figure 4.12 - Variations in Trends. Earth metrics and fire frequency for a site located at the *Sudoeste Piauiense*.



The long-term decrease in land productivity is represented in red color by the trajectory metric (a), while the recent short-term declines in productivity (2013-2015) are expressed in red color by the state metric (b). Areas of potential degradation (red color) are indicated in (c) from the combination of both metrics. Fire frequency, determined from the MODIS MCD64A1 product, is illustrated on a per-pixel basis in (d).

Source: Author's production.

Figure 4.13 - Relationship between the proportion of land-degraded areas and fire frequency for a site located at the *Sudoeste Piauiense* (mesoregion 8).



Results are presented as a function of native vegetation and agricultural classes. Land degradation was determined from the Trends.Earth algorithm using MODIS NDVI, while fire frequency was obtained from the MODIS MCD64A1 product.

Source: Author's production.

#### 4.4 Discussion

The present study makes some important contributions to understanding the dynamics of land occupation in the newest agricultural frontier in Brazil. To the best of our knowledge, this is the first long-term study using temporal segmentation of Landsat NDVI that has tracked quantitatively savanna clearings since 1985 over the different mesoregions of MATOPIBA. In addition, it presents for the first time a spectro-temporal trajectory analysis of MODIS NDVI to detect patterns of land degradation in the region. Finally, it relates topographic attributes and fire frequency with savanna clearings and land degradation. All this knowledge is important to make reliable decisions on agricultural and environmental planning (SPERA et al., 2016; ARAÚJO et al., 2019). The analysis of this large amount of data was facilitated by cloud processing on the GEE platform, which saved considerable computational time.

Our findings from satellite data showed patterns of increasing savanna clearings over time (1985-2018) with well-defined peaks in 1986, 1991, and 2012. In general, these patterns were consistent with the dynamics of soybean production (1990-2015) reported by Araújo et al. (2019) when using qualitative information from the Instituto Brasileiro de Geografia e Estatística (IBGE). The soybean production was estimated by IBGE using questionnaires applied by government agents to local farmers and technicians. In agreement with our LandTrendr results, Araújo et al. (2019) also pointed out the mesoregions Extremo Oeste Baiano and Sudoeste Piauiense as representative of the most recent soybean expansion in MATOPIBA.

The focus of our work was not to identify the best method to detect savanna clearings. From our validation strategy, the performance of the LandTrendr algorithm to capture savanna clearings presented an overall accuracy of 74.3%. However, we observed larger omission errors than commission errors, indicating accuracy uncertainties from the point of view of the map producer. On the other hand, we also confirmed the consistency of our results through comparison with cleared-area estimates provided by the PRODES *Cerrado* project (INPE 2018). This project has covered only the most recent period of agricultural expansion, using Landsat images interpretation since 2000. Despite the significant differences in methodologies, our estimates of the cumulative clearing were only 5.24% lower than the estimates provided by the PRODES *Cerrado* in the MATOPIBA region.

Another important aspect of our analysis is the spillover effects of the Amazon Soy Moratorium to a different biome (*Cerrado*). Such effects should be considered in the evaluation and planning of conservation efforts because they produce displacement of environmental pressure from one area to another area (DOU et al., 2018). Some studies claim that one of the consequences of the Amazon Soy Moratorium, signed in 2006, has been just the opening of new agricultural frontiers over the savannas in Brazil (NEPSTAD et al., 2019). Other investigations indicate that the association between policies to reduce Amazonian tropical deforestation and the increased clearing over time in MATOPIBA is not necessarily a cause-and-effect relationship (ZALLES et al.,

2019). Both views seem to be correct. Our results confirmed that the Amazon Soy Moratorium was an important factor to explain the soybean expansion in MATOPIBA. The cleared areas expanded 41% in the decade post-agreement and the savanna-clearing peak in 2012 (Figure 4) was inversely related to the reduction in deforestation areas in the Amazon. From our results, savanna-cleared and tropical-deforested areas presented a non-linear relationship ( $R^2 = 0.50$ ) in the decade post-moratorium.

However, the expansion of 41% in cleared areas was not homogeneous over the entire MATOPIBA region. In addition to the Amazon Soy Moratorium, other local factors promoting clearing expansion for agriculture cannot be ignored. Some of them reported in the literature include market oscillations in agricultural commodities and land prices; local policies of credit incentives to agriculture; infrastructure improvement; and technological advances in soil/crop management practices (MESQUITA, 2011; SPAGNOLO, 2011; BOLFE et al., 2016). For instance, the clearing expansion over the *Extremo Oeste Baiano* followed the availability of low-tax loans offered by the federal government since 2000. The strategy has been part of various programs to increase and modernize agricultural production in the state of Bahia (SPAGNOLO, 2011; ARAÚJO et al., 2019). One example of these programs is the Investment Program for the Modernization of Agriculture in Bahia (AGRINVEST). This program was implemented in 2000, thus before the signature of the Amazon Soy Moratorium in 2006. It helped to consolidate the soybean production in this mesoregion even before the moratorium.

For the protection of native vegetation, a similar type of moratorium does not exist for the *Cerrado*. From a political point of view, the expansion of the Soy Moratorium into the *Cerrado* would probably prevent the direct conversion of 3.6 Mha of savannas until 2050 (SOTERRONI et al., 2019). Other actions of savanna-clearing control could include incentives for agricultural expansion in already cleared areas and adaptation of the rural properties to the environmental legislation (RAUSCH et al., 2019; SANO et al., 2019b). In terms of environmental legislation, the *Cerrado* biome is also more vulnerable to clearing/deforestation than the Amazon ecosystem. For instance, the Brazilian Forest Code established

the retention of 20-35% of the area with native vegetation as a legal reserve for the Cerrado against 80% for the Amazon (LIMA et al., 2019). The more permissive legislation in *Cerrado* areas, compared to the Amazon biome, is, therefore, a factor that has contributed to the recent high rates of savanna clearings observed in our study in MATOPIBA. Another critical point for conservation of the biome is the low proportion of protected areas in the form of conservation units and indigenous lands. The allocation of land to conservation units and indigenous territories is an effective way to decrease deforestation (FRANÇOSO et al., 2015).

Our land degradation map was consistent with the natural vulnerability of the mesoregions and with the use of fire in cleared areas. The main degraded areas (*Sudoeste Piauiense* and *Centro Maranhense*) presented the lowest average annual precipitation and the greatest amounts of sandy soils, especially in the transition zone with the semi-arid *Caatinga* biome in northeastern Brazil. In agreement with our results, Araújo et al. (2019) also reported more occurrences of sandy soils over the *Sudoeste Piauiense*. They considered this mesoregion as the most sensitive to drought effects. The association between climate, great amounts of sandy soils, crop/soil management practices, and fire events of variable frequency can explain the decrease in long-term land productivity captured by the Trends.Earth algorithm. However, further studies are necessary to confirm this pattern, including the need of fieldwork for soil sampling and physicochemical analyses. Because of the lack of acceptable accuracy for MATOPIBA, we did not consider the soil organic carbon information available on the GEE platform. On the other hand, we corrected for the effects of climate to ensure confidence in human-induced causes of land productivity changes. At the *Sudoeste Piauiense*, the amount of land degradation areas detected by Trends.Earth increased also with fire frequency over agricultural areas. In contrast, we did not observe this relationship over the savanna native vegetation. This vegetation type is composed of a high diversity of species well adapted to natural and human-induced fires (RATTER; BRIDGEWATER; RIBEIRO, 2006). However, in other study areas, the negative effects of fire frequency on floristic diversity, carbon emissions, and tree mortality have been well described in the

literature (MIRANDA et al., 2009; PIVELLO et al., 2010; BUSTAMANTE et al., 2012).

The current investigation can be extrapolated to other savanna environments because of the worldwide availability of the satellite images and products used here and the facilities provided by the GEE platform. However, our study has some constraints that require attention in future studies. One of them is the lack of ground observations to validate savanna-clearing detection over time and land degradation mapping. To overcome this limitation, face to the absence of reference maps to track clearing over a long time, we adopted a validation approach used in several studies (OLOFSSON et al., 2014; MURILLO-SANDOVAL; HOEK; HILKER, 2017). The approach followed the good practices recommended in the literature for this purpose. In MATOPIBA, the LandTrendr-clearing detection over woodland savannas is probably more accurate than the clearing detection over savanna grasslands. As indicated in Figure 4.3, it occurs because of the larger NDVI modifications due to disturbance observed over woodland savannas when compared to grassland areas. Another constraint is the need to confirm in the field the potentially degraded areas detected by Trends.Earth. The comprehension of the effects of savanna clearing and agricultural expansion on the long-term decrease in land productivity can benefit from paired-site analysis using control areas (reference sites). NDVI time series having better spatial resolution than the MODIS datasets, along with adequate temporal resolution, may complement the land degradation analysis. Examples include the new Harmonized Landsat and Sentinel-2 product and the recent advent of satellite constellations (CLAVERIE et al., 2018; BREUNIG et al., 2020). Finally, there were also uncertainties associated with data upscaling. Although the analyses of savanna clearing (30-m pixel size) and land degradation (250-m pixel size) were performed independently from each other, the evaluation of their relationships with topography and fire involved data resampling. As a result, the transition from different levels of spatial resolution in the data analysis represented distinct spectral mixture conditions viewed by the optical instruments.

## 4.5 Conclusions

From investigating the dynamics of savanna clearings and land degradation in the newest agricultural frontier over the savannas in Brazil, we concluded that:

- 1) In the 1985-2005 period, the savanna clearing progressed from the south (mesoregions *Ocidental do Tocantins* and *Extremo Oeste Baiano*) to the center and southeast of MATOPIBA (*Sudoeste Piauiense* and *Sul Maranhense*), especially over terrain slopes lower than 3° (plateaus). After the signature of the Amazon Soy Moratorium in 2006, the expansion of savanna-cleared areas followed the soybean planting at the *Extremo Oeste Baiano* and *Sudoeste Piauiense*. For the entire time series (1985-2018), the LandTrendr detected well-defined clearing peaks in 1986, 1991, and 2012.
- 2) The Amazon Soy Moratorium, signed in 2006 to reduce Amazonian tropical deforestation, contributed indirectly to accelerating savanna clearings in the *Cerrado* biome. In MATOPIBA, the savanna clearing increased 41% in the decade post-moratorium (2007-2016) when compared to the 10 years preceding the agreement (1996-2005). However, this moratorium was not the only factor promoting clearing expansion over the mesoregions.
- 3) The number of fire events increased with vegetation clearing. However, because fire is used for clearing and crop management practices, affecting both the native vegetation and agricultural areas, the amount of cleared areas was only moderately correlated with that of burned areas ( $r = +0.50$ ).
- 4) The mesoregions that showed the largest proportions of land degradation areas were the *Sudoeste Piauiense* and *Centro Maranhense*, which presented distinct patterns of precipitation and soil composition. The amount of land-degraded areas increased with fire frequency over agricultural areas but remained relatively stable over native-vegetated areas.

## 5 ON A DATA-DRIVEN APPROACH FOR DETECTING DISTURBANCE IN THE BRAZILIAN SAVANNAS USING TIME SERIES OF VEGETATION INDICES<sup>2</sup>

### 5.1 Introduction

Savannas in Brazil comprise a global hotspot of biodiversity that has already lost half of the native vegetation cover to crops and pastures (SANO et al., 2010; PARENTE et al., 2021). Locally known as the *Cerrado*, the savannas are the second largest biome in the country and the second-largest terrestrial source of carbon emissions after the Amazon biome (FERREIRA et al., 2011; OLIVERAS et al., 2013; DE MIRANDA et al., 2014). Savannas show gradients ranging from grasslands to woodlands, having species well adapted to natural and human-induced fires as well as to the strong seasonality of precipitation (SILVA; BATES, 2002; RATTER; BRIDGEWATER; RIBEIRO, 2006; JACON et al., 2021).

In addition to its biodiversity, the *Cerrado* is also very important for agriculture and has half of the croplands in Brazil (GRAESSER et al., 2015; SPERA, 2017; RAUSCH et al., 2019). The recent expansion of soybean over native vegetation of the northern portion of the *Cerrado* (new agricultural frontier) has increased the number of disturbance events in this region (MIRANDA et al., 2009; DOU et al., 2018; LIMA et al., 2019; NEPSTAD et al., 2019; ZALLES et al., 2019). As in other regions of the *Cerrado*, clearing and fire are the main drivers of disturbance. However, the seasonal pattern of occurrence of these two types of disturbance is not entirely understood. The comprehension of the relationships between fire and clearing over each year requires further studies. For land management, fire is a common practice that generally invades the native vegetation areas. Although part of the savanna vegetation is adapted to fire, an excessive number of events may cause biodiversity loss and land degradation (PIVELLO, 2011; SOUZA et al., 2020a). Fire is also used in recently cleared areas to burn and

---

<sup>2</sup> This chapter is an adapted version of the paper: SOUZA, A. A. et al. On a Data-Driven Approach for Detecting Disturbance in the Brazilian Savannas Using Time Series of Vegetation Indices. **Remote Sensing**, v. 13, n. 24, 2021.

clean the non-photosynthetic vegetation left on the ground after disturbance (e.g., rest of leaves, branches, and trunks).

To monitor vegetation disturbance caused by clearing and fire in the *Cerrado*, remote sensing programs have been developed in Brazil. The use of satellite imagery is perhaps the only way for large-scale monitoring of this biome (SANO et al., 2007). An example of these initiatives is the project for monitoring the *Cerrado* developed by the Brazilian National Institute of Space Research (INPE), which is mostly based on the visual interpretation of several satellite data. The objective of the INPE's project is to provide annual rates and warning alerts of savanna clearings (PARENTE et al., 2021). Monitoring disturbance in the *Cerrado* is part of the strategies used to mitigate greenhouse gas emissions and conserve biodiversity. For instance, if a similar agreement to the Amazonian Soy Moratorium is adopted to the *Cerrado*, such types of remote sensing programs can adequately support the major exporting companies to not buy and finance soybean production from new savanna-cleared areas. This would probably reduce savanna-clearing rates, as was observed in the last decade for tropical deforestation in the Amazon region.

However, satellite monitoring of human-induced disturbance in the *Cerrado* is not a trivial task. It still requires the development and testing of new approaches for the detection of disturbance and the reduction of uncertainties in data analysis. Some factors that affect detection are the distinct resilience of savanna vegetation types to disturbance events, the significant changes in satellite spectral response due to vegetation phenology, the natural soil exposure due to the presence of more open canopies in the savanna formations, and the frequency of satellite observations affected by cloud cover. To reduce the influence of vegetation phenology on clearing detection, vegetation indices (VIs) calculated in a fixed period of each year (e.g., dry season) can be used as input data for algorithms. When compared to band reflectance, VIs can reduce data variability associated with the geometry of data acquisition and with terrain illumination or topographic effects. This is especially valid for VIs with a band reflectance normalization on their formulations (GALVÃO; SOUZA; BREUNIG, 2019; SILVEIRA et al., 2019; DE OLIVEIRA; GALVÃO; PONZONI, 2021).

Algorithms like the Landsat-based detection of Trends in Disturbance and Recovery (LandTrendr) retrieve the annual rates of disturbance from the Landsat time series (KENNEDY; YANG; COHEN, 2010; SOUZA et al., 2020a). In this case, early warning alerts of disturbance cannot be generated. Alternatively, algorithms that consider the seasonal response of vegetation can be used for near real-time detection of disturbance. This is the case of the Continuous Change Detection and Classification (CCDC), which can detect land cover changes continuously using all available Landsat data or every time a new image is collected (ZHU; WOODCOCK, 2014).

When compared to other methods, CCDC has the advantage of working with multiple input variables for providing robust detection of land covers, especially when working with high quantities of missing data in the time series, as demonstrated in a simulation study by Awty-Carroll et al. (AWTY-CARROLL et al., 2019). CCDC uses ordinary least squares in a time series model that has components of seasonality, trend, and overall values. The CCDC algorithm has been successfully used in forest environments (SHIMIZU; OTA; MIZOUE, 2019; TANG et al., 2019). As far as we know, no studies are using CCDC over the savannas in Brazil. When VIs are considered for change detection in other environments, most studies generally focus on the Normalized Difference Vegetation Index (NDVI). However, in the *Cerrado*, it is particularly important to consider adding other VIs that capture the information of different savanna properties associated with canopy structure, biochemistry, and plant physiology (JACON et al., 2017). There are also specific VIs proposed to be sensitive to disturbance by fire, such as the Normalized Burn Ratio (NBR) (KEY; BENSON, 2006). For detecting disturbances in the Brazilian savannas, the performance of each VI, or all VIs in a multivariate approach with CCDC (henceforth named “ensemble VIs”), has not been evaluated yet.

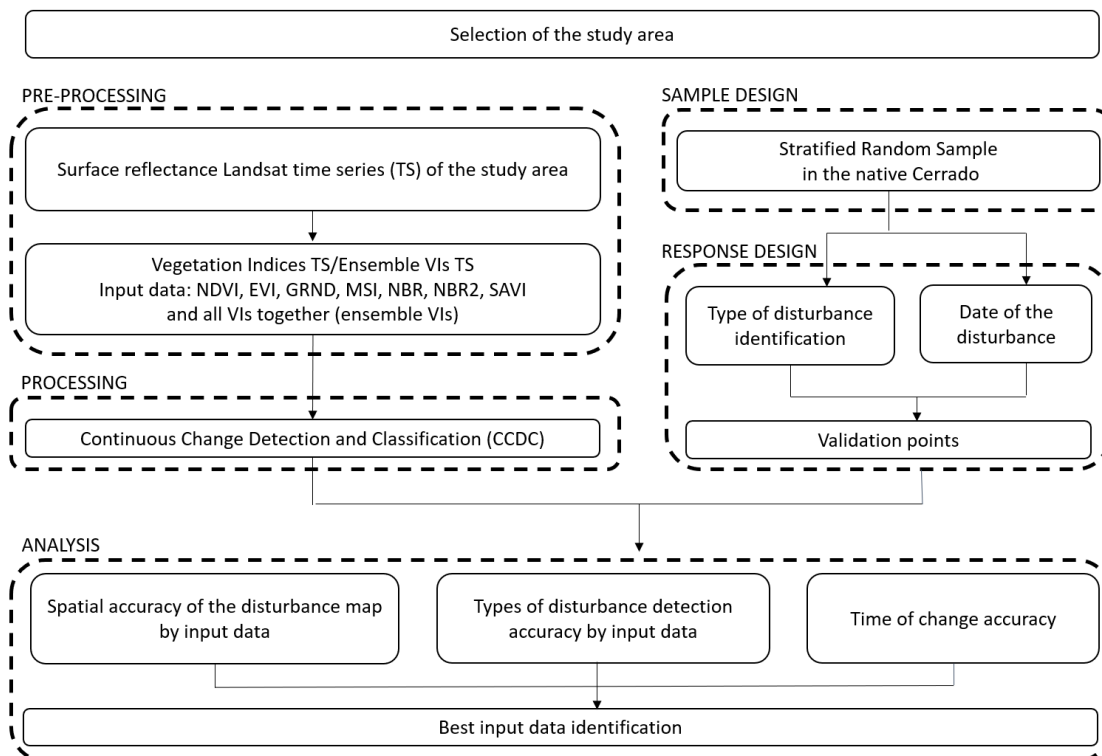
In this study, we investigated the detection of disturbance over the savannas in Brazil using seven VIs calculated from a Landsat time series (2017–2019) and the CCDC algorithm. The specific objectives were to evaluate: (1) the effects of disturbance on savanna reflectance spectra and VIs time series; (2) the accuracy of CCDC-detection in 2019, considering single VIs, ensemble VIs, and the type

of disturbance (savanna clearing and fire) in the analysis; and (3) the possible existence of seasonal patterns of occurrence of fire and clearing for a better understanding of the dynamics of disturbance in the savannas.

## 5.2 Data and methodology

The main methodological steps for the detection and analysis of disturbance in the savannas are presented in Figure 5.1. In the accuracy assessment of the CCDC-derived maps of disturbance, the detections were compared with reference data (validation points). Such high-quality data were collected through a sample-based approach (sampling design), allowing for a careful interpretation of specific areas of the map (response design). Response design was the step to determine whether the map and reference data would agree. The reference data were then used to compare the results and finally estimate the accuracy and area of the changes, and their related confidence intervals (data analysis). The steps are detailed in the next sub-sections.

Figure 5.1 Main methodological steps used for detecting disturbance over the savannas.



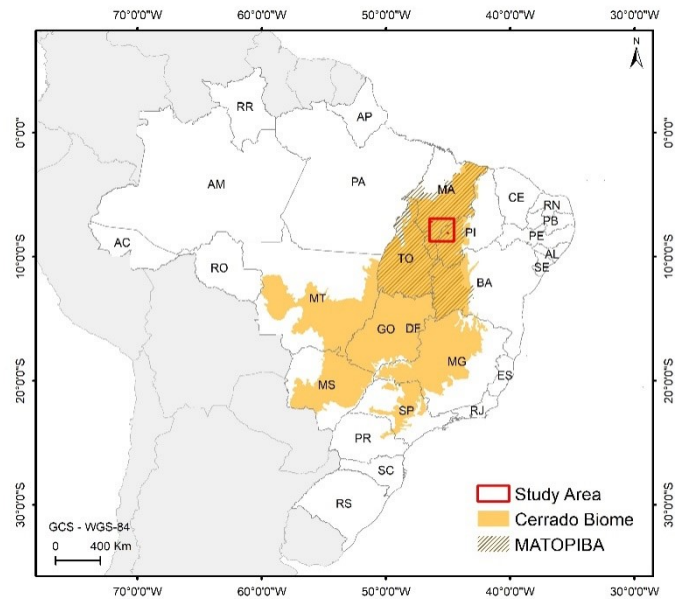
Source: Author's production.

### 5.2.1 Selection of the study area

The study area is located in MATOPIBA, an acronym for the names of four Brazilian states that compose this region (Maranhão, Tocantins, Piauí, and Bahia). Intensive savanna clearing for single cropping (soybean, maize, and cotton plantations) or double cropping (soybean-corn or soybean-cotton rotations) activities in this region is a consequence of several factors. These factors include the spillover effect of the Amazon Soy Moratorium to the *Cerrado* biome and several local actions for promoting recent agriculture expansion (DOU et al., 2018; LIMA et al., 2019; NEPSTAD et al., 2019). Savanna clearing rates vary with: market oscillations in commodities and land prices; local policies of credit incentives to agriculture; infrastructure improvement; and technological advances in soil/crop management practices (MIRANDA et al., 2009; ZALLES et al., 2019).

We selected a study area of 215 km × 215 km located close to the municipalities of Balsas and Uruçuí in the Brazilian states of Maranhão (MA) and Piauí (PI), respectively (Figure 5.2). Intensive savanna clearing, especially for soybean expansion, has already removed 22% of the native vegetation cover. Native vegetation is mainly composed of savanna grasslands (*Formações Campestres*), shrub savannas (*Formações Savânicas*), and woodland savannas (*Formações Florestais*) (SOUZA et al., 2020b).

Figure 5.2 - Location of the study area in the *Cerrado* biome in Brazil.

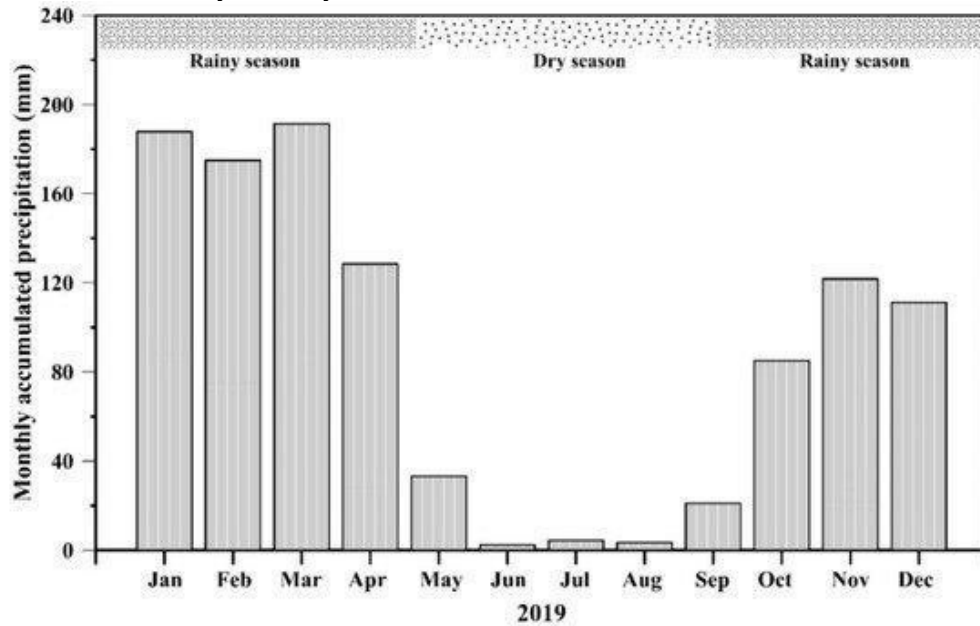


The MATOPIBA region, indicated by the hatched area in yellow, is the newest agricultural frontier of the country.

Source: Author's production.

The study area has well-defined rainy and dry seasons, with an average annual precipitation of 1100 mm (SANO et al., 2019a). In 2019, the year of our analysis of disturbance, the total precipitation was 1065 mm. From May to September (dry season), the monthly accumulated precipitation was generally lower than 35 mm. During the rainy season, rainfall reached values higher than 170 mm per month between January and March (Figure 5.3).

Figure 5.3 - Variations in monthly accumulated precipitation over the study area during the rainy and dry seasons of 2019.



Source: Author's production.

From a geomorphological point of view, there are plateaus and depressions in the study area. The elevation ranges from 160 m to 663 m with plateaus having more than 400 m of elevation. In contrast to depressions, plateaus allow mechanized agriculture because of the more favorable slope conditions for the displacement of tractors (SOUZA et al., 2020c). Crops are mostly planted over oxisols that are managed to improve soil fertility.

### 5.2.2 Pre-processing of Landsat time series and selection of VIs for CCDC

We used surface reflectance data obtained from 1 January 2017 to 31 December 2019 by the Enhanced Thematic Mapper Plus (ETM+)/Landsat-7 and Operational Land Imager (OLI)/Landsat-8. Despite the data gaps associated with the Scan Line Corrector (SLC) failure in ETM+ imagery, the remaining pixel observations are useful because they maintain the same radiometric and geometric corrections as data collected prior to the failure. All the available images from both sensors in the period were considered in the data analysis, including 469 images from four tiles: 215 images from Landsat-7 and 254 images from Landsat-8.

On the Google Earth Engine (GEE) cloud-computing platform (GORELICK et al., 2017), the reflectance of the ETM+ bands was radiometrically adjusted to that of the OLI bands using slopes and intercepts reported by Roy et al. (2016). This procedure is recommended to face the spectral differences in spectral response functions of the bands from both sensors. Such differences tend to produce, for instance, greater NDVI values for OLI than for ETM+ (ROY et al., 2016). Therefore, statistical functions to adjust the band reflectance between the sensors ensure the temporal continuity of the time series generated from ETM+ and OLI. Moreover, we excluded pixels under clouds and cloud shadows using the CF-mask algorithm (ZHU; WOODCOCK; OLOFSSON, 2012; FOGA et al., 2017).

From the surface reflectance data, we calculated seven VIs for detecting disturbance (savanna clearing and burned areas). Equations and references of the VIs are listed in Table 5.1 (ROUSE et al., 1973; HUETE, 1988; HUNT; ROCK, 1989; HUETE et al., 2002; KEY; BENSON, 2006; MOURA et al., 2017). They were selected because of their sensitivity to different biophysical parameters of the savannas. For instance, the Enhanced Vegetation Index (EVI) and the Soil-Adjusted Vegetation Index (SAVI) are the VIs more sensitive to changes in vegetation structure produced by disturbance. They were proposed to reduce constraints of the NDVI that are mainly associated with signal saturation over dense vegetation, or with soil background influence over sparse vegetation. On the other hand, the Green-Red Normalized Difference (GRND) and the Moisture Stress Index (MSI) may detect changes in old/new foliage and leaf/canopy water stress resulting from gradual processes of savanna clearing or degradation, respectively. Finally, we also considered in the data analysis the Normalized Burn Ratio (NBR) and its variant (NBR2), which are VIs sensitive to fire disturbance. They use near-infrared (NIR) and shortwave infrared (SWIR) bands on their formulations (Table 5.1). Therefore, besides their sensitivity to different biophysical parameters of the savannas, such VIs explore different band combinations of OLI and ETM+ in the visible, NIR, and SWIR spectral regions.

Table 5.1 - Vegetation indices (VIs) used in the CCDC algorithm for detecting disturbance over the savannas.

VIs	Equation
Enhanced Vegetation Index (EVI)	$2.5 \times ((\text{NIR} - \text{Red})/(\text{NIR} + 6 \times \text{Red} - 7.5 \times \text{Blue} + 1))$
Green-Red Normalized Difference (GRND)	$(\text{Green} - \text{Red})/(\text{Green} + \text{Red})$
Moisture Stress Index (MSI)	$(\text{NIR} - \text{SWIR1})/(\text{NIR} + \text{SWIR1})$
Normalized Burn Ratio (NBR)	$(\text{NIR} - \text{SWIR2})/(\text{NIR} + \text{SWIR2})$
Normalized Burn Ratio2 (NBR2)	$(\text{SWIR1} - \text{SWIR2})/(\text{SWIR1} + \text{SWIR2})$
Normalized Difference Vegetation Index (NDVI)	$(\text{NIR} - \text{Red})/(\text{NIR} + \text{Red})$
Soil-Adjusted Vegetation Index (SAVI)	$1.5 \times ((\text{NIR} - \text{Red})/(\text{NIR} + \text{Red} + 0.5))$

Source: Author's production.

### 5.2.3 Continuous Change Detection and Classification (CCDC)

The selected VIs of Table 5.1 were used individually as input data (univariate approach) and in an ensemble approach (multivariate) for the detection of disturbance with the CCDC algorithm on the GEE platform. Thus, the algorithm was run eight times: one run for each of the seven VIs and another run for the ensemble approach (VIs together as seven input variables). The ensemble approach explored indirectly the distinct spectral-biophysical information provided by the seven VIs for disturbance detection. The CCDC is an online algorithm that uses a data-driven statistic threshold (adjusted for each pixel) to detect changes in the time series (ZHU; WOODCOCK, 2014). An online approach means that a model is fitted to observations from the beginning to the end of the time series, being updated as new observations become available. Thus, if new observations over the time series do not diverge widely from the fitted model, they are added to the time series before updating the model.

The time series modeled by CCDC have components of overall value (mean VI throughout the time series), seasonality, and trend. In our study, Least Absolute Shrinkage and Selection Operator (LASSO) regression fitting estimated the coefficients of the model. After testing different parameters in pixels with available

information of disturbance, the model based on the overall value was then selected for analysis. When we considered single VIs as input data for CCDC, a disturbance caused by clearing or fire was flagged when the difference between observed and predicted values by the model exceeded three times the normalized root mean square error (RMSE) for three consecutive observations. In the ensemble approach, the algorithm averages and normalizes such differences (observed minus predicted) by three times the RMSE for all VIs. A disturbance was marked in the time series when the result was larger than one for three consecutive observations. This number of observations was set to avoid the pseudo-detection of disturbance caused by noise in the time series (ZHU; WOODCOCK; OLOFSSON, 2012). While noise factors tend to be ephemeral, land cover change is more persistent through time. The results of the first disturbance detection that occurred in 2019 were evaluated.

#### **5.2.4 Data analysis from sampling and response designs**

The data analysis was divided into three parts. In the first one, the CCDC's ability to correctly detect a disturbance in 2019 was evaluated per VI and ensemble VIs, considering also the performance of the metrics as a function of the type of disturbance (savanna clearing or fire). In the second part, the ability of the algorithm for precise detection of the time of disturbance occurrence was analyzed. Finally, the last part looked for the possible existence of temporal patterns of clearing and fire in 2019. The strategy used for accuracy assessment is described below.

##### **5.2.4.1 Accuracy assessment per VI, ensemble VIs, and type of disturbance**

The sampling and response design for the accuracy assessment of the CCDC disturbance detection in 2019 was based on the Area Two (BULLOCK, 2020) and Collect Earth Online (<https://collect.earth/>; accessed on 30 June 2021) tools, respectively. These applications provide the necessary tools to comply with the recommended practices and international guidelines for assessing map accuracy. Using these approaches, we estimated the optimal number of samples and randomly located them in the study area (sampling design). In addition, we built a reference dataset for these sample locations (response design) to support

the validation of the results. The sampling design considered only the native vegetation areas in 2018. Land cover changes observed until 2018 and reported by the INPE's program of *Cerrado* monitoring were masked.

A stratified random sample design with equal sample allocation on each class (disturbed and non-disturbed) was adopted in the work. The stratification was based on the classes (disturbed by fire, clearing, and non-disturbed) and on the inspection of ancillary maps. There are two main purposes for stratification. First, the strata are important to report accuracy per class. Second, the stratification ensures a sufficient representation of each class, even that occupying a small proportion of the area (e.g., disturbance class). The sample unit is the pixel. We choose an equal number of samples per strata to make possible the comparison of accuracy per type of disturbance. We selected 588 samples for the spatial accuracy assessment and area estimation of disturbance in 2019. In addition to the visual inspection of the Landsat time series, we used other satellite data with more detailed spatial resolution than the Landsat instruments for the identification of disturbed and non-disturbed areas. Examples of these satellites include the Multispectral Instrument (MSI)/Sentinel-2 images having some bands with 10-m spatial resolution, and the PlanetScope satellite constellation with 3-m spatial resolution data.

From the 588 allocated samples, we selected 294 non-disturbed sites and 294 disturbed sites. We divided also the set of 294 disturbed areas into two groups having an equal number of samples: one group affected by fire and another one affected by clearing. The cross-tabulation of the class label (disturbed and non-disturbed) assigned from the CCDC results against the reference dataset generated the error matrix. The error matrix was the basis for quantification of the overall accuracy, user's accuracy (and its complementary measure, commission error), and producer's accuracy (and its complementary measure, omission error) estimates. Based on these estimates, we identified the performance of each VI and the ensemble VIs for overall detection of disturbance and specific detection of savanna-cleared and fire-affected areas.

#### **5.2.4.2 Accuracy of the detected time of disturbance**

For evaluating the accuracy of time detection of disturbance by CCDC, we used the set of 294 disturbed samples by clearing and fire. We tracked them over time in the Landsat images and VI profiles using the Collect Earth Online. This tool was customized here to record the type and date of each disturbance in the attributes of the validation points (shapefile). Thus, the date of change was obtained visually for the reference data and was compared with the CCDC output to obtain the difference between them. The evaluation of the date of disturbance occurrence was affected by the number of clear observations in the images. In other words, the reference date of disturbance occurrence can be different from the exact time of the event due to the limitations imposed by cloud cover, cloud shadows, and the temporal resolution of the instruments.

The date of change for clearing events considered the time when the vegetation was completely removed (clear-cutting). The date of change for fire events considered the time when active fire or burned areas were first recorded in the reference samples. The accuracy of time detection of disturbance by the CCDC algorithm was then calculated by comparing this reference dataset with the CCDC outputs of the time of occurrence of each disturbance type in 2019.

#### **5.2.4.3 Seasonal patterns of savanna clearing and fire events**

The relationships between savanna clearing and fire are not completely understood in the *Cerrado* environment. In order to look for temporal patterns of occurrence of these events in the study area, we first inspected our reference dataset by plotting the type of disturbance on a per-month basis in 2019. We compared these results with the CCDC-derived disturbance maps.

Because of the difficulties of CCDC to separate both types of disturbance in the time series, we complemented our analysis using ancillary data from savanna clearing in 2019 provided by the INPE's program entitled "*Sistema de Detecção de Desmatamento em Tempo Real*" (DETER *Cerrado*; <http://terrabrasilis.dpi.inpe.br/>; accessed on 21 July 2021). In addition, we used the 250-m Moderate Resolution Imaging Spectroradiometer (MODIS) FireCCI v.5.1 product (European Space Agency—ESA) to compare the

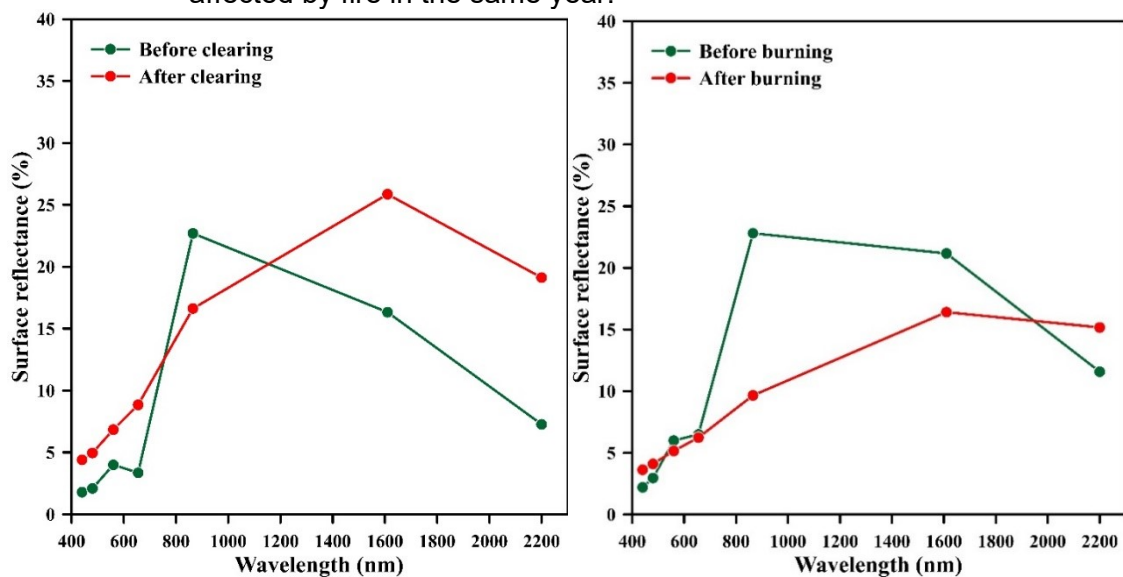
CCDC results with the burned areas detected by MODIS in 2019. Such comparisons used the validation points of disturbance that were also recorded on each product.

### 5.3 Results

#### 5.3.1 Time series of vegetation indices and the detection of disturbance

Savanna clearing and fire produced a great variety of changes in surface reflectance that depended on the intensity of disturbance, the disturbed savanna physiognomy, and the soil background composition before and after disturbance. For instance, when a woodland savanna area was cleared in the study area, we observed a reflectance increase in the visible and SWIR spectral intervals and a reflectance decrease in the NIR region (Figure 5.4a). This response was a combination of the soil reflectance with the reflectance of non-photosynthetic vegetation left on the ground after clearing (e.g., litter, branches, and twigs). In contrast, the effect of fire on shrub savannas was to decrease the reflectance of the NIR and SWIR-1 OLI/Landsat-8 bands (Figure 5.4b). Recently burned areas over savanna grasslands had low reflectance for the sensor, which gradually increased from the visible and NIR (VNIR) to the SWIR.

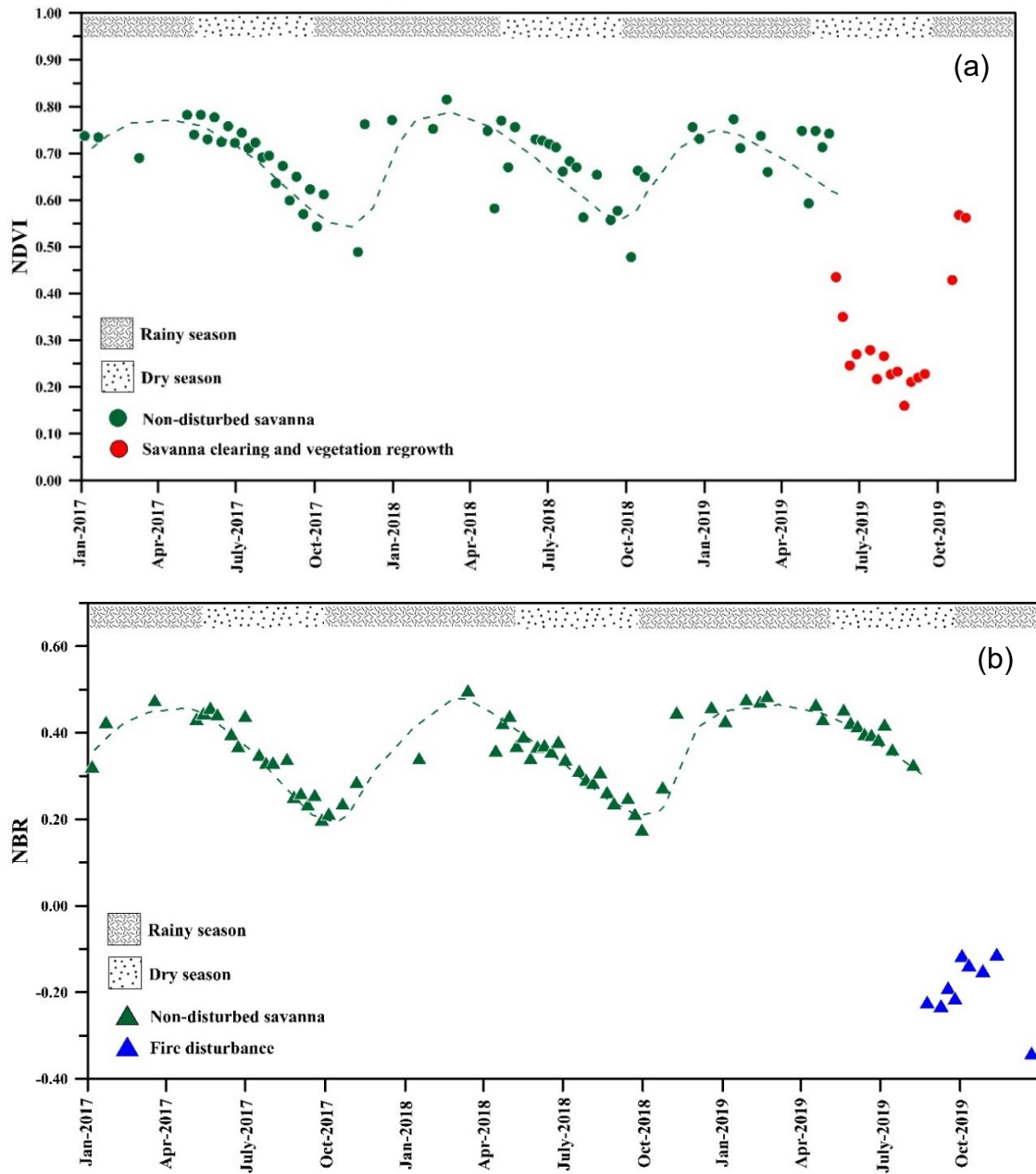
Figure 5.4 - (a) OLI/Landsat-8 surface reflectance spectra of woodland savanna before and after a clearing event in 2019. (b) Spectra from a shrub savanna area affected by fire in the same year.



Source: Author's production.

Both events of disturbance reduced the VIs response. Because the reflectance after savanna clearing increased in the red band (640–670 nm) of OLI/Landsat-8 and decreased in its NIR band (850–880 nm) (Figure 5.4a), this type of disturbance produced a significant change in the temporal profile of NDVI (Figure 5.5a). To be labeled as a disturbance (“break” in the time series) by the CCDC algorithm, such NDVI modifications for a given pixel should be distinct from the seasonal NDVI variations produced by vegetation phenology. NDVI decreased from the rainy to the dry season of each year, reaching the lowest values toward September under maximum water stress for the plants. As demonstrated in Figure 5.5a, clearing can be also followed by a quick vegetation regrowth that may produce an increase in NDVI and a new pattern of seasonal profile (see NDVI after October 2019 in Figure 5.5a).

Figure 5.5 - Landsat time-series examples of disturbance in 2019 in seasonal profiles.



(a) NDVI (savanna clearing in July) and (b) NBR (disturbance by fire in September). In both figures, dashed lines indicate the seasonal cycles of the savannas during the rainy and dry seasons of the 2017–2019 period. In (a), savanna clearing is followed by vegetation regrowth after October 2019.

Source: Author's production.

For detecting disturbance by fire, VIs like NBR were especially important when used with CCDC because they tracked the reflectance changes over time in the NIR and SWIR spectral intervals (Table 5.1; Figure 5.4b). In our study area,

disturbance by fire over the savannas generally transformed positive NBR values into negative ones. Therefore, “breaks” in the NBR time series were created because of the NIR reflectance decrease and the SWIR reflectance increase caused by biomass burning (Figure 5.5b).

### **5.3.2 Variations in accuracy metrics per VI, ensemble VIs, and type of disturbance**

The CCDC algorithm detected  $1.24 \pm 0.12$  Mha of total disturbance (clearing plus fire) in 2019. This result is based on the ensemble approach. The other VI-area estimates presented approximately similar results since the estimates were based on a stratified estimator. This number represents an area equivalent to 41.8% of the native vegetation of our site. The overall accuracy of detection ranged from  $51.2 \pm 4.2\%$  for GRND to  $65.9 \pm 4.2\%$  for NBR2 and increased to  $71.2 \pm 4.0\%$  for ensemble VIs (Table 5.2). The best single VIs for detecting total disturbance were therefore metrics that used NIR, SWIR-1, and SWIR-2 reflectance bands of the Landsat instruments on their equations (NBR2, NBR, and MSI in Table 5.1).

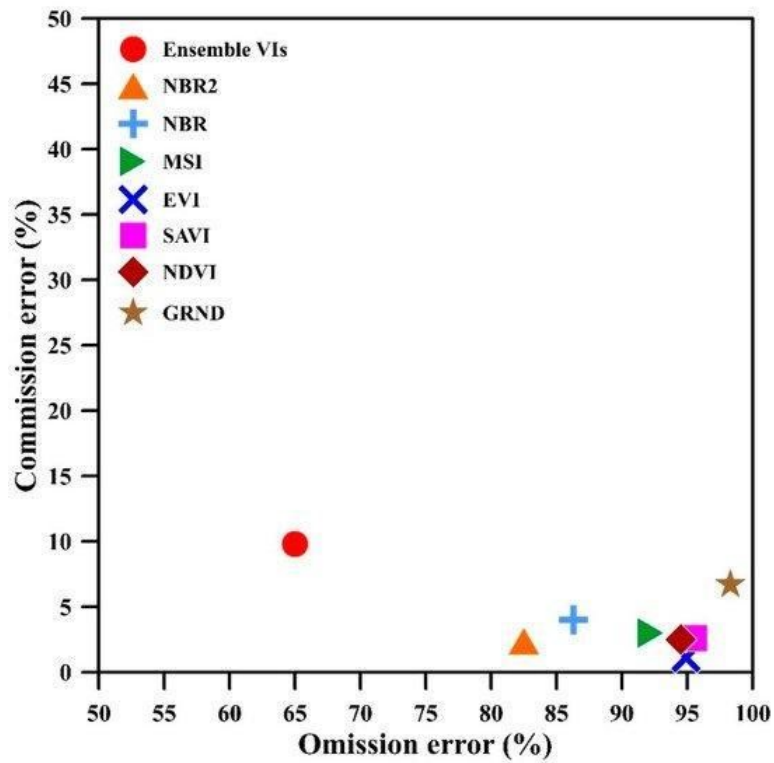
Table 5.2 - Overall accuracy (OA) with confidence intervals (CI) for the CCDC detection of disturbance over savannas using different vegetation indices (VIs) and ensemble VIs. Producer's (PA) and User's (UA) accuracies are also indicate for the disturbance and non-disturbance classes.

Input Data	OA (%)	95% CI	PA (%)	UA (%)	PA (%)	UA (%)
			Disturbance Class	Disturbance Class	Non-Disturbance Class (%)	Non-Disturbance Class
Ensemble VIs	71.2	4.0	35.0	90.2	97.3	67.5
NBR2	65.9	4.2	17.5	97.6	99.7	63.4
NBR	64.9	4.3	13.7	96.0	99.6	63.0
MSI	61.0	4.3	7.8	97.0	99.8	59.7
EVI	59.6	4.4	5.1	98.9	100	58.7
SAVI	57.9	4.3	4.5	97.4	99.9	57.1
NDVI	57.9	4.3	4.5	97.4	99.9	57.1
GRND	51.2	4.2	1.7	93.3	99.9	50.8

Source: Author's production.

For ensemble VIs, the producer's accuracy varied from 35.0% (high omission error) to 97.3% (low omission error) for the disturbance and non-disturbance classes, respectively (Table 5.2). On the other hand, user's accuracy ranged from 90.2% to 67.5%, indicating a low commission error for detecting disturbances. In Table 5.2, the contrast between producer's and user's accuracies occurs because of the differences in the proportion of the disturbed and non-disturbed classes. The disturbance class had higher user's accuracy (small commission error) and lower producer's accuracy (large omission error) than the predominant non-disturbance class in the scene. The use of an unbiased estimator accommodates the effects of map classification errors in the area estimates. Compared to the use of single VIs, a practical effect of the ensemble CCDC approach was to reduce the omission error and slightly increase the commission error (Figure 5.6).

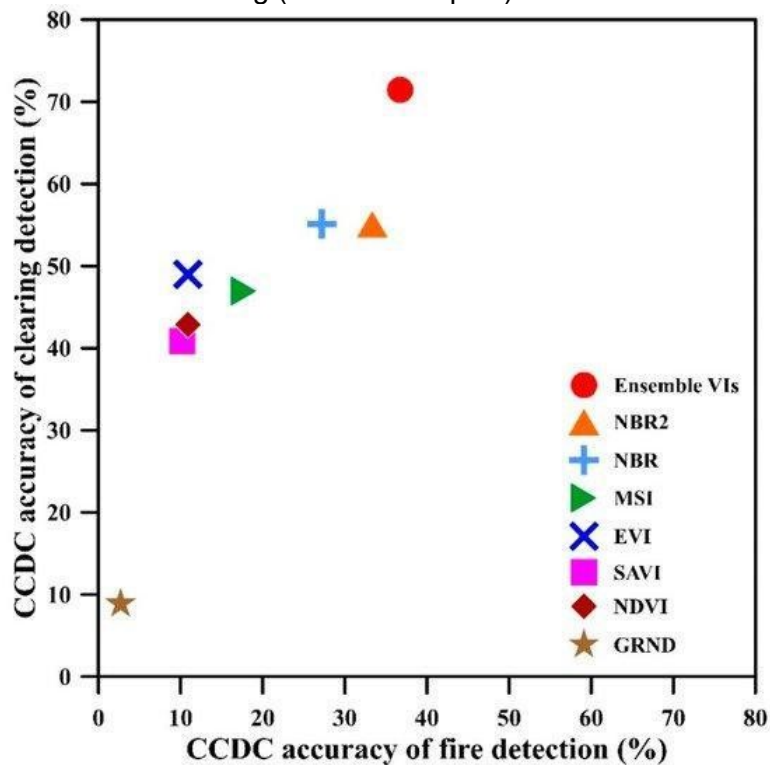
Figure 5.6 - Variations in commission and omission errors for the CCDC detection of disturbance (clearing plus fire), using different vegetation indices (VIs) and ensemble VIs.



Source: Author's production.

When we considered the performance of detection of each VI or ensemble VIs per type of disturbance, we observed higher accuracies over cleared areas than over burned areas (Figure 5.7). NBR2 had the highest accuracy values for detecting fire (34.0%) and clearing (55.2%) disturbance. Such values increased to 36.7% and 71.4%, respectively, when ensemble VIs were used as input data to CCDC (Figure 5.7).

Figure 5.7 - CCDC performance of each vegetation index (VI) and ensemble VIs to correctly detect disturbance over areas affected by fire ( $n = 147$  samples) and savanna clearing ( $n = 147$  samples).



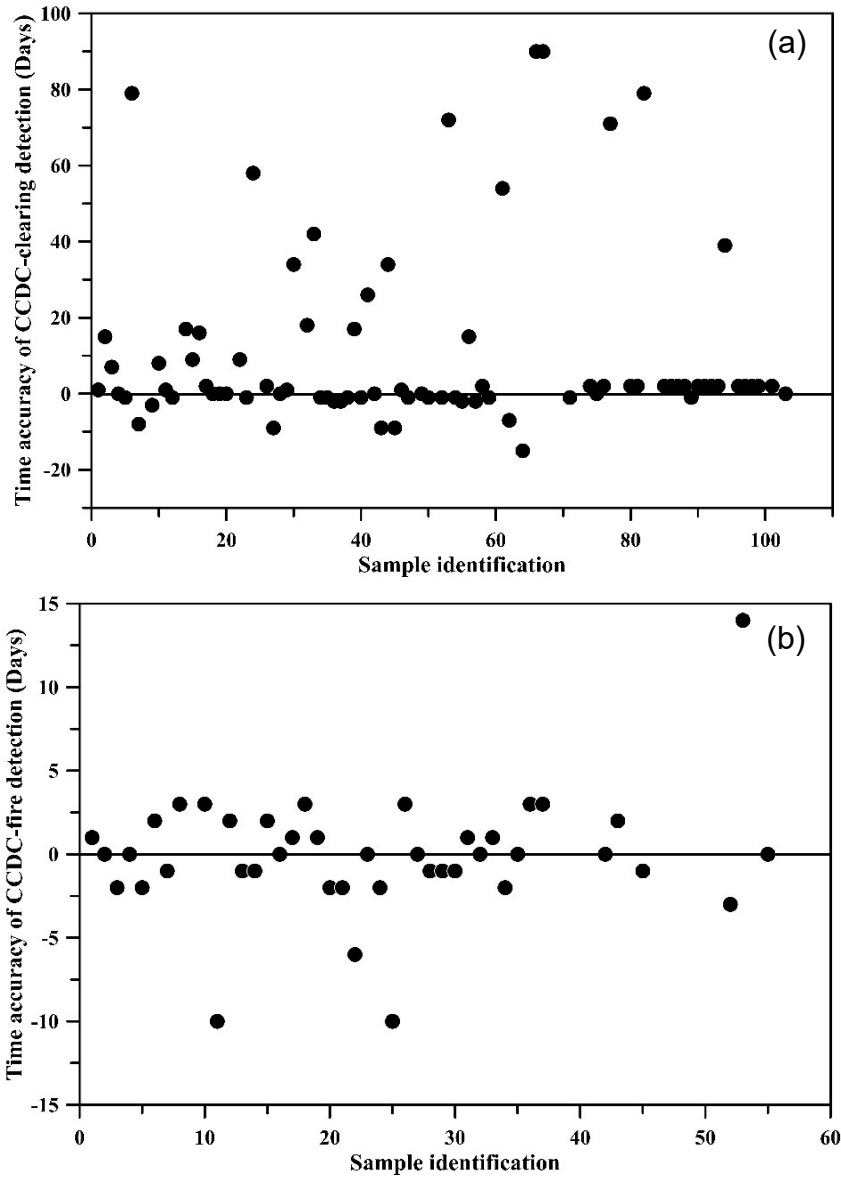
Source: Author's production.

### 5.3.3 Assessment of the correct time of disturbance

The evaluation of the correct time of CCDC-detection of disturbance occurrence from the ensemble VI approach showed larger uncertainties in days for events of savanna clearing than for events caused by fire. This fact was indicated in Figure 5.8 by the lower data dispersion around the zero-day line recorded for fire disturbance detection (Figure 5.8b) when compared to clearing detection (Figure 5.8a). Disturbance by fire comprised more abrupt events than savanna clearing, which usually includes gradual processes of degradation before the complete removal of vegetation cover. The degradation process produces uncertainties in establishing the exact date of vegetation suppression. On the other hand, clearing events are more detectable than disturbance by fire because of the predominant period of their occurrence in the beginning and middle of the dry season. The great availability of cloud-free images in this period favors the detection of three

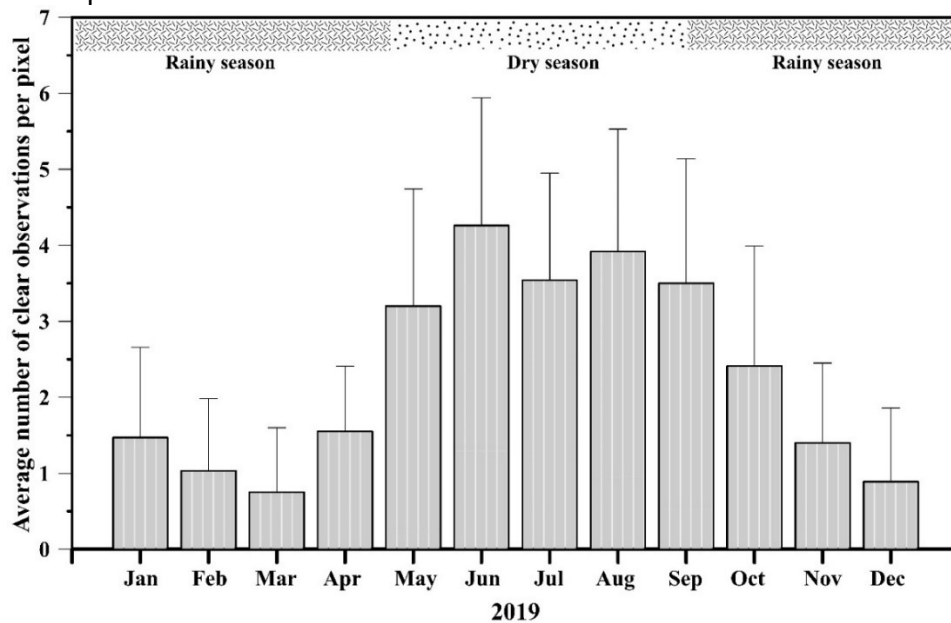
consecutive observations of clearing change by the CCDC algorithm, which does not occur for fire. Using single VIs in the data analysis, results were approximately similar to those observed with the ensemble approach.

Figure 5.8 - Time accuracy of CCDC-detection over (a) cleared- and (b) burned-savanna areas.



The availability of clear observations in the images of the study area was variable over space and time. The greatest difficulties of tracking over time such disturbance events were noted during the rainy season when the frequency of satellite observations decreased due to cloud cover and related shadows. For instance, the average number of Landsat clear observations per pixel reached its maximum value in the dry season between July and August (Figure 5.9). Therefore, the assessment of the correct time of disturbance occurrence detected by the CCDC was biased to some extent by the dry season period. Moreover, disturbances that occurred in areas with a low number of clear observations can be detected with greater delay when compared to the real date of its occurrence.

Figure 5.9 - Monthly average of Landsat cloud-free pixels in the study area during the rainy and dry seasons of 2019. The standard deviation bars are also plotted.



Source: Author's production.

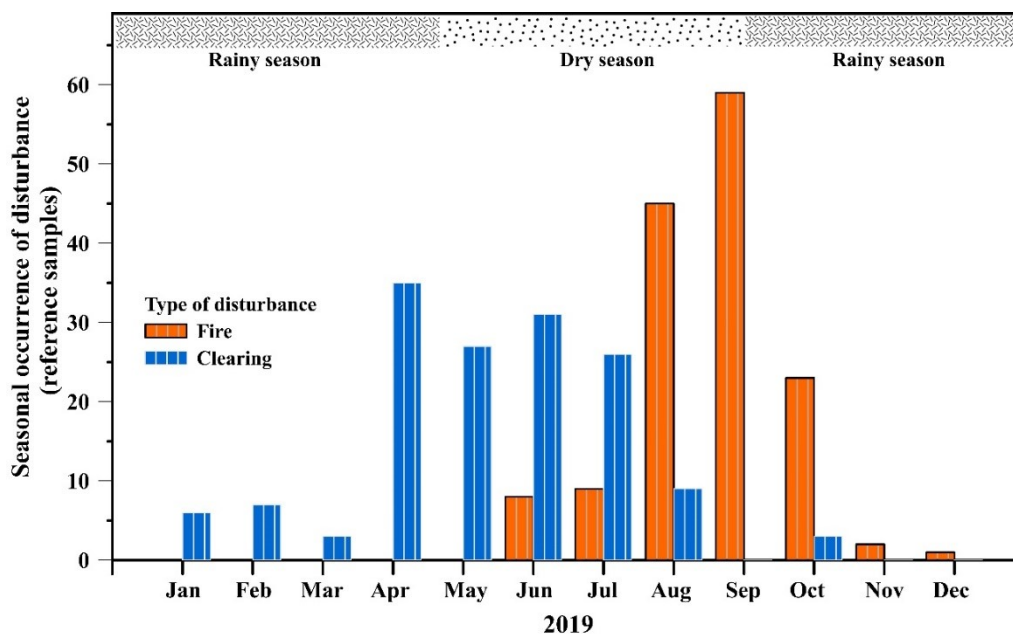
From the set of reference samples detected as disturbance by CCDC, 74% of them matched  $\pm 5$  days of the occurrence of fire. Considering the most favorable period of imagery (dry season), when the combination of sensors can generate up to four monthly observations (Figure 5.9), this difference in days is likely non-statistically significant. It is lower than the 8-day spaced interval of data acquisition in the dry season. For clearing, 70% of the reference samples

matched  $\pm 30$  days of the occurrence of the events. As mentioned before for savanna clearing, early detection by the CCDC was generally associated with processes of vegetation degradation preceding the complete removal of vegetation.

#### 5.3.4 Seasonal patterns of occurrence between savanna clearing and fire

Inspection in the reference dataset of the date of occurrence of clearing and fire events revealed the existence of a seasonal pattern of disturbance in the study area (Figure 5.10). Savanna clearing predominated between April and July, while fire disturbance mainly occurred between August and October. This result is important because the discrimination between these two types of disturbance is not an easy task using data-driven procedures. Therefore, there is a period more favorable to detect cleared areas (April to July) that precedes the largest occurrence of biomass burning (August to October) (Figure 5.10).

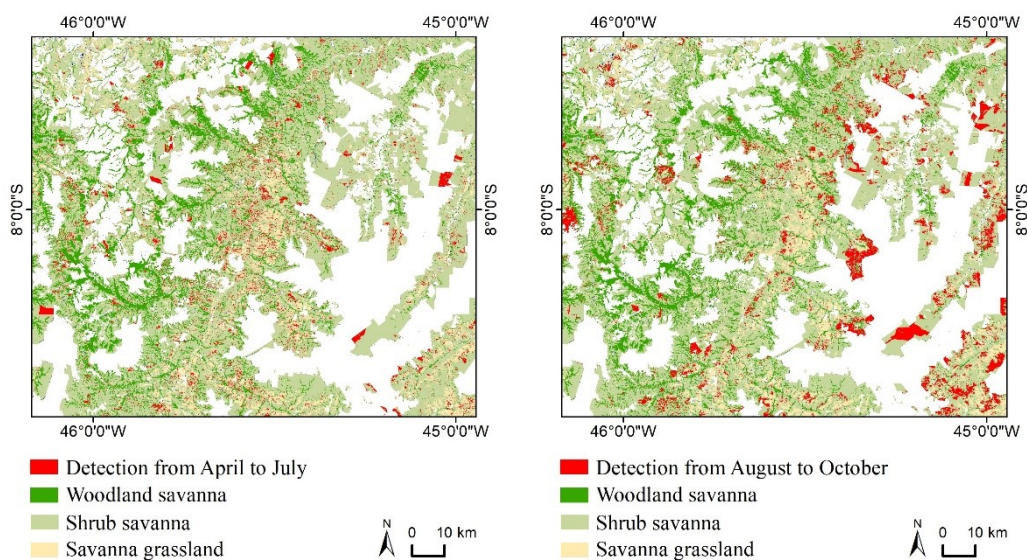
Figure 5.10 - Temporal local patterns of disturbance over areas affected by clearing and fire in 2019 for the reference samples. Savanna clearing events predominate between April and July, while fire disturbance mainly occurs between August and October.



Source: Author's production.

We plotted the CCDC-detected disturbed areas for the two periods of analysis: April to July (Figure 5.11a), and from August to October (Figure 5.11b). Assuming the existence of the seasonal pattern of disturbance observed in Figure 5.10, we anticipate that the extension of cleared areas is much smaller than that of burned areas. Furthermore, most of the disturbed areas between August and October occurred predominantly near the consolidated areas of agriculture (areas in white in Figure 5.11), indicating possible land conversion for agriculture expansion. Low air humidity, high temperatures, water stress for the plants, and great amounts of non-photosynthetic vegetation occur at the end of the dry season. These factors favor fire expansion.

Figure 5.11 - CCDC-detected disturbance over two periods of predominant occurrence of (a) savanna clearing (April–July) and (b) fire (August–October).



(a)

(b)

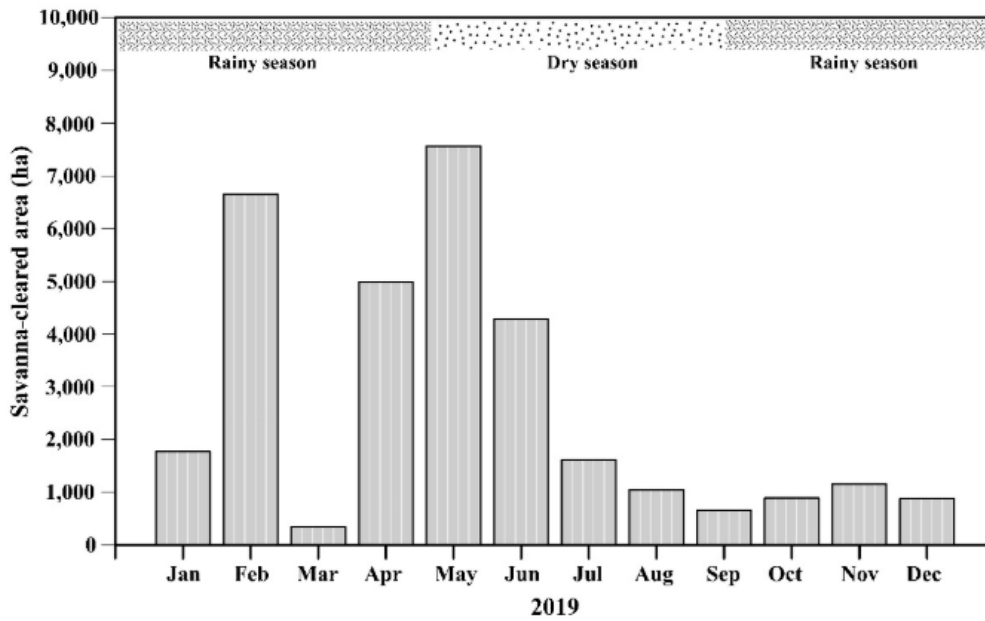
White represents consolidated areas of agriculture that have been masked before data analysis.

Source: Author's production.

The consistency of the results of Figure 5.10 and Figure 5.11 was confirmed after the inspection of cleared areas mapped in 2019 by the DETER *Cerrado* program (Figure 5.12) and of the burned areas mapped in both periods by the 250-m

MODIS FireCCI v.5.1 product (Figure 5.14). Figure 5.12 confirmed the predominance of savanna clearing events between April and July, while Figure 5.13 showed the highest frequency of fire disturbance events recorded in the second period of observation (August to October) in the vicinities of the agricultural areas (areas in white).

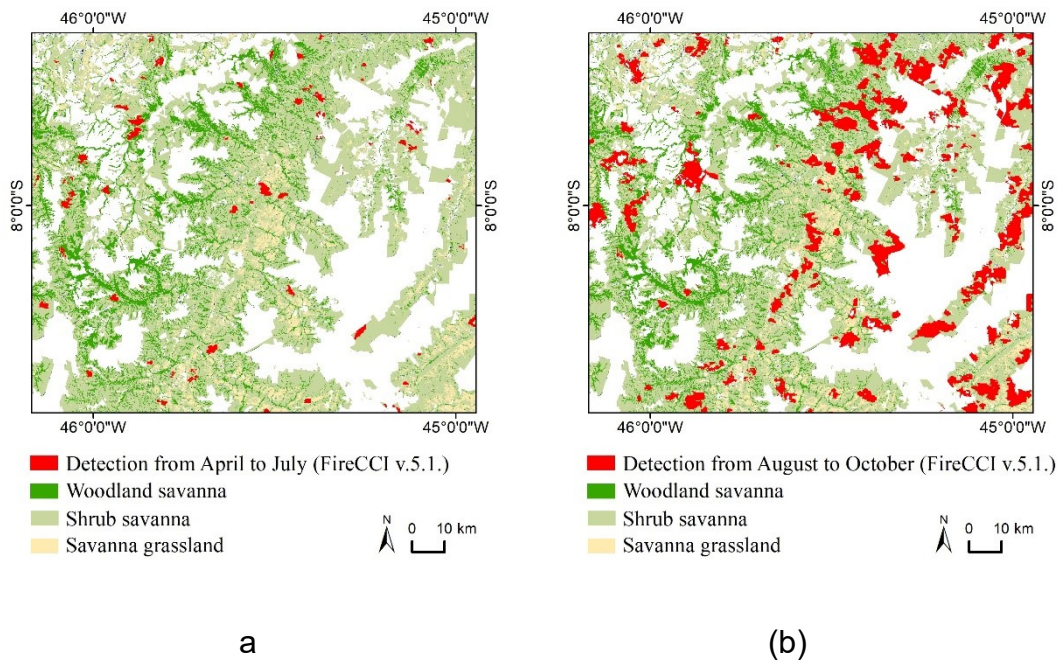
Figure 5.12 - Savanna-cleared area in 2019 mapped in the study area by the *Sistema de Detecção de Desmatamento em Tempo Real* (DETER Cerrado) from the Brazilian National Institute of Space Research (INPE).



Results confirm the existence of a predominant period of clearing (April–July) in the study area indicated in Figure 5.10.

Source: Author’s production.

Figure 5.13 - Burned area in two distinct periods of 2019, registered by the 250-m MODIS FireCCI v.5.1 product (European Space Agency—ESA): (a) April to June and (b) August to October.



Results confirmed the higher frequency of fire disturbance events observed in the second period, as indicated in Figure 10. White represents consolidated areas of agriculture that have been masked before the data analysis.

Source: Author's production.

## 5.4 Discussion

Our study has important contributions for the remote sensing of disturbance in the savanna environment. As far as we know, this is the first investigation using univariate and multivariate approaches that evaluates the detection of disturbance in the Brazilian savannas from a set of VIs that respond differently to biophysical attributes of vegetation. In addition, our investigation demonstrates for the first time the performance of each VI and ensemble VIs to detect two types of disturbance (savanna clearing and fire). Finally, it shows the existence of a seasonal pattern of occurrence between these two drivers of disturbance in the MATOPIBA region.

When compared to the available projects of *Cerrado* monitoring that are mostly based on visual interpretation of satellite data, the current approach is automated and does not require training samples to detect disturbance. This is very important because we have observed a large reflectance variability over the savanna physiognomies in response to different types and intensities of disturbance. In this context, our approach using CCDC and ensemble VIs can optimize the generation of early warning alerts of disturbance to be further inspected in the field. Our data-driven approach can be extended into other savanna areas from Brazil since the selected site is representative of the different patterns of land use, vegetation physiognomy, and geomorphology observed in a great part of the biome.

Our findings showed that the most important VIs to detect savanna clearing and fire used NIR and SWIR Landsat bands on their formulations (e.g., NBR, NBR2, and MSI). This result is not a surprise, since the first two VIs have been designed to detect burned areas (KEY; BENSON, 2006). Moreover, MSI is sensitive to changes in canopy water that may result from gradual processes of vegetation degradation (SILVA; BATES, 2002; JACON et al., 2017). It also expresses modifications in non-photosynthetic vegetation leftover in the soil surface after events of savanna clearing (e.g., dry leaves, branches, and twigs). Our findings also agree with results obtained by Bueno et al. (BUENO et al., 2019), who showed the importance of the SWIR-derived VIs (e.g., NBR and NBR2) to detect clearing at highly seasonal areas of Brazilian savannas. When using the Breaks For Additive Season and Trend (BFAST) algorithm over a savanna site located in southeastern Brazil, Bueno et al. (BUENO et al., 2020) obtained an overall accuracy ranging from 54.7% to 59.6% for different VIs. This accuracy was approximately consistent with results obtained in our work with the use of single VIs. On the other hand, it was comparatively lower than the accuracy reported for our ensemble approach (71.2%).

From a visual comparison between the VI disturbance maps, we observed that their similarity depended on the intensity of disturbance and the spectral range of VI operation. For instance, most VIs detected intense disturbance, while VIs operating at a similar spectral interval (e.g., NDVI and SAVI) produced more

similar maps. The ensemble approach using CCDC took advantage of these aspects. Using the CCDC algorithm, the ensemble approach had a better performance for detecting overall disturbance than the use of single VIs. When compared to NBR2, the ensemble VIs increased the overall accuracy of detection from 65.9% to 71.2%. This result indicates an advantage of the CCDC over other time-series algorithms that do not run with multiple input data (KENNEDY; YANG; COHEN, 2010; VERBESSELT; ZEILEIS; HEROLD, 2012b; BROOKS et al., 2017; JOSEPH HUGHES; DOUGLAS KAYLOR; HAYES, 2017). However, even for these algorithms, our results are useful when indicating single VIs that deserve attention and testing over other savanna areas of the world.

In the literature, it is very difficult to compare the results of different products generated from distinct approaches, satellite data, and sensor specifications. For instance, our approach uses a data-driven procedure with Landsat data, while the DETER *Cerrado* program involves the visual interpretation of medium spatial resolution CBERS/WFI and endmember-fraction images. Even considering the limitations of such a comparison, we observed that 73.14% of our reference samples detected as disturbed sites by CCDC were also assigned as savanna-cleared areas by the DETER *Cerrado*. On the other hand, when we compared our CCDC-detected reference samples of fire disturbance with the burned areas mapped by the 250-m MODIS FireCCI v.5.1 product, the agreement was only 40.7% on a per-pixel basis.

The differences in agreement between the clearing and burning products are explained by different factors. For instance, there is a greater duration of the signals of clearing disturbance over the OLI/Landsat-8 images when compared to burning events. Overall, our results showed that the CCDC accuracy was generally higher for detecting clearing than for mapping burned areas, but the contrary was observed for the accuracy of the actual date of disturbance occurrence. As mentioned before, the great availability of cloud-free images in the predominant period of savanna clearing favors the record of three consecutive observations in the CCDC algorithm for the assignment of change. On the other hand, fire comprises more abrupt events than savanna clearing,

which may include gradual processes of degradation. Such processes add uncertainties in establishing the exact date of vegetation suppression.

Another interesting result obtained here is the existence of a seasonal pattern of disturbance occurrence in MATOPIBA. Our results showed the predominance of savanna clearing between April and July, and of disturbance caused by fire between August and October. They were consistent with reports published by Schmidt and Eloy (SCHMIDT; ELOY, 2020) on the fire regime in the Brazilian savannas. According to them, the lack of fire management causes wildfires over native vegetated areas, especially during the late dry season (August–October) and near the agricultural fields. From 2000 to 2018, the new agricultural frontier of MATOPIBA was responsible for approximately 40% of the total cleared areas of the *Cerrado* biome and for 57% of the burned areas, as indicated by data of the MapBiomas and INPE's projects of savanna monitoring (SCHMIDT; ELOY, 2020).

Finally, our study has some constraints to consider in future investigations of savannas. For instance, we did not consider other algorithms in the analysis of disturbance. Recent studies have proposed also the use of an ensemble of time series algorithms to monitor land cover changes (BULLOCK; WOODCOCK; HOLDEN, 2020). By comparing four dense time series algorithms using simulated data, Awty-Carroll et al. (AWTY-CARROLL et al., 2019) discussed the advantages and limitations of each approach. They demonstrated the advantage of CCDC in working with multiple input variables for providing robust detection of land covers, especially when high quantities of missing data occur in the time series. This is the case with our datasets, which have distinct frequencies of satellite observations in the rainy and dry seasons of MATOPIBA due to cloud cover. In this context, we did not consider the inclusion of other satellites than Landsat (e.g., MSI/Sentinel-2) to produce denser time series. This would require strategies of data harmonization that may add other uncertainties in the data analysis. The number of images was still a limiting factor for disturbance detection in MATOPIBA, adding commission errors during the rainy season and omission errors at the end of the dry season. This limiting factor also added uncertainties in the definition of the date of disturbance occurrence. Despite these constraints,

our results reinforce the importance of data-driven procedures for the fast generation of near-real-time warning alerts of disturbance to be carefully inspected in the images and further checked in the field.

Therefore, future studies should consider hybrid satellite datasets to produce denser time series. By increasing the number of consecutive observations, the accuracy of disturbance detection by CCDC will probably increase. Future studies should also consider the use of high spatial and temporal resolution data from a constellation of satellites, especially if reflectance data from the NIR, SWIR-1 and SWIR-2 spectral regions are available for disturbance analysis. For instance, daily observations from the PlanetScope satellite constellation with a spatial resolution of 3 m should be tested over the savannas.

## **5.5 Conclusions**

The use of a time series of VIs with different sensitivities to biophysical attributes of savannas in an ensemble approach improved the CCDC-detection of disturbance when compared to the detection using single VIs. Considering the specific objectives of the work, we concluded that:

(a) The disturbance caused by clearing and fire produced significant reflectance modifications in the NIR and SWIR-1,2 Landsat bands that explained the better performance of NBR2, NBR, and MSI to detect such events.

(b) The ensemble VI approach with CCDC had an accuracy of  $71.2 \pm 4.0\%$  for detecting total disturbance (savanna clearing plus fire), reducing the omission errors when compared to the use of single VIs in the analysis. The accuracy was generally higher for detecting clearing rather than for mapping burned areas, but the opposite was observed concerning the recorded date of the occurrence of disturbance.

(c) Savanna clearing predominated in the transition from the rainy to the dry season (April to July), while most events of fire disturbance occurred between August and October toward the end of the dry season.

Finally, the results highlight the importance of data-driven approaches for generating early warning alerts of disturbance in the *Cerrado* to support programs of monitoring of savannas.

## 6 GENERAL DISCUSSION

The results of both studies presented in this thesis (Chapters 4 and 5) fill an important gap on the need of new approaches for detecting vegetation disturbances in the Cerrado. Some of the algorithms used in this study have not been evaluated in this biome yet. Such approaches have shown promising results for use in the Cerrado and may resolve some of the limitations of the change detection methods that are based on fixed thresholds. Their accuracy is affected by the existing diversity of savanna phytophysionomies and their distinct resilience to different types and intensities of disturbances (BAYMA; SANO, 2015; PESSOA et al., 2015; BARROSO et al., 2017). The current data-driven approach based on the temporal trajectory of each pixel overcomes the problem of using fixed thresholds. The data cloud processing in GEE is another highlight because it makes processing faster to allow large-scale monitoring with big data.

In addition to the change detection method itself, our study demonstrated the importance of using the complementary information retrieved from VIs calculated from different spectral bands of Landsat positioned in the visible, NIR, and SWIR regions. The complementary information of the indices reduces the omission errors of the detection methods, as demonstrated by the results using the CCDC algorithm (Chapter 5). Although not addressed in the present study, it can be anticipated that omission errors during disturbance detection will decrease after adding different VIs in the LandTrendr analysis when compared to the use of single VIs as input data (results not shown).

Despite the better performance in detecting vegetation clearing than fire events, this CCDC result is affected to some extent by the variability in the quality of the time series across years rather than the type of event. Thus, the use of a denser time series, especially in the rainy season, tends to equalize the detection performance by type of disturbance. Moreover, we observed that the quality of the time series was a decisive factor in selection of the CCDC monitoring model based on the average values of the time series of VIs. More complex models, which also consider the components of trend and seasonality, require more observations for calibration. This is sometimes difficult to obtain especially during

the rainy season when the availability of cloud-free pixels is reduced in the study area. Furthermore, as indicated by Souza and Galvão (2019), the seasonal component does not make a significant contribution to the detection of disturbance. On the other hand, the trend component is important for detecting long-term processes (e.g., land degradation). Another disadvantage of complex models is the loss of ability to detect successive disturbance events that occur within 15 observations.

The present work also contributes to the understanding of the interannual and seasonal dynamics of disturbance in the Cerrado by showing the complexity of anthropic actions over the landscapes. In addition to the behavior of cutting and burning guided by the intra-annual climatic seasonality, we observed that several regional factors (e.g., spillover effects of Soy Moratorium in Amazonia) also had a strong influence on the vegetation suppression in the Cerrado. Our results corroborate previous studies based on the topic (DOU et al., 2018; NEPSTAD et al., 2019). The suppression of the Cerrado was also strongly influenced by the geomorphological compartments of the plateaus and depressions, which is important to consider, for instance, in modeling studies of deforestation predictions. The difference between plateaus and depressions in MATOPIBA was also highlighted by Favareto et al. (2018; 2019), given its relevance in the territorial and socioeconomic dynamics of the region.

Concerning the dynamics of disturbance, our study highlights the importance of time series of VIs for detecting abrupt changes (clear-cut and fire) and subtle changes (degradation by fire) in the Cerrado vegetation. Our results show that the fire resilience of the native Cerrado is distinct from agricultural areas. The proportion of land-degraded areas increased with fire frequency over the agricultural areas. By contrast, it remained stable over the savanna areas of native vegetation. However, although the use of fire does not show evident effects on the current NDVI time series over native vegetation, its impact on species composition has already been reported in several studies (MIRANDA et al., 2009; PIVELLO et al., 2010; BUSTAMANTE et al., 2012; GARCIA; BALLESTER, 2016; TRABAQUINI et al., 2017). For instance, Loiola et al. (2010) concluded that different fire conditions may change species composition without affecting the

functional diversity of the herbaceous layer of savannas, corroborating the idea that savannas are more stable in functional aspect than in floristic terms. This agrees with the current findings. Santana (2018) also found negative trends of NDVI over agricultural areas without relation to the occurrence of fire. Indeed, fire frequency is probably not the only reason for the degradation of agricultural areas in MATOPIBA, which depends on other factors such as soil types and precipitation.

Although the studies reported in two articles and presented in this thesis (Chapters 4 and 5) had different objectives, their results complemented each other. For instance, Chapter 5 indicated the preferred periods of clearing and fire occurrence of native vegetation in MATOPIBA, which can better guide the selection of the acquisition period for LandTrendr analysis (Chapter 4), or for any other change detection approach focused on specific disturbances. Our results suggest that the selection of images from April to July tends to capture clear-cut of the Cerrado, while the images from August to October record the predominant burning events over native vegetation. In our study, we used images from the July-August-September quarter to compose the annual images that served as input data to LandTrendr, which captured the presence of both types of disturbance events.

## 7 CONCLUSIONS

Considering the hypotheses and objectives of the thesis, we concluded that:

- The largest spectral magnitude of change (pos-disturbance minus pre-disturbance value) in an annual time series was related to native vegetation clearing in the Cerrado, as shown in the first article (Chapter 4). We confirmed this hypothesis by visually inspecting the native vegetation suppression in the images in the time series. Considering one year of a confidence interval, the year of the Cerrado clearing was correctly detected by the LandTrendr algorithm in 96% of the cases. However, it is important to highlight that this result was valid for LandTrendr's strategy, which can avoid transitory disturbances. For instance, fire disturbance can result in a bigger magnitude of change, but it may quickly disappear for the satellite sensor due to vegetation recovery of some physiognomies. The generalization of this result to other methods requires further studies.
- The indiscriminate use of fire in the Cerrado causes land degradation, which is detectable using a time series of VIs. However, its effects differ between the native vegetation of Cerrado and the agricultural areas.
- The detection of clearing and fire in the Cerrado has distinct sensitivities to the VIs used as input data for detecting changes in time series. The combined use of different VIs in the analysis provides disturbance maps with higher accuracy than those obtained with single VIs. For instance, the ensemble metric approach increased the CCDC overall accuracy by 5.3% compared with the use of a single VI (e.g., NBR2).

### 7.1 Future Works

Based on the results from this thesis, we suggest using denser time series (better temporal resolution) as input data for the change detection algorithms evaluated in our work. The influence of selecting other periods to compose the annual images that served as input to LandTrendr and, consequently, on the results of omission and commission errors of detections requires further studies. The use of products with a better spatial resolution for land degradation analysis needs to be tested as well. That is the case of satellite constellations (e.g., PlanetScope).

The fast identification of the type of change (e.g., disturbance by savanna clearing or fire), by integrating other ancillary data or other spectral metrics not explored here, is also important to be tested in future studies for defining early warning alerts of disturbance.

## REFERENCES

- ALENCAR, A.; SHIMBO, J. Z.; LENTI, F.; MARQUES, C. B.; ZIMBRES, B.; ROSA, M.; ARRUDA, V.; CASTRO, I.; FERNANDES, M.; ALENCAR, I.; PIONTEKOWSKI, V.; RIBEIRO, V. Savanna Native Vegetation Using Landsat Data Processed in the Google Earth Engine Platform. **Remote Sensing**, v. 12, n. 924, p. 1–23, 2020.
- ARAÚJO, M. L. S. DE; SANO, E. E.; BOLFE, É. L.; SANTOS, J. R. N.; DOS SANTOS, J. S.; SILVA, F. B. Spatiotemporal dynamics of soybean crop in the Matopiba region, Brazil (1990–2015). **Land Use Policy**, v. 80, p. 57–67, 2019.
- ARRUDA, V. L. S.; PIONTEKOWSKI, V. J.; ALENCAR, A.; PEREIRA, R. S.; MATRICARDI, E. A. T. An alternative approach for mapping burn scars using Landsat imagery, Google Earth Engine, and Deep Learning in the Brazilian Savanna. **Remote Sensing Applications: Society and Environment**, v. 22, e100472, 2021.
- AWTY-CARROLL, K.; BUNTING, P.; HARDY, A.; BELL, G. An evaluation and comparison of four dense time series change detection methods using simulated data. **Remote Sensing**, v. 11, n. 23, 2019.
- BAI, Z. G.; DENT, D. L.; OLSSON, L.; SCHAEPMAN, M. E. Proxy global assessment of land degradation. **Soil Use and Management**, v. 24, n. 3, p. 223–234, 2008.
- BANSKOTA, A.; KAYASTHA, N.; FALKOWSKI, M. J.; WULDER, M. A.; FROESE, R. E.; WHITE, J. C. Forest monitoring using Landsat Time Series Data: a review. **Canadian Journal of Remote Sensing**, v. 40, n. 5, p. 362–384, 2014.
- BARROSO, A. G.; SANO, E. E.; FREITAS, D. M. DE; UNB, U. D. B. Identificação de desmatamentos no Cerrado utilizando técnicas de diferença de imagens e índice de queima por diferença normalizada. **Revista Brasileira de Cartografia**, v. 7, n. 69, p. 1397–1409, 2017.
- BAYMA, A. P.; SANO, E. E. Time series of vegetation indices (NDVI and EVI) from MODIS for detecting deforestation in the Cerrado biome. **Boletim de Ciências Geodésicas**, v. 21, n. 4, p. 797–813, 2015.
- BENDINI, H. DO N. **Agricultural land classification based on phenological information from dense time-series Landsat-like imagens in the Brazilian Cerrado**. 2018. 122 p. Thesis (PhD in Remote Sensing) - Instituto Nacional de Pesquisas Espaciais, São José dos Campos, 2018.
- BEUCHLE, R.; GRECCHI, R. C.; SHIMABUKURO, Y. E.; SELIGER, R.; EVA, H. D.; SANO, E.; ACHARD, F. Land cover changes in the Brazilian Cerrado and

Caatinga biomes from 1990 to 2010 based on a systematic remote sensing sampling approach. **Applied Geography**, v. 58, p. 116–127, 2015.

BOLFE, É. L.; VICTÓRIA, D. C.; CONTINI, E.; SILVA, G. B.; ARAUJO, L. S.; GOMES, D. MATOPIBA em crescimento agrícola. **Revista de Política Agrícola**, v. 1, n. 4, p. 38–62, 2016.

BRASIL. MINISTÉRIO DO MEIO AMBIENTE.

**Metodologia\_TCCerrado\_2013.pdf**. 2015. Disponível em:

<[http://www.dpi.inpe.br/tccerrado/Metodologia\\_TCCerrado\\_2013.pdf](http://www.dpi.inpe.br/tccerrado/Metodologia_TCCerrado_2013.pdf)>.

BREUNIG, F. M.; GALVÃO, L. S.; DALAGNOL, R.; DAUVE, C. E.; PARRAGA, A.; SANTI, A. L.; DELLA FLORA, D. P.; CHEN, S. Delineation of management zones in agricultural fields using cover–crop biomass estimates from PlanetScope data. **International Journal of Applied Earth Observation and Geoinformation**, v. 85, e102004, 2020.

BRITO, A.; VALERIANO, D. M.; FERRI, C.; SCOLASTRICI, A.; SESTINI, M.

**Metodologia da detecção do desmatamento no Bioma Cerrado**. São José dos Campos, SP: INPE, 2018. Disponível em:

<[http://www.obt.inpe.br/cerrado/report\\_funcate\\_metodologia\\_mapeamento\\_bioma\\_cerrado.pdf](http://www.obt.inpe.br/cerrado/report_funcate_metodologia_mapeamento_bioma_cerrado.pdf)>.

BROOKS, E. B.; YANG, Z.; THOMAS, V. A.; WYNNE, R. H. Edyn: dynamic signaling of changes to forests using exponentially weighted moving average charts. **Forests**, v. 8, n. 9, p. 1–18, 2017.

BUENO, I.; ACERBI JÚNIOR, F.; SILVEIRA, E.; MELLO, J.; CARVALHO, L.; GOMIDE, L.; WITHEY, K.; SCOLFORO, J. Object-based change detection in the Cerrado biome using Landsat Time Series. **Remote Sensing**, v. 11, n. 5, p. 570, 2019.

BUENO, I. T.; MCDERMID, G. J.; SILVEIRA, E. M. O.; HIRD, J. N.; DOMINGOS, B. I.; ACERBI JÚNIOR, F. W. Spatial agreement among vegetation disturbance maps in tropical domains using Landsat time series. **Remote Sensing**, v. 12, n. 18, 2020.

BULLOCK, E. **gee-assessment-tools documentation**. [S.l.: s.n.], 2020.

BULLOCK, E. L.; WOODCOCK, C. E.; HOLDEN, C. E. Improved change monitoring using an ensemble of time series algorithms. **Remote Sensing of Environment**, v. 238, e111165, 2020.

BUSTAMANTE, M.; NARDOTO, G.; PINTO, A.; RESENDE, J.; TAKAHASHI, F.; VIEIRA, L. Potential impacts of climate change on biogeochemical functioning of Cerrado ecosystems. **Brazilian Journal of Biology**, v. 72, n. 3 suppl, p. 655–671, 2012.

CÂMARA, G.; ASSIS, L. F.; RIBEIRO, G.; FERREIRA, K. R.; LLAPA, E.; VINHAS, L. Big earth observation data analytics: matching requirements to

system architectures. In: ACM SIGSPATIAL INTERNATIONAL WORKSHOP ON ANALYTICS FOR BIG GEOSPATIAL DATA, 5., 2016. **Proceedings...** 2016.

CLAVERIE, M.; JU, J.; MASEK, J. G.; DUNGAN, J. L.; VERMOTE, E. F.; ROGER, J. C.; SKAKUN, S. V.; JUSTICE, C. The Harmonized Landsat and Sentinel-2 surface reflectance data set. **Remote Sensing of Environment**, v. 219, p. 145–161, 2018.

COHEN, W. B.; HEALEY, S. P.; YANG, Z.; STEHMAN, S. V.; BREWER, C. K.; BROOKS, E. B.; GORELICK, N.; HUANG, C.; HUGHES, M. J.; KENNEDY, R. E.; LOVELAND, T. R.; MOISEN, G. G.; SCHROEDER, T. A.; VOGELMANN, J. E.; WOODCOCK, C. E.; YANG, L.; ZHU, Z. How similar are forest disturbance maps derived from different Landsat time series algorithms? **Forests**, v. 8, n. 4, p. 1–19, 2017.

COHEN, W. B.; YANG, Z.; KENNEDY, R. Detecting trends in forest disturbance and recovery using yearly Landsat time series: 2. TimeSync - tools for calibration and validation. **Remote Sensing of Environment**, v. 114, n. 12, p. 2911–2924, 2010.

CONSERVATION INTERNATIONAL. **Trends Earth documentation**. [S.l.: s.n.], 2019.

COPPIN, P.; JONCKHEERE, I.; NACKAERTS, K.; MUYS, B.; LAMBIN, E. Digital change detection methods in ecosystem monitoring: a review. **International Journal of Remote Sensing**, v. 25, n. 9, p. 1565–1596, 2004.

COSTA, W. S. **Mapeamento de formações campestres nativas e de pastagens cultivadas no cerrado brasileiro utilizando mineração de dados**. 2014. 107 p. Dissertação (Mestrado em Computação Aplicada) - Instituto Nacional de Pesquisas Espaciais, São José dos Campos, 2014.

DE MIRANDA, S. C.; BUSTAMANTE, M.; PALACE, M.; HAGEN, S.; KELLER, M.; FERREIRA, L. G. Regional variations in biomass distribution in Brazilian Savanna Woodland. **Biotropica**, v. 46, n. 2, p. 125–138, 2014.

DE OLIVEIRA, L. M.; GALVÃO, L. S.; PONZONI, F. J. Topographic effects on the determination of hyperspectral vegetation indices: a case study in southeastern Brazil. **Geocarto International**, v. 36, n. 19, p. 2186–2203, 2021.

DOU, Y.; DA SILVA, R. F. B.; YANG, H.; LIU, J. Spillover effect offsets the conservation effort in the Amazon. **Journal of Geographical Sciences**, v. 28, n. 11, p. 1715–1732, 2018.

EASDALE, M. H.; FARIÑA, C.; HARA, S.; PÉREZ LEÓN, N.; UMAÑA, F.; TITTONELL, P.; BRUZZONE, O. Trend-cycles of vegetation dynamics as a tool for land degradation assessment and monitoring. **Ecological Indicators**, v. 107, e105545, 2019.

EMBRAPA TERRITORIAL. **GeoMatopiba**: inteligência territorial estratégica para o Matopiba. Campinas, 2020. Disponível em: < [www.embrapa.br/geomatopiba](http://www.embrapa.br/geomatopiba) >. Acesso em: 24 maio 2022

FAVARETO, A. **Entre chapadas e baixões do MATOPIBA**: dinâmicas territoriais e impactos socioeconômicos na fronteira da expansão agropecuária no Cerrado. São Paulo: Prefixo Editorial, 2019. 272 p. ISBN 9788592545093.

FAVARETO, A. S.; NAKAGAWA, L.; KLEEB, S. C.; SEIFER, P. G.; PÓ, M. A expansão do agronegócio e a disputa pelo cerrado. **Greenpeace**, p. 100, 2018.

FERREIRA, N. C.; FERREIRA, L. G.; FERREIRA, M. E.; BUSTAMANTE, M.; OMETTO, J. Assessing deforestation related carbon emission in the Brazilian Savanna based on moderate resolution imagery. **International Geoscience and Remote Sensing Symposium (IGARSS)**, p. 748–751, 2011.

FLOOD, N. Seasonal composite landsat TM/ETM+ Images using the medoid (a multi-dimensional median). **Remote Sensing**, v. 5, n. 12, p. 6481–6500, 2013.

FOGA, S.; SCARAMUZZA, P. L.; GUO, S.; ZHU, Z.; DILLEY, R. D.; BECKMANN, T.; SCHMIDT, G. L.; DWYER, J. L.; JOSEPH HUGHES, M.; LAUE, B. Cloud detection algorithm comparison and validation for operational Landsat data products. **Remote Sensing of Environment**, v. 194, p. 379–390, 2017.

FRANÇOSO, R. D.; BRANDÃO, R.; NOGUEIRA, C. C.; SALMONA, Y. B.; MACHADO, R. B.; COLLI, G. R. Habitat loss and the effectiveness of protected areas in the Cerrado Biodiversity Hotspot. **Natureza e Conservação**, v. 13, n. 1, p. 35–40, 2015.

FUENTES, M.; MILLARD, K.; LAURIN, E. Big geospatial data analysis for Canada's Air Pollutant Emissions Inventory (APEI): using google earth engine to estimate particulate matter from exposed mine disturbance areas. **GIScience and Remote Sensing**, v. 57, n. 2, p. 245–257, 2020.

GALVÃO, L. S.; SOUZA, A. A.; BREUNIG, F. M. A hyperspectral experiment over tropical forests based on the EO-1 orbit change and PROSAIL simulation change and PROSAIL simulation. **GIScience & Remote Sensing**, p. 1–17, 2019.

GAO, Q.; LI, Y.; WAN, Y.; LIN, E.; XIONG, W.; JIANGCUN, W.; WANG, B.; LI, W. Grassland degradation in Northern Tibet based on remote sensing data. **Journal of Geographical Sciences**, v. 16, n. 2, p. 165–173, 2006.

GARCIA, A. S.; BALLESTER, M. V. R. Land cover and land use changes in a Brazilian Cerrado landscape: drivers, processes, and patterns. **Journal of Land Use Science**, v. 11, n. 5, p. 538–559, 2016.

GIBBS, H. K.; RAUSCH, L.; MUNGER, J.; SCHELLY, I.; MORTON, D. C.; NOOJIPADY, P.; SOARES-FILHO, B.; BARRETO, P.; MICOL, L.; WALKER, N.

F. Brazil's Soy Moratorium. **Science**, v. 347, n. 6220, p. 377–378, 2015.

GIROLAMO NETO, C. D. **Identificação de fitofisionomias de Cerrado no Parque Nacional de Brasília utilizando Random Forest aplicado a imagens de alta e média resoluções espaciais**. 2018. Tese (Doutorado em Sensoriamento Remoto) - Instituto Nacional de Pesquisas Espaciais, São José dos Campos, 2018. Disponível em: <<http://urlib.net/8JMKD3MGP3W34R/3RU6Q68>>.

GÓMEZ, C.; WHITE, J. C.; WULDER, M. A. Optical remotely sensed time series data for land cover classification: a review. **ISPRS Journal of Photogrammetry and Remote Sensing**, v. 116, p. 55–72, 2016.

GONZALEZ-ROGLICH, M.; ZVOLEFF, A.; NOON, M.; LINIGER, H.; FLEINER, R.; HARARI, N.; GARCIA, C. Synergizing global tools to monitor progress towards land degradation neutrality: Trends.Earth and the World Overview of Conservation Approaches and Technologies sustainable land management database. **Environmental Science and Policy**, v. 93, p. 34–42, 2019.

GORELICK, N.; HANCHER, M.; DIXON, M.; ILYUSHCHENKO, S.; THAU, D.; MOORE, R. Google Earth Engine: planetary-scale geospatial analysis for everyone. **Remote Sensing of Environment**, v. 202, p. 18–27, 2017.

GRAESSER, J.; AIDE, T. M.; GRAU, H. R.; RAMANKUTTY, N. Cropland/pastureland dynamics and the slowdown of deforestation in Latin America. **Environmental Research Letters**, v. 10, n. 3, 2015.

GRIFFITHS, P.; JAKIMOW, B.; HOSTERT, P. Reconstructing long term annual deforestation dynamics in Pará and Mato Grosso using the Landsat archive. **Remote Sensing of Environment**, v. 216, p. 497–513, 2018.

GUIDOTTI, V.; FREITAS, F. L. M.; SPAROVEK, G.; PINTO, L. F. G.; HAMAMURA, C.; CARVALHO, T.; CERIGNONI, F. Números detalhados do novo Código Florestal e suas implicações para os principais resultados e considerações. **Sustentabilidade em Debate**, n.5, p. 1–11, 2017.

GUMMA, M. K.; THENKABAIL, P. S.; TELUGUNTLA, P. G.; OLIPHANT, A.; XIONG, J.; GIRI, C.; PYLA, V.; DIXIT, S.; WHITBREAD, A. M. Agricultural cropland extent and areas of South Asia derived using Landsat satellite 30-m time-series big-data using random forest machine learning algorithms on the Google Earth Engine cloud. **GIScience and Remote Sensing**, v. 57, n. 3, p. 302–322, 2020.

HUETE, A.; DIDAN, K.; MIURA, T.; RODRIGUEZ, E. .; GAO, X.; FERREIRA, L. Overview of the radiometric and biophysical performance of the MODIS vegetation indices. **Remote Sensing of Environment**, v. 83, n. 1, p. 195–213, 2002.

HUETE, A. R. A Soil-Adjusted Vegetation Index (SAVI). **Remote Sensing of**

**Environment**, v. 25, n. 1, p. 295–309, 1988.

HUNT, E. R.; ROCK, B. N. Detection of changes in leaf water content using Near- and Middle-Infrared reflectances. **Remote Sensing of Environment**, v. 30, n. 1, p. 43–54, 1989.

HUSSAIN, M.; CHEN, D.; CHENG, A.; WEI, H.; STANLEY, D. Change detection from remotely sensed images: From pixel-based to object-based approaches. **ISPRS Journal of Photogrammetry and Remote Sensing**, v. 80, p. 91–106, 2013.

INSTITUTO BRASILEIRO DE GEOGRAFIA E ESTATÍSTICA (IBGE). **Manual técnico da vegetação brasileira**. Rio de Janeiro: IBGE, 2012. ISBN 9788524042225.

INSTITUTO NACIONAL DE PESQUISAS ESPACIAIS (INPE). **Metodologia utilizada nos projetos PRODES e DETER**. São José dos Campos, SP: INPE, 2019. Disponível em:  
<[http://www.obt.inpe.br/OBT/assuntos/programas/amazonia/prodes/pdfs/Methodologia\\_Prodes\\_Deter\\_revisada.pdf](http://www.obt.inpe.br/OBT/assuntos/programas/amazonia/prodes/pdfs/Methodologia_Prodes_Deter_revisada.pdf)>.

JACON, A. D. **Caracterização espectro-sazonal de fitofisionomias do Cerrado e estimativa de biomassa usando dados do sensor Hyperion/EO-1**. 2016. 144. Dissertação (Mestrado em Sensoriamento Remoto) - Instituto Nacional de Pesquisas Espaciais, São José dos Campos, 2016. Disponível em:  
<<http://urlib.net/8JMKD3MGP3W34P/3LD4TUP>>.

JACON, A. D.; GALVÃO, L. S.; DALAGNOL, R.; DOS SANTOS, J. R. Aboveground biomass estimates over Brazilian savannas using hyperspectral metrics and machine learning models: experiences with Hyperion/EO-1. **GIScience & Remote Sensing**, p. 1–18, 2021.

JACON, A. D.; GALVÃO, L. S.; SANTOS, J. R. DOS; SANO, E. E. Seasonal characterization and discrimination of savannah physiognomies in Brazil using hyperspectral metrics from hyperion/EO-1. **International Journal of Remote Sensing**, v. 38, n. 15, p. 4494–4516, 2017.

JACQUIN, A.; SHEEREN, D.; LACOMBE, J. P. Vegetation cover degradation assessment in Madagascar savanna based on trend analysis of MODIS NDVI time series. **International Journal of Applied Earth Observation and Geoinformation**, v. 12, Suppl. 1, p. 3–10, 2010.

JOSEPH HUGHES, M.; DOUGLAS KAYLOR, S.; HAYES, D. J. Patch-based forest change detection from Landsat time series. **Forests**, v. 8, n. 5, p. 1–22, 2017.

KENNEDY, R. E.; ANDRÉFOUËT, S.; COHEN, W. B.; GÓMEZ, C.; GRIFFITHS, P.; HAIS, M.; HEALEY, S. P.; HELMER, E. H.; HOSTERT, P.; LYONS, M. B.; MEIGS, G. W.; PFLUGMACHER, D.; PHINN, S. R.; POWELL,

S. L.; SCARTH, P.; SEN, S.; SCHROEDER, T. A.; SCHNEIDER, A.; SONNENSCHNEIN, R.; VOGELMANN, J. E.; WULDER, M. A.; ZHU, Z. Bringing an ecological view of change to landsat-based remote sensing. **Frontiers in Ecology and the Environment**, v. 12, n. 6, p. 339–346, 2014.

KENNEDY, R. E.; YANG, Z.; COHEN, W. B. Detecting trends in forest disturbance and recovery using yearly Landsat time series: 1. LandTrendr - Temporal segmentation algorithms. **Remote Sensing of Environment**, v. 114, n. 12, p. 2897–2910, 2010.

KENNEDY, R. E.; YANG, Z.; GORELICK, N.; BRAATEN, J.; CAVALCANTE, L.; COHEN, W. B.; HEALEY, S. Implementation of the LandTrendr algorithm on Google Earth Engine. **Remote Sensing**, v. 10, n. 5, p. 1–10, 2018.

KEY, C. H.; BENSON, N. C. **Landscape Assessment (LA) sampling and analysis methods**. [S.I.]: USDA Forest Service, 2006.

LEITE, L. R.; DE CARVALHO, L. M. T.; DA SILVA, F. M. Detecção de mudanças em florestas e savanas utilizando análise estatística baseada em objetos geográficos. **Boletim de Ciências Geodesicas**, v. 23, n. 2, p. 284–295, 2017.

LIESENBERG, V.; GALVÃO, L. S.; PONZONI, F. J. Variations in reflectance with seasonality and viewing geometry: Implications for classification of Brazilian savanna physiognomies with MISR/Terra data. **Remote Sensing of Environment**, v. 107, n. 1–2, p. 276–286, 2007.

LIMA, J. E. F. W.; SILVA, E. M. Estimativa da produção hídrica superficial do Cerrado brasileiro. **Cerrado: Ecologia, Biodiversidade e Conservação**, p. 61–72, 2005.

LIMA, M.; SILVA JUNIOR, C. A.; RAUSCH, L.; GIBBS, H. K.; JOHANN, J. A. Demystifying sustainable soy in Brazil. **Land Use Policy**, v. 82, p. 349–352, 2019.

LIU, L.; XIAO, X.; QIN, Y.; WANG, J.; XU, X.; HU, Y.; QIAO, Z. Mapping cropping intensity in China using time series Landsat and Sentinel-2 images and Google Earth Engine. **Remote Sensing of Environment**, v. 239, 2020.

LU, D.; MAUSEL, P.; BRONDÍZIO, E.; MORAN, E. Change detection techniques. **International Journal of Remote Sensing**, v. 25, n. 12, p. 2365–2401, 2004.

MEIRA, M. B.; EDUARDO, L.; MAURANO, P.; ALMEIDA, C. A.; ALESSANDRA, B.; GOMES, R.; ADAMI, M.; RAFAEL, R.; OLIVEIRA, S.; LOPES, G.; GURGEL, R. S. Avaliação da acurácia temática do mapeamento de desmatamento no bioma Cerrado na região do MATOPIBA. In: SIMPÓSIO BRASILEIRO DE SENSORIAMENTO REMOTO, 19., 2019. **Anais...** São José dos Campos: INPE, 2019

MESQUITA, B. A. **O desenvolvimento desigual da agricultura: a dinâmica do agronegócio e da agricultura familiar.** [S.l.]: EDUFMA, 2011. ISBN 9788578622022.

MIRANDA, H. S.; SATO, M. N.; NETO, W. N.; AIRES, F. S. Fires in the cerrado, the Brazilian savanna. **Tropical Fire Ecology**, v. 2, p. 427–450, 2009.

MOURA, Y. M.; GALVÃO, L. S.; HILKER, T.; WU, J.; SALESKA, S.; DO AMARAL, C. H.; NELSON, B. W.; LOPES, A. P.; WIEDEMAN, K. K.; PROHASKA, N.; DE OLIVEIRA, R. C.; MACHADO, C. B.; ARAGÃO, L. E. O. C. Spectral analysis of amazon canopy phenology during the dry season using a tower hyperspectral camera and modis observations. **ISPRS Journal of Photogrammetry and Remote Sensing**, v. 131, p. 52–64, 2017.

MURILLO-SANDOVAL, P. J.; HOEK, J. VAN DEN; HILKER, T. Leveraging multi-sensor time series datasets to map short- and long-term tropical forest disturbances in the Colombian Andes. **Remote Sensing**, v. 9, n. 2, p. 1–17, 2017.

MYERS, N.; A, M. R.; MITTERMEIER, C. G.; FONSECA, G. A. .; KENT, F. Biodiversity hotspots for conservation priorities. **Nature**, v. 468, n. 7326, p. 895, 2000.

NEPSTAD, L. S.; GERBER, J. S.; HILL, J. D.; DIAS, L. C. P.; COSTA, M. H.; WEST, P. C. Pathways for recent Cerrado soybean expansion: extending the soy moratorium and implementing integrated crop livestock systems with soybeans. **Environmental Research Letters**, v. 14, n. 4, 2019.

NOOJIPADY, P.; MORTON, C. D.; MACEDO, N. M.; VICTORIA, C. D.; HUANG, C.; GIBBS, K. H.; BOLFE, L. E. Forest carbon emissions from cropland expansion in the Brazilian Cerrado biome. **Environmental Research Letters**, v. 12, n. 2, 2017.

OLIVERAS, I.; MEIRELLES, S. T.; HIRAKURI, V. L.; FREITAS, C. R.; MIRANDA, H. S.; PIVELLO, V. R. Effects of fire regimes on herbaceous biomass and nutrient dynamics in the Brazilian savanna. **International Journal of Wildland Fire**, v. 22, n. 3, p. 368–380, 2013.

OLOFSSON, P.; FOODY, G. M.; HEROLD, M.; STEHMAN, S. V.; WOODCOCK, C. E.; WULDER, M. A. Good practices for estimating area and assessing accuracy of land change. **Remote Sensing of Environment**, v. 148, p. 42–57, 2014.

PARENTE, L.; NOGUEIRA, S.; BAUMANN, L.; ALMEIDA, C.; MAURANO, L.; AFFONSO, A. G.; FERREIRA, L. Quality assessment of the PRODES Cerrado deforestation data. **Remote Sensing Applications: Society and Environment**, v. 21, 2021.

PEREIRA, A. A.; TEIXEIRA, F. R.; LIBONATI, R.; MELCHIORI, E. A.;

- MARCELO, L.; CARVALHO, T. Avaliação de índices espectrais para identificação de áreas queimadas no Cerrado utilizando dados Landsat TM. **Revista Brasileira de Cartografia**, v. 68, n. 8, p. 1665–1680, 2016.
- PEREIRA, O. J. R.; FERREIRA, L. G.; PINTO, F.; BAUMGARTEN, L. Assessing pasture degradation in the Brazilian Cerrado based on the analysis of MODIS NDVI time-series. **Remote Sensing**, v. 10, n. 11, 2018.
- PESSOA, O. A. A.; BAPTISTA, G. M. M.; ALMEIDA, T.; MENESES, P. R. Monitoramento da reflectância espectral após extinção do fogo e uma proposta para a detecção de áreas queimadas em vegetação campestre de Cerrado. **Revista Brasileira de Cartografia**, v. 67, n. 6, p. 1131–1143, 2015.
- PICOLI, M. C. A.; CAMARA, G.; SANCHES, I.; SIMÕES, R.; CARVALHO, A.; MACIEL, A.; COUTINHO, A.; ESQUERDO, J.; ANTUNES, J.; BEGOTTI, R. A.; ARVOR, D.; ALMEIDA, C. Big earth observation time series analysis for monitoring Brazilian agriculture. **ISPRS Journal of Photogrammetry and Remote Sensing**, v. 145, p. 328–339, 2018.
- PIVELLO, V. R. The use of fire in the cerrado and Amazonian rainforests of Brazil: Past and present. **Fire Ecology**, v. 7, n. 1, p. 24–39, 2011.
- PIVELLO, V. R.; OLIVERAS, I.; MIRANDA, H. S.; HARIDASAN, M.; SATO, M. N.; MEIRELLES, S. T. Effect of fires on soil nutrient availability in an open savanna in Central Brazil. **Plant and Soil**, v. 337, n. 1, p. 111–123, 2010.
- RADKE, R. J.; ANDRA, S.; AL-KOFAHI, O.; ROYSAM, B. Image change detection algorithms: a systematic survey. **IEEE Transactions on Image Processing**, v. 14, n. 3, p. 294–307, 2005.
- RATANA, P.; HUETE, A. R.; FERREIRA, L. Analysis of cerrado physiognomies and conversion in the MODIS seasonal-temporal domain. **Earth Interactions**, v. 9, n. 1, 2005.
- RAUSCH, L. L.; GIBBS, H. K.; SCHELLY, I.; BRANDÃO, A.; MORTON, D. C.; FILHO, A. C.; STRASSBURG, B.; WALKER, N.; NOOJIPADY, P.; BARRETO, P.; MEYER, D. Soy expansion in Brazil's Cerrado. **Conservation Letters**, 2019.
- ROUSE, J. W.; HASS, R. H.; SCHELL, J. A.; DEERING, D. W. Monitoring vegetation systems in the great plains with ERTS. In: EARTH RESOURCES TECHNOLOGY SATELLITE SYMPOSIUM, 3., 1973. **Proceedings...** 1973. p. 309–317.
- ROY, D. P.; KOVALSKYY, V.; ZHANG, H. K.; VERMOTE, E. F.; YAN, L.; KUMAR, S. S.; EGOROV, A. Characterization of Landsat-7 to Landsat-8 reflective wavelength and normalized difference vegetation index continuity. **Remote Sensing of Environment**, v. 185, p. 57–70, 2016.
- SANO, E. E.; FERREIRA, L. G.; ASNER, G. P.; STEINKE, E. T. Spatial and

temporal probabilities of obtaining cloud-free Landsat images over the Brazilian tropical savanna. **International Journal of Remote Sensing**, v. 28, n. 12, p. 2739–2752, 2007.

SANO, E. E.; RODRIGUES, A. A.; MARTINS, E. S.; BETTIOL, G. M.; BUSTAMANTE, M. M. C.; BEZERRA, A. S.; COUTO, A. F.; VASCONCELOS, V.; SCHÜLER, J.; BOLFE, E. L. Cerrado ecoregions: a spatial framework to assess and prioritize Brazilian savanna environmental diversity for conservation. **Journal of Environmental Management**, v. 232, p. 818–828, 2019a.

SANO, E. E.; ROSA, R.; BRITO, J. L. S.; FERREIRA, L. G. Land cover mapping of the tropical savanna region in Brazil. **Environmental Monitoring and Assessment**, v. 166, n. 1–4, p. 113–124, 2010.

SANO, E. E.; ROSA, R.; SCARAMUZZA, C. A. M.; ADAMI, M.; BOLFE, E. L.; COUTINHO, A. C.; ESQUERDO, J. C. D. M.; MAURANO, L. E. P.; NARVAES, I. S.; OLIVEIRA FILHO, F. J. B.; SILVA, E. B.; VICTORIA, D. C.; FERREIRA, L. G.; BRITO, J. L. S.; BAYMA, A. P.; OLIVEIRA, G. H.; BAYMA-SILVA, G. Land use dynamics in the Brazilian Cerrado in the period from 2002 to 2013. **Pesquisa Agropecuária Brasileira**, v. 54, 2019b.

SANTANA, N. C. Fire recurrence and normalized difference vegetation index (NDVI) dynamics in Brazilian savanna. **Fire**, v. 2, n. 1, p. 1–17, 2019.

SANTOS, H. G.; CARVALHO JÚNIOR, W.; DART, R. O.; ÁGLIO, M. L. D.; SOUSA, J. S.; PARES, J. G.; FONTANA, A.; MARTINS, A. L. S.; OLIVEIRA, A. P. O. **O novo mapa de solos do Brasil**: legenda atualizada. Rio de Janeiro: Embrapa Solos, 2011.

SCHMIDT, I. B.; ELOY, L. Fire regime in the Brazilian Savanna: Recent changes, policy and management. **Flora: Morphology, Distribution, Functional Ecology of Plants**, v. 268, e151613, 2020.

SCHUCKNECHT, A.; ERASMI, S.; NIEMEYER, I.; MATSCHULLAT, J. Assessing vegetation variability and trends in north-eastern Brazil using AVHRR and MODIS NDVI time series. **European Journal of Remote Sensing**, v. 46, n. 1, p. 40–59, 2013.

SCHWIEDER, MARCEL; LEITÃO, PEDRO J.; BUSTAMANTE, M.M.C.; FERREIRA, LAERTE GUIMARÃES, RABE A.; HOSTERT, P. Mapping Brazilian savanna vegetation gradients with Landsat time series. **International Journal of Applied Earth Observation and Geoinformation**, v. 52, p. 318–327, 2016.

SCHWIEDER, M.; LEITÃO, P. J.; PINTO, J. R. R.; TEIXEIRA, A. M. C.; PEDRONI, F.; SANCHEZ, M.; BUSTAMANTE, M. M.; HOSTERT, P. Landsat phenological metrics and their relation to aboveground carbon in the Brazilian Savanna. **Carbon Balance and Management**, v. 13, n. 1, p. 1–15, 2018.

SHIMIZU, K.; OTA, T.; MIZOUE, N. Detecting forest changes using dense Landsat 8 and Sentinel-1 time series data in tropical seasonal forests. **Remote Sensing**, v. 11, n. 16, p. 1–22, 2019.

SILVA, C. V. J.; COSTA, O. B.; MATRICARDI, E. A. T. Detecção de cicatrizes de fogo na vegetação Cerrado do Distrito Federal entre 1999 a 2011. **Revista Brasileira de Cartografia**, v. 69/4, p. 687–699, 2017.

SILVA, J. M. C.; BATES, J. M. Biogeographic patterns and conservation in the South American Cerrado: a tropical Savanna hotspot. **BioScience**, v. 52, n. 3, p. 225, 2002.

SILVEIRA, E. M. O.; ESPÍRITO-SANTO, F. D. B.; ACERBI-JÚNIOR, F. W.; GALVÃO, L. S.; WITHEY, K. D.; BLACKBURN, G. A.; DE MELLO, J. M.; SHIMABUKURO, Y. E.; DOMINGUES, T.; SCOLFORO, J. R. S. Reducing the effects of vegetation phenology on change detection in tropical seasonal biomes. **GIScience and Remote Sensing**, v. 56, n. 5, p. 699–717, 2019.

SILVEIRA, E. M. O.; BUENO, I. T.; ACERBI-JUNIOR, F. W.; MELLO, J. M.; SCOLFORO, J. R. S.; WULDER, M. A. Using spatial features to reduce the impact of seasonality for detecting tropical forest changes from landsat time series. **Remote Sensing**, v. 10, n. 6, 2018.

SIMS, N. C.; ENGLAND, J. R.; NEWNHAM, G. J.; ALEXANDER, S.; GREEN, C.; MINELLI, S.; HELD, A. Developing good practice guidance for estimating land degradation in the context of the United Nations Sustainable Development Goals. **Environmental Science and Policy**, v. 92, p. 349–355, 2019.

SIMS, N. C.; GREEN, C.; NEWNHAM, G. J.; ENGLAND, J. R.; HELD, A.; WULDER, M. A.; HEROLD, M.; COX, S. J. D.; HUETE, A. R.; KUMAR, L.; VISCARRA-ROSSEL, R. A.; ROXBURGH, S. H.; MCKENZIE, N. J. **Good practice guidance: SDG Indicator 15.3.1. Version 1.0. [S.I.]**: UNCCD, 2017.

SOTERRONI, A. C.; RAMOS, F. M.; MOSNIER, A.; FARGIONE, J.; ANDRADE, P. R.; BAUMGARTEN, L.; PIRKER, J.; OBERSTEINER, M.; KRAXNER, F.; CÂMARA, G.; CARVALHO, A. X. Y.; POLASKY, S. Expanding the soy moratorium to Brazil's Cerrado. **Science Advances**, v. 5, n. 7, 2019.

SOUZA, A. A.; GALVÃO, L. S.; KORTING, T. S.; ALMEIDA, C. A. On a data-driven approach for detecting disturbance in the Brazilian Savannas using time series of vegetation indices. **Remote Sensing**, v. 13, n. 24, 2021.

SOUZA, A. A.; GALVÃO, L. S.; KORTING, T. S.; PRIETO, J. D. Dynamics of savanna clearing and land degradation in the newest agricultural frontier in Brazil. **GIScience and Remote Sensing**, v. 57, n. 7, p. 965–984, 2020a.

SOUZA, A. A.; GALVÃO, L. S.; SANTOS, J. R. Relationships between Hyperion-derived vegetation indices, biophysical parameters, and elevation data in a Brazilian savannah environment. **Remote Sensing Letters**, v. 1, n. 1,

p. 55–64, 2010.

SOUZA, C. M.; SHIMBO, J. Z.; ROSA, M. R.; PARENTE, L. L.; ALENCAR, A. A.; RUDORFF, B. F. T.; HASENACK, H.; MATSUMOTO, M.; FERREIRA, L. G.; SOUZA-FILHO, P. W. M.; DE OLIVEIRA, S. W.; ROCHA, W. F.; FONSECA, A. V.; MARQUES, C. B.; DINIZ, C. G.; COSTA, D.; MONTEIRO, D.; ROSA, E. R.; VÉLEZ-MARTIN, E.; WEBER, E. J.; LENTI, F. E. B.; PATERNOST, F. F.; PAREYN, F. G. C.; SIQUEIRA, J. V.; VIERA, J. L.; NETO, L. C. F.; SARAIVA, M. M.; SALES, M. H.; SALGADO, M. P. G.; VASCONCELOS, R.; GALANO, S.; MESQUITA, V. V.; AZEVEDO, T. Reconstructing three decades of land use and land cover changes in brazilian biomes with landsat archive and earth engine. **Remote Sensing**, v. 12, n. 17, 2020b.

SOUZA, A. A. DE; GALVÃO, L. S. Trajetórias de mudança no uso e cobertura da terra e seu impacto na temperatura de superfície MODIS em áreas de Cerrado. In: SIMPÓSIO BRASILEIRO DE SENSORIAMENTO REMOTO, 19., 2019. **Anais...** São José dos Campos: INPE, 2019.

SOUZA, A. A.; GALVÃO, L. S.; KORTING, T. S.; SOUZA, A. A. Dynamics of savanna clearing and land degradation in the newest agricultural frontier in Brazil Dynamics of savanna clearing and land degradation in the newest agricultural. **GIScience & Remote Sensing**, p. 1–20, 2020c.

SPAGNOLO, T. F. DE O. **Análise da dinâmica espacial da expansão agrícola no oeste baiano entre 1984 E 2008: estudo de caso do município de São Desidério-BA.** 2011. 77p. Dissertação (Mestrado em Geografia) - Universidade de Brasília, Brasília, 2011. Disponível em: <<https://repositorio.unb.br/handle/10482/8830>>.

SPAROVEK, G.; BERNDES, G.; BARRETTO, A. G. O. P.; KLUG, I. L. F. The revision of the brazilian forest act: Increased deforestation or a historic step towards balancing agricultural development and nature conservation? **Environmental Science and Policy**, v. 16, p. 65–72, 2012.

SPERA, S. Agricultural intensification can preserve the brazilian Cerrado: applying lessons from Mato Grosso and Goiás to Brazil's last agricultural frontier. **Tropical Conservation Science**, v. 10, 2017.

SPERA, S. A.; GALFORD, G. L.; COE, M. T.; MACEDO, M. N.; MUSTARD, J. F. Land-use change affects water recycling in Brazil's last agricultural frontier. **Global change biology**, v. 22, n. 10, p. 3405–3413, 2016.

TAMIMINIA, H.; SALEHI, B.; MAHDIANPARI, M.; QUACKENBUSH, L.; ADELI, S.; BRISCO, B. Google Earth Engine for geo-big data applications: a meta-analysis and systematic review. **ISPRS Journal of Photogrammetry and Remote Sensing**, v. 164, p. 152–170, 2020.

TANG, X.; BULLOCK, E. L.; OLOFSSON, P.; ESTEL, S.; WOODCOCK, C. E. Near real-time monitoring of tropical forest disturbance: new algorithms and

assessment framework. **Remote Sensing of Environment**, v. 224, p. 202–218, 2019.

THONFELD, F.; HECHELTJEN, A.; MENZ, G. Bi-temporal change detection, change trajectories and time series analysis for forest monitoring. **Photogrammetrie - Fernerkundung - Geoinformation**, v. 2015, n. 2, p. 129–141, 2015.

TRABAQUINI, K.; GALVÃO, L. S.; FORMAGGIO, A. R.; DE ARAGÃO, L. E. O. E. C. Soil, land use time, and sustainable intensification of agriculture in the Brazilian Cerrado region. **Environmental Monitoring and Assessment**, v. 189, n. 2, 2017.

TUCKER, C.J., PINZON, J. **Using spectral vegetation indices to measure gross primary productivity as an indicator of land degradation**. [S.l.]: Conservation International, 2016.

VERBESSELT, J.; ZEILEIS, A.; HEROLD, M. Near real-time disturbance detection using satellite image time series. **Remote Sensing of Environment**, v. 123, p. 98–108, 2012a.

VERBESSELT, J.; ZEILEIS, A.; HEROLD, M. Near real-time disturbance detection in terrestrial ecosystems using satellite image time series: drought detection in Somalia. **Remote Sensing of Environment**, p. 19, 2012b.

VOGELMANN, J. E.; GALLANT, A. L.; SHI, H.; ZHU, Z. Perspectives on monitoring gradual change across the continuity of Landsat sensors using time-series data. **Remote Sensing of Environment**, v. 185, p. 258–270, 2016.

WESSELS, K. J.; VAN DEN BERGH, F.; SCHOLES, R. J. Limits to detectability of land degradation by trend analysis of vegetation index data. **Remote Sensing of Environment**, v. 125, p. 10–22, 2012.

XIE, Z.; PHINN, S. R.; GAME, E. T.; PANNELL, D. J.; HOBBS, R. J.; BRIGGS, P. R.; MCDONALD-MADDEN, E. Using Landsat observations (1988–2017) and Google Earth Engine to detect vegetation cover changes in rangelands: a first step towards identifying degraded lands for conservation. **Remote Sensing of Environment**, v. 232, e111317, 2019.

ZALLES, V.; HANSEN, M. C.; POTAPOV, P. V.; STEHMAN, S. V.; TYUKAVINA, A.; PICKENS, A.; SONG, X. P.; ADUSEI, B.; OKPA, C.; AGUILAR, R.; JOHN, N.; CHAVEZ, S. Near doubling of Brazil's intensive row crop area since 2000. **Proceedings of the National Academy of Sciences of the United States of America**, v. 116, n. 2, p. 428–435, 2019.

ZHU, Z. Change detection using landsat time series: a of frequencies, preprocessing, algorithms, and applications. **ISPRS Journal of Photogrammetry and Remote Sensing**, v. 130, p. 370–384, 2017.

ZHU, Z.; WOODCOCK, C. E. Continuous change detection and classification of

land cover using all available Landsat data. **Remote Sensing of Environment**, v. 144, p. 152–171, 2014.

ZHU, Z.; WOODCOCK, C. E.; OLOFSSON, P. Continuous monitoring of forest disturbance using all available Landsat imagery. **Remote Sensing of Environment**, v. 122, p. 75–91, 2012.